1-1-2021

Experimental and computational studies of the growth plate reserve zone and chondro-osseous junction

Masumeh Massie Kazemi

EXPERIMENTAL AND COMPUTATIONAL STUDIES OF THE GROWTH PLATE RESERVE ZONE AND CHONDRO-OSSEOUS JUNCTIONS

By

Masumeh (Massie) Kazemi-Moghadam-Beydokhti

A Dissertation

Submitted in Partial Fulfillment of the

Requirements for the Degree of

Doctor of Philosophy

Major: Biomedical Engineering

The University of Memphis

May 2021

To my Mom, and my Husband, Ahmad,

For your unconditional

love and support

And to the memory of my Dad

ACKNOWLEDGEMENTS

First and foremost, I would like to sincerely thank my supervisor, Professor John L. Williams for giving me the opportunity to work on this project. I wish to express my deepest gratitude for his time and support during my research. His assistance and guidance were essential to the organization, analysis and presentation of my work. I am profoundly indebted to him for genuine caring and patient supervision, support, valuable comments and suggestions without which I may have never been able to finish this project. Thank you so much Dr. Williams for having faith in me and sharing with me your valuable experiences, you have always been there to listen to my problems and give invaluable advice and suggestions.

In addition, I would like to thank my committee member Dr. Omar Skalli for helping me learn the histology and microscopy techniques required for this work. I would also like to express my gratitude to Dr. Amy Curry and Dr. Aaryani Sajja for their kind acceptance to be a member of my examination committee. Furthermore, I would like to thank Dr. Felio Perez and Ms. Lauren Thompson for their help with histology and SEM/EDX studies and for their hours of assistance and support.

I would also like to thank my fellow graduate students particularly Ronald Perrone and Paola James with whom I had the pleasure of working during my PhD.

And behind everything, throughout my PhD, I have benefitted tremendously from the support of my family in life and science. I would like to thank my wonderful mom, my supportive sisters, Shiva, Tahmine and Mahboube, and my caring brothers, Kamran and Mahdi, for all their love and their continuous support and encouragements throughout this long journey from primary school to doctoral degree.

And at last, but not least, I want to thank my kind husband, Ahmad, for his love, patience, technical advice, critics and enthusiastic supports during my PhD. He has always been very supportive and helped me deal with difficulties.

PREFACE

This dissertation consists of four manuscripts that have been published or submitted for publication to different peer-reviewed journals. The manuscript in Chapter 2 entitled ‘Properties of cartilage–subchondral bone junctions: a narrative review with specific focus on the growth plate’ was published in the Journal of Cartilage in May 2020. The manuscript in Chapter 3 entitled ‘On the role of the reserve zone and mechano-regulatory stimuli in the development and maturation of the growth plate: Observations and models’ was accepted to publish in the Mechanobiology Journal in April 2021. The manuscript in Chapter 4 entitled ‘Chondrocyte and pericellular matrix deformation and strain in the growth plate cartilage reserve zone under compressive loading’ was published in the International Symposium on Computer Methods in Biomechanics and Biomedical Engineering in August 2019. The manuscript in Chapter 5 entitled ‘Depth and strain-rate dependent mechanical response of chondrocytes in reserve zone cartilage subjected to compressive loading’ was accepted to publish in the Journal of Biomechanics and Modeling in Mechanobiology in April 2021.

ABSTRACT

The growth plate of a long bone is an organ comprised of a thin layer of hyaline cartilage sandwiched between epiphyseal and metaphyseal bone and surrounded by fibrous tissues. The cartilage tissue can be divided into three histological zones reflecting the activities of the chondrocytes from the epiphysis toward the metaphysis: a reserve, proliferative and hypertrophic zone. Longitudinal growth occurs by a process of endochondral ossification in which cartilage in the hypertrophic zone at the metaphyseal border is calcified and then replaced by bone while new cartilage is produced in the proliferative zone. Application of mechanical loading modulates the chondrocyte activity in the proliferative and hypertrophic zones. As growth continues the growth plate develops into a three-dimensional interlocking interface of hills and valleys, termed mammillary processes, and a layer of compact subchondral bone arises at the border of the reserve zone and epiphysis. The undulations on the metaphyseal side of the growth plate are formed by endochondral ossification. The mechanism by which the undulations between the reserve zone and subchondral epiphysis form has not been elucidated. Recent discoveries of stem-like cells in the reserve zone suggest that reserve zone cells may also modulate growth under mechanical loading. To explore this possible function the present work examined the histology and chemistry of the interface between the reserve zone and epiphyseal bone in a pig model. Elastic and poroelastic multiscale finite element models of the growth plate were developed to investigate the depth-dependent biomechanical microenvironment of reserve zone chondrocytes, particularly cells close to the subchondral bone and proliferative zone. The histological, chemical, and computational results suggest that reserve zone chondrocytes near the epiphysis participate in a slower second endochondral ossification front that develops the subchondral bone plate forming undulations that match those on the metaphyseal side. Computational results indicate that dynamic loading engenders fluid shear stresses around reserve zone cells that may signal dividing cells to orient and align in columns. The depth-dependent micro-mechanical environment of the reserve zone cell is highly sensitive to the permeability of the subchondral bone plate and to the rate of loading.

Table of Contents

List of Tables

List of Figures

List of Abbreviations

AC	Articular cartilage
AFM	Atomic force microscopy
ALP	Alkaline phosphatase
CC	Calcified cartilage
ECM	Extracellular matrix
EDX	Energy dispersive X-ray spectroscopy
EP	Epiphyseal bone (Epiphysis)
GP	Growth plate cartilage
H&E	Hematoxylin and eosin
HZ	Hypertrophic zone
MMPs	Matrix metalloproteinases (enzymes)
MP	Metaphyseal bone (Metaphysis)
MTX	Methotrexate
OA	Osteoarthritis
PC	Provisional calcification
PCM	Pericellular matrix
PSR	Picro-Sirius Red
PZ	Proliferative zone
RZ	Reserve zone
SB	Subchondral bone
SCFE	Slipped capital femoral epiphysis
SEM	Scanning Electron Microscopy

Chapter 1

INTRODUCTION

1.1 Motivation for this study and objectives

During embryonic development, long bones are formed from a cartilaginous anlage through a process of cartilage ossification, known as endochondral ossification (Brighton 1984). Throughout this process, chondrocytes within the tissue undergo a series of phenotypical changes towards a terminal hypertrophic state that promotes tissue calcification. This process is continued after birth, in a structure known as the growth plate or physis. Endochondral ossification is regulated by many factors including hormones, genetics, nutrition, and the mechanical environment. The growth plate can be divided into three distinct zones based on the stage of differentiation of its chondrocytes: two highly cellular regions of proliferative and hypertrophic chondrocytes located in tubular structures, which contribute to further bone formation, and a region that is more sparsely populated by chondrocytes called the germinal layer, resting zone, or reserve zone (Brighton 1978). As these names imply, the function of the reserve zone has remained largely unknown, but it has recently been shown to contain stem-like cells that give rise to proliferative chondrocytes (Newton et al. 2019). The growth plate reserve zone connects to a plate of subchondral bone on the epiphyseal side through the calcified cartilage layer. During skeletal development, undulations termed mammillary processes appear in the cartilage-bone interfaces that affect the biomechanical stability of the joint and tissue. The metaphyseal undulations are matched by epiphyseal undulations that are formed by an as yet unknown mechanism that may also involve mechanical factors. Both physiological and pathological patterns of growth have been linked to external loading considerations.

Many theories and principles have been developed to explain bone formation and bone remodeling. Clinical observation indicates that physiological compression is critical for normal bone growth. Wolff's law suggests that bone modeling and remodeling is in part a tissue response to mechanical force (Frost 1994; Strokes 2002). Based on the Hueter-Volkmann law, reduced static compression acting on the growth plate accelerates ossification while increased static compression retards ossification (Hueter 1863; Volkman 1862). The effects of dynamic versus static mechanical modulation on bone growth were addressed by Frost (Frost 1990; 1997). He proposed that dynamic compression within the physiological range results in bone growth acceleration; conversely, increased compression exceeding the physiological range inhibits ossification. More recently, the concepts of mechanobiological parameters have been used to describe cartilage growth and endochondral ossification. Pauwels (1960) developed a tissue differentiation theory implemented by others in computational models (Carter ad Wong 1988, 2003; Carter and Beaupre 2001; Claes and Heigele 1999) in which the effect of applied stress on tissue differentiation has been explained by the combination of two scalar components of the applied stress tensor, the octahedral shear stress (deviatoric stress), which tends to accelerate bone formation, and the hydrostatic stress (volumetric or dilatational stress), which tends to maintain cartilage. While mechanical forces can act as stimuli for bone modeling and remodeling, abnormal physiological loading of the growth plate can cause various growth deformities and injuries. For instance, slipped capital femoral epiphysis (SCFE) is the most common hip disorder in children aged nine to sixteen years. It is most likely caused by multiple factors, including those that are mechanical in nature. SCFE occurs when shear stress across the capital femoral epiphysis becomes greater than the resistance provided by the mechanical stability of the growth plate tissue and the interlocking mammillary processes. Deficiencies in the development of the mammillary processes may result in bone growth problems and could contribute to conditions of SCFE. Therefore, investigating the biomechanical and biochemical properties of cartilage-bone interface and mammillary processes development may help in understanding the mechanical factors associated with SCFE and aid in its early diagnosis.

Moreover, idiopathic scoliosis is another cartilage deformity caused in part by asymmetrical forces across the vertebral body growth plate generating asymmetrical growth, which is most prevalent during the growth spurt before puberty. Stress-strain states across the vertebral body growth plate can modulate spine growth and induce scoliosis in animal models. Characterizing such patterns within the growth plate and the relationship between these and bone growth could provide guidance in developing less invasive treatments of progressive scoliosis. However, there is no direct way to measure stress either at the cellular or tissue level. Although several studies have measured growth plate cartilage strains at the tissue level, measurements at the scale of the cell are still challenging. Therefore, computational modeling and finite element techniques are particularly valuable to provide information on biomechanical parameters, which are not easy to measure experimentally, while avoiding limitations and difficulties associated with experiments. By finite element analysis, we can evaluate the mechano-transduction phenomenon in terms of stress and strain in zonal cartilage and chondrocyte cells. The result of such numerical approaches will give us insight into the behavior of cartilage and cells under different loading conditions, which can be of potential benefit to the diagnosis and treatment of physeal injuries and growth abnormalities.

On the other hand, bone fracture healing follows a process similar to that of endochondral ossification. Fracture healing is regulated by a variety of factors, including mechanical ones. Developing a mechanobiology model of growth plate to relate mechanical parameters to bone growth may also benefit our understanding and design of fracture healing studies in animal models by connecting the extrinsic factors of loading and displacement to cell-level stress-strain states and treatment modalities. Such modeling brings about a better understanding of how the cells respond to these mechanical stimuli and how they might function as mechanoreceptors within the tissue.

1.2 Outline of the dissertation

This thesis is divided into seven chapters and is submitted as an article-based thesis:

Chapter 2. Properties of the cartilage–subchondral bone junctions: a narrative review with specific focus on the growth plate. This chapter includes literature reviews on what is currently known about the histological, chemical, and mechanical properties of the chondro-osseous junction for both articular and growth plate cartilage. We focused on those aspects of the growth plate reserve zone-subchondral bone junction that relate to the development and adaptation of epiphyseal mammillary processes during skeletal development. We also included some of our histology studies on the microstructure of reserve zone chondro-osseous junction and cells boarding on this interface.

Chapter 3. On the role of the reserve zone and mechano-regulatory stimuli in the development and maturation of the growth plate: Observations and models. This chapter includes both experimental and computational results with a focus on reserve zone chondro-osseous junction in tissue and cell levels. In order to investigate a possible secondary bone growth front at the epiphyseal border of the growth plate, contributing to epiphyseal mammillary processes, the histological and elemental analysis of this border were studies at three different age groups. Furthermore, a series of multiscale elastic models of growth plate with four different thicknesses, subjected to 15% strain, were developed. Then, the mechano-regulatory parameters of reserve zone chondrocytes were explained based on tissue differentiation graphs.

Chapter 4. Chondrocyte and pericellular matrix deformation and strain in the growth plate cartilage reserve zone under compressive loading. Several multiscale elastic models of a single chondrocyte at four different locations within the reserve zone were developed to determine the chondrocyte functionality under physiological loads. Moreover, the influence of the pericellular matrix (PCM) on mechano-transduction mechanisms of reserve zone chondrocytes was investigated.

Chapter 5. Depth and strain-rate dependent mechanical response of chondrocytes in reserve zone cartilage subjected to compressive loading. Due to fluid flow throughout the porous solid matrix, growth

plate cartilage has time-dependent deformation characteristics. To consider the effects of interstitial fluid flow on stress-strain states around reserve zone chondrocytes and examine the transient response of the cell, a multiscale poroelastic model was developed. The computational studies compare the stress-strain state around cells at four different strain rates and also two fluid flow boundary conditions of chondro-epiphysis border.

Finally, a summary and conclusion of the dissertation and recommendations for future work are presented in Chapter 6 and Chapter 7, respectively. Generally, this dissertation addresses some fundamental aspects of mechanical stimulation of reserve zone chondrocytes within the growth plate. The motivation of these parts is to better understand mechanical mechanisms involved in the functional adaptation of the reserve zone of growth plate cartilage. In the long term, this knowledge will be useful for the development of treatment approaches based on the local mechanical modulation of bone growth.

Chapter 2

Properties of cartilage-subchondral bone junctions. A narrative review with specific focus on the growth plate.

2.1 Introduction

The interface between cartilage and bone is a unique region, which provides tissue integrity across a bi-material interface of two very different structural materials. Maintaining the interface at the chondro-osseous junction is a key factor for normal bone growth and articular cartilage function and maintenance. Unlike the interface between articular cartilage and bone, growth plate cartilage has two chondro-osseous junctions. The reserve zone of the mature growth plate is intimately connected to a plate of subchondral bone on the epiphyseal side. This interface resembles that between the subchondral bone and articular cartilage, although much less is known about its makeup and formation. On the other side of the growth plate, the hypertrophic zone attaches to the metaphysis through calcified cartilage, which is formed by endochondral ossification. Although endochondral bone growth occurs at the metaphyseal side of the growth plate, there is evidence of a slower growth front at the interface between the reserve zone and the subchondral bone plate of the epiphysis. The existence of such a growth front may help explain the mechanism of physeal mammillary process development which creates matching involutions at both cartilage-bone junctions. Although there have been several publications on the elemental distribution and biomechanical properties of the chondro-osseous junction of articular cartilage, there is surprisingly little information on the biochemical, morphology and biomechanical parameters of growth plate-subchondral bone interface.

This review paper focuses on those aspects of the growth plate reserve zone-subchondral bone junction that relate to the development and adaptation of this interface during bone growth. Following a

review of the overall structural and functional characteristics of the physis the literature on histological studies of the articular cartilage-subchondral bone interface is briefly reviewed, followed by histological studies on the growth plate cartilage-subchondral bone interface. Next, the literature on the biochemical properties of these interfaces is reviewed, specifically the literature on elemental analyses across the cartilage-subchondral bone junctions. Finally, the literature on biomechanical studies of these junctions at the articular and physeal interfaces is reviewed and compared.

2.2 Growth plate zonal structure and function

The growth plate is a thin layer of hyaline cartilage, which separates epiphyseal bone from the metaphysis at the end of each long bone and provides bone growth during skeletal development. The growth plate consists of at least three major zones: reserve zone, proliferative zone, and hypertrophic zone. Fig. 2.1 shows these histological zones of the growth plate for a yearling bovine cow. In all zones, chondrocytes are enveloped by a thin layer of the pericellular matrix (PCM) consisting of proteoglycans and acting as a diffusion barrier for large molecules[1]. The PCM is characterized by type VI collagen. Several studies suggested that the PCM seems to function as a mechano-transducer and transitional zone between cells and the extracellular matrix (ECM), which converts mechanical signals from and to chondrocytes[1-5.] Primary cilia on the surface of the cell can also act as mechanosensory organelles, which transduce mechanical forces into biological signals[5,6]. Understanding the sequence of events by which cells and ECM communicate and transduce biomechanical and biochemical signals is still providing a challenge to investigators[7,8].

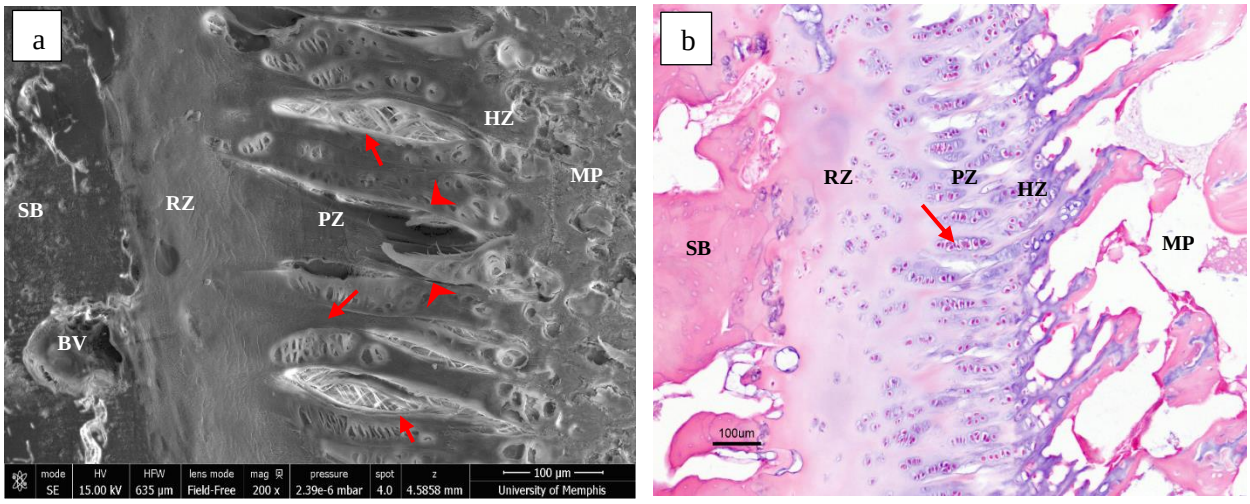

Fig. 2.1. Growth plate images of a bovine (12-18 month) growth plate; a) SEM image, and b) light microscopy image, stained with H&E. Red arrows show the intact chondrons within the proliferative zone, red arrowhead demonstrate tears between neighboring chondrons. SB=Subchondral Bone, BV=Blood vessel, RZ=Reserve Zone, PZ=Proliferative Zone, HZ=Hypertrophic Zone, MP=Metaphysis (from the authors' laboratory).

2.2.1 Reserve Zone Structure and Function

Many terms have been used for the reserve zone, such as the germinal layer, resting zone, stem-cell zone, and small-size-cartilage-cells zone[9-12]. Reserve zone chondrocytes are scattered irregularly within the ECM. Although the exact function of the reserve zone cells is not quite clear, some potential roles have been postulated.

First, the higher lipid concentration in chondrocyte vacuoles supports the idea that reserve zone cells might store nutrients for later nutritional requirements[10,11,13,14]. Early studies mentioned that these cells do not have any proliferative capacity and they are sometimes called undifferentiated cells[10,11,15]. Later authors reported that these cells might have the capability to generate new chondrocytes[16]. Cells in the reserve zone may be linked to stem cells, which have the proliferative capacity and can generate clones of chondrocytes for the proliferative zone. Therefore, one of the postulated functions of the reserve zone is to provide a pool of stem-like cells[12,16,17]. However, not all chondrocytes in the reserve zone can function as stem cells[18]. The average reserve zone chondrocyte cycle time for 35-day-old rats was

measured as 4-5 days, which shows reserve zone stem cells rarely divide or proliferate and have a slow proliferation rate, which is one of the characteristics of stem cells[12,19].

Second, chondrocytes in the reserve zone also secrete a morphogen that causes the chondrocyte proliferative clones to align to form a chondron by an as yet unknown mechanism[16,18]. The reserve zone can be divided into two parts; reserve cartilage, closer to the proliferative zone with flatted chondrocytes, and epiphyseal cartilage, nearer to the epiphyseal bone and chondro-osseous junction with round/elliptical cells[16]. However, most studies have reported the reserve zone cells as being spherical and round[10,11,20,21]. With increasing age and decreasing growth rate, the reserve zone chondrocytes become flatter[14]. Reserve zone chondrocytes are randomly distributed as single or paired cells[9,11,12,13,15], and have about the same dimensions as chondrocytes in the proliferative zone[10,11].

Third, chondrocytes may release hypertrophy-inhibiting morphogens to prevents premature hypertrophy of proliferative cells. Therefore, proliferative chondrocytes near the reserve zone cannot differentiate to hypertrophic cells, while towards metaphyseal end of the chondrons, cells not exposed to such factors enlarge and become hypertrophic cells[18].

2.2.2 Proliferative Zone Structure and Function

Chondrocytes and their surrounding PCM and territorial matrix were called chondrons by Benninghof [22] who described chondrons as being the basic anatomic and functional units of cartilage in analogy to osteons, which are the basic functional units of Haversian bone. In this context, we also refer to the columns of chondrocytes in the growth plate that consist of the proliferative zone[1,3,7,23], zone of maturation and hypertrophic zone as the growth plate chondrons. The chondrons are clustered around nutrient arteries that pass through the subchondral bone plate and reserve zone and end at the base of the proliferative zone of a cluster of chondron columns. It has been noted that after uniaxial tensile testing to failure of isolated growth plate samples, failure occurred within the proliferative zone/reserve zone interface with clusters of chondrons torn out of the reserve zone, but otherwise remaining intact on the side of the metaphysis after separation from the epiphyseal end of the sample; chondrons remained joined

to each other in clusters appearing to converge at the reserve zone junction around the source of the vascular supply[24], suggesting that this connection, as a unit of chondrons with a central blood supply, is relatively strong. This can be seen in the microradiography studies of rabbit (see Figs. 11 & 14 in ref. [25]) and rat (see plate I, Figs. 4 & 5 in ref. [26]) growth plates and in the freeze-fracture studies of the authors' laboratory (Fig. 2.2). Morgan[25] described blood vessels penetrating the subchondral bone plate through openings at the summit of from eight to twelve columns of proliferating epiphysial cartilage cells, "the rounded tops of the columns inclining towards the central aperture in the calcified zone". In mammals the small arteries from the epiphyseal side do not penetrate beyond the proliferative zone, making proliferative and hypertrophic zones dependent on diffusion[9,10,15,27,28]. Two main functions of the proliferative zone are matrix production (proteoglycan and collagen) and cell proliferation (chondrocytes), which together with the hypertrophic zone contribute to longitudinal bone growth[9,10,15,18].

Chondrocytes migrate from the reserve zone and arrange themselves to align with the longitudinal chondrons[29,30]. The flattened chondrocytes near the reserve zone-proliferative zone interface, at the base of the chondron are sometimes called mother cells[9,15,29], which can ultimately give rise to approximately 30 hypertrophic chondrocytes[17]. The linear growth rate of the growth plate is proportional to the rate of daily cell proliferation (cells/day) in the proliferative zone of the mother cells multiplied by the average height of mature chondrocytes (μm/cell) in the hypertrophic zone[10,13,31]. The average number of newly formed chondrocytes in each chondron is about 5 per day in the rat model (six to eight weeks old)[32]. Another study found the daily rate of cellular turnover in hypertrophic zone to be about 8 cells, which was calculated by dividing daily longitudinal growth by the mean height of hypertrophic cells[33]. This means that every three hours, a chondrocyte will be replaced at the end of the hypertrophic zone. The average cell cycle time or chondrocyte replication rate for the proliferative zone was reported to be about 48 hours in 35-day-old-rat, compared with 20 days in 5 to 8-year-old children[12]. These values may be factors of age and the animal species.

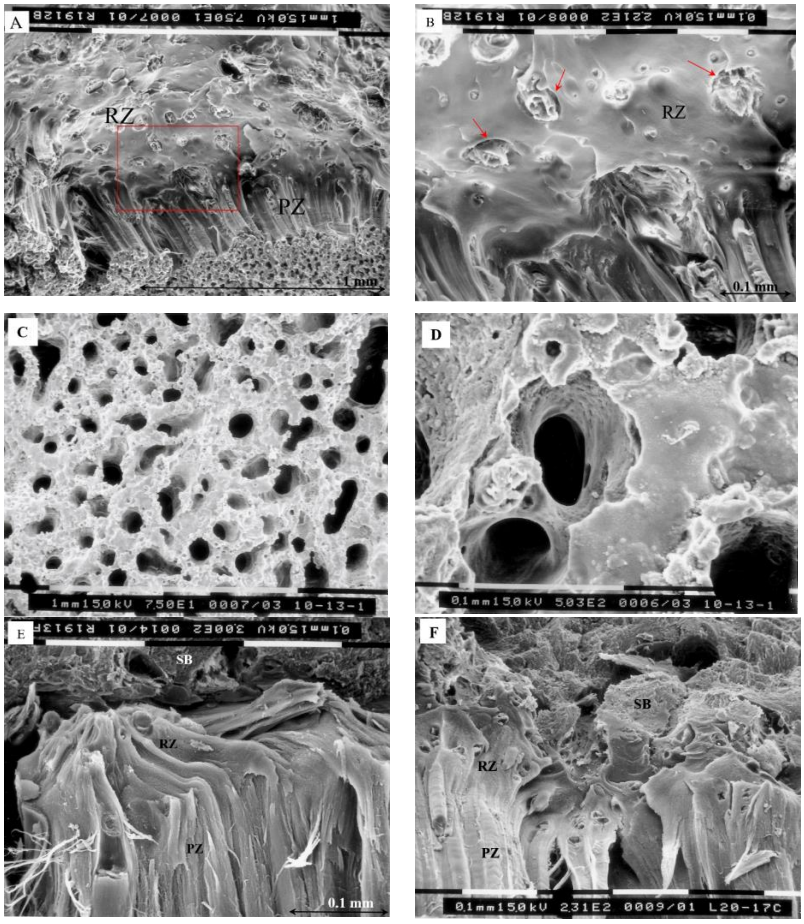

Fig. 2.2. SEM (Philips SEM 515) images of a yearling bovine proximal tibial growth plate. A) freeze-fracture sample showing fractured chondrons (bottom half of image) and the underneath exposed surface (top half of image) of the reserve zone from which clusters of chondrons have been torn. Torn blood vessels can be seen passing through the reserve zone. B) Higher magnification of red rectangular in (A), red arrows showing blood vessels. C) Surface of the subchondral bone and remaining calcified cartilage following digestion of organic matrix with 3% sodium hypochlorite to expose the pores for blood vessels. D) higher magnification of (C), view of a subchondral bone pore following sodium hypochlorite treatment. Several pores to side channels can be seen deeper inside the middle pore. E) Freeze-fracture showing an intact cluster of chondrons entering the reserve zone and arching toward the supplying blood vessel. F) Freeze-fractured sample. A cluster of chondrons has been torn from the reserve zone/subchondral bone plate (middle of image) exposing the pore containing the blood vessel that supplied the cluster. This can be compared to histology (Fig 14 in Morgan, 1959). From the authors' laboratory, SB = Subchondral Bone, RZ = Reserve Zone, PZ = Proliferative Zone.

2.2.3 Hypertrophic Zone Structure and Function

The hypertrophic zone plays a dominant role in endochondral ossification. Hypertrophic chondrocytes are formed by the final differentiation of the proliferative cells. As chondrocytes progress

from flattened cells in the upper proliferative zone close to the reserve zone, they begin to enlarge eventually reaching diameters up to five times greater (~ 50 μm in diameter) in the hypertrophic zone as reported in some studies, including birds[10,34]. Other studies have shown that the horizontal and vertical diameters of the cell increase by a factor of 1.6 and 4, respectively in rats[33,35], which results in an increased cell/matrix ratio in the hypertrophic zone. In contrast, confocal microscope studies of 4-week-old pigs show a higher cell/matrix volume ratio in the proliferative zone compared with the hypertrophic zone. It was measured to be around 11-13% in the reserve zone, 17% in the proliferative and 15% in the hypertrophic zone[20,21]. These parameters may vary with the species, the age of the animal and perhaps with specimen preparation and measurement technique (2D or 3D)[36]. Comparing these values with our histology images of a yearling bovine calf (Fig. 2.1) and early pubertal human growth plate (see Fig. 2 in ref. [37]) in which there are larger cells within a lower matrix volume in the hypertrophic zone, we expect to have higher cell/matrix volume ratios in the hypertrophic zone than the two other zones. In addition to the large changes in size and shape, the terminally differentiated cells undergo a change in phenotype[18]. Hypertrophic cells can either undergo cell death through apoptosis or, as some have suggested, transform into osteoblasts through trans-differentiation, which reprograms cells to change their phenotype. Hypertrophic cell differentiation is regulated by the cell's microenvironment, local factors like matrix metalloproteinases (MMPs), Wnt/β-catenin and the Ihh/PTHrP signaling pathway[3,37-39]. Trans-differentiation is a mechanism to generate osteoblasts as osteoprogenitor cells by an unknown mechanism while apoptosis is a mechanism to permit tissue remodeling[18,39,40]. A recent study proposed a model in which chondrocytes transform to osteoblasts directly [41]. The main function of the hypertrophic zone is to prepare the matrix for calcification by depositing calcium-phosphate mineral in the matrix[42].

Cartilage calcification occurs as the extracellular matrix volume decreases while the relative volume of chondrocytes gradually increases. At the initiation site of mineralization, the concentration of proteoglycan, type II collagen, alkaline phosphatase, and hyaluronic acid are maximum[3,43]. The concentration of type II collagen might be a function of its binding to hydroxyapatite[43]. However, by the end of the calcification process, proteoglycan and type II collagen have been split to form type X collagen

and release hyaluronic acid. Matrix metalloproteinase-13 (MMP-13) degrades type II collagen and contributes to the production of type X collagen (COL10A1: collagen gene) from type II collagen (CoL2a1: collagen gene). Then type X collagen is synthesized in the hypertrophic zone and is regulated by Runx2 factor[3,43,44].

2.2.4 Growth plate mammillary processes

Growth plate mammillary processes are the undulations of cartilage-bone interfaces, which form an interlocking interface of hills and valleys that continue to evolve as the bone grows in length and circumference (Fig. 2.3). These can be considered at various levels: primary, secondary and tertiary, depending on the relative size of the processes in relation to the epiphyseal dimension. On the metaphyseal side, the mammillary processes are formed by endochondral ossification. On the epiphyseal side, mammillary undulations closely match the 3D topographical pattern of the metaphyseal side forming a mechanical interlocking interface[45-47]. After the secondary center of ossification ceases to form bone and leaves a thickened 'endplate' of subchondral bone at both the articular and growth plate interfaces, the undulations along the interface with the growth plate reserve zone continue to evolve to match those on the metaphyseal side. The mechanism by which the epiphyseal side achieves this is unknown and will require future study. These two chondron-osseous interfaces play a dominant role in the structural integrity of the tissue and successful attachment of the soft and hard tissues and may have relevance to conditions such as slipped capital femoral epiphysis and cam morphology[48]. Therefore, further histological, biochemical and biomechanical studies of the chondro-osseous junctions are warranted.

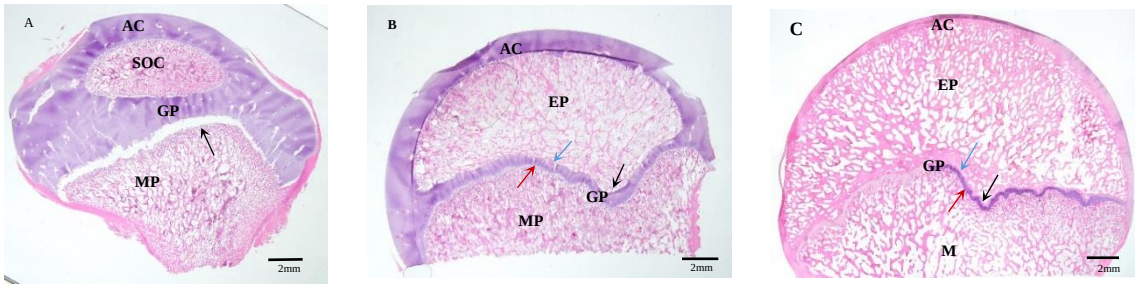

Fig. 2.3. Stereo-microscopy (Olympus, SZX16, Japan) sections cut in the same middle plane relative to pig femoral heads for three different age groups, which show the development of mammillary processes with aging. A) 20-day-old. B) 35-day-old. C) 480-day-old. AC=Articular cartilage, GP=Growth Plate cartilage, EP=Epiphysis, MP=Metaphysis. Black arrows show the undulation of the tubercle in the femoral head, red arrows indicate the metaphyseal secondary mammillary process and blue arrows point to the epiphyseal secondary mammillary process. The scale bar is 2 mm (from the authors' laboratory).

As the structural properties of the growth plate chondro-osseous junction, specifically the interface on the epiphysis side, are still mostly unexplored, the purpose of this study is to focus on those features. Experimental observations show that there are some structural similarities between the chondro-osseous junction of articular cartilage and that of the growth plate reserve zone with the epiphysis. Although the chemical and mechanical features of the articular cartilage-subchondral bone interface have been studied, almost no attention has been paid to the growth plate-subchondral bone interface. Chemical and mechanical studies of this interface may elucidate the mechanism of the successful attachment of these two dissimilar tissues of bone and cartilage and reveal more information related to mammillary process development. To develop a more complete understanding of these cartilage-bone interfaces, which evolve over time, we need more studies that examine the development and evolution of these interfaces during growth, aging, and disease.

2.3 Chondro-osseous junction structure

Histological studies have revealed details of the collagenous network and orientation and cell shape in the tissue at the chondro-osseous interface. The structural integrity between articular cartilage as a soft tissue and stiffer calcified cartilage is aided by collagen fibers that cross the tidemark[49]. The anisotropic architecture of collagen fibers within the cartilage matrix has a crucial role in cell protection and biomechanical strength and anchors the articular cartilage into the calcified base[50,51]. In the

hypertrophic and proliferative zones, collagen fibers are mostly oriented longitudinally[1,52]. Collagenous fibers are said to be arranged to give the appearance of arches and make a honeycomb-like network at the base of the proliferative zone, near the reserve zone of growth plate cartilage, which is similar to what has been noted for the superficial zone of articular cartilage[51,53]. At the interface of the reserve zone and the epiphyseal subchondral bone plate, collagen fibers orient transversely (radially) and in some parts obliquely. This structure is said to be similar to that in subchondral bone-articular cartilage interface[50,51].

2.3.1 Structure of articular chondro-osseous junction

In articular cartilage, the chondro-osseous junction includes the non-calcified cartilage, tidemark, calcified cartilage, cement line, and subchondral bone plate[54-56]. The tidemark is a strong hematoxylin-staining border between avascular non-calcified cartilage and vascular calcified cartilage, which forms as a result of an advancing ossification front. Calcified cartilage is a distinct mineralized layer intermediate between compliant articular cartilage and its stiff substrate of the bone plate. It provides a transition zone between soft and hard tissue, which facilitates load transfer at the interface by its intermediate Young modulus[57,58]. It has been reported that calcified cartilage is 10-100 times stiffer than articular cartilage and 10 times softer than bone[59]. The upper boundary on one side is demarcated by the tidemark and on the other boundary by the cement line, which is at the interface between calcified cartilage and lamellar bone[60,61]. The tidemark was first named and noted by Fawns and Landells[61], who described it as a zone of weakness in comparison with the interface between bone and cartilage which is a “double layer of a stain-free line and a granular layer of polysaccharide” somewhat, resembling the tidemark, but without its weakness and never duplicated. It has been shown that there is an increased alignment in collagen fiber orientation, predominantly perpendicular to the tidemark, and an increase in packing density through the tidemark towards calcified cartilage, which provides a smoother transfer of stress from articular cartilage with type II collagen to rigid calcified cartilage with type X collagen[49,62-64]. The dynamic structure and irregular geometry of the tidemark provide shearing resistance of the interface and it is frequently duplicated, both as a normal process of aging as well as due to cartilage pathologies[54,62,65]. Therefore, the

appearance of multiple tidemarks or tidemark duplication is not necessarily a significant identification for joint disorders such as osteoarthritis (OA)[66-68] and can be seen in normal tissue (Fig. 2.4).

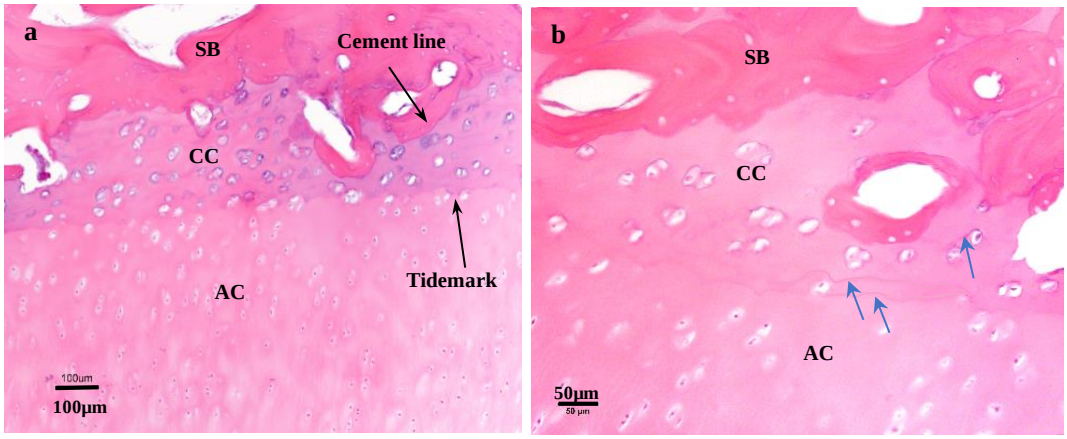

Fig. 2.4. Articular cartilage chondro-osseous junction of a yearling cow (12-18 months), stained with H&E; blue arrows show multiple tidemark lines. SB=Subchondral Bone plate, CC=Calcified Cartilage, AC=Articular Cartilage (from the authors' laboratory).

In normal tissue, tidemark duplication represents an advance of the calcification front and can be the result of metabolic activities. With cartilage degradation and disease like OA, tidemark duplication also occurs in which the tidemarks become more distinct and are duplicated between chondrocyte lacunae[59]. Cartilage lesions cause the formation of bony spicules with a central canal, originating from Haversian canals within the subchondral bone, which advances toward calcified cartilage[69]. The higher density of these spicules in OA makes the cement line more irregular and decreases the calcified cartilage thickness by gradual replacement with new less-structurally-organized Haversian canals[59,69]. The tidemark thickness varies from 2 to 10 microns[54,66]. The interface surface roughness values (Rs, which is the unitless surface roughness parameter) for the articular calcified cartilage/subchondral bone tidemark and cement line of the normal human femoral condyle were measured to be 1.14 ± 0.04 and 1.99 ± 0.38, respectively[70]. The thickness and shape of the tidemark are related to the loading sustained. Load-bearing areas have thicker tidemarks with more undulations to provide more stability and resistance to shear forces during articulation[68].

There are different definitions for the structure referred to as the subchondral bone plate. Duncan et al.[77] defined it as a region, which separates articular cartilage from bone marrow cavities including the calcified cartilage region. In the current review paper, we use the term 'subchondral bone' to refer to the cortical bone-like endplate, lying adjacent to the calcified cartilage. The subchondral bone plate thickness varies in the range of 0.1-1.5 mm, with numerous intercommunication spaces, which provide a direct connection between the non-calcified cartilage and the marrow cavity of the trabecular bone[72,73]. Bone plate composition, thickness, and perfusion vary with the region of the joint surface. The thickness is determined by joint function, the stress distribution, and changes with the joint disease[73]. For example, OA results in subchondral bone thickening and increases its porosity[74]. Clark et al.[72] showed that the subchondral bone plate is thicker in the center of the adult tibial plateau and a thinner on the lateral side; however, Mila et. al.[73] reported a uniform thickness of subchondral bone for the same region.

A 3D reconstruction of samples from histological serial sections of a human knee joint revealed that non-calcified cartilage islands pass beyond the tidemark interface and go through calcified cartilage to reach into the bone marrow[54]. This 'invagination' by non-calcified cartilage islands could also provide a nutritional pathway for articular cartilage and allow crosstalk within the chondro-osseous junction[54]. It has been hypothesized that subchondral bone may also protect articular cartilage through endogenous bone-mediated factors for cartilage chondrocyte survival[75]. In explant experiments in which articular cartilage was cultured without subchondral bone, most chondrocytes did not survive, whereas they survived in samples in which the subchondral bone remained attached[75].

2.3.2 Structure of growth plate chondro-osseous junction

After the growth plate cartilage-subchondral bone plate unit has formed following completion of growth by the secondary center of ossification, the growth plate cartilage is protected with a dense subchondral bone plate, bordering on the reserve zone[76]. The formation of subchondral bone may begin with the mineralization of cartilage on the reserve zone side through a mechanism, which is not completely elucidated. There is no tidemark formation at the metaphyseal growth plate cartilage-bone

interface where the hypertrophic zone merges into the zone of provisional calcification; however, there is evidence demonstrating the presence of a tidemark at the reserve zone-subchondral bone interface[77,78]. The formation of this tidemark would be the result of cartilage calcification[67]. Therefore, in addition to an endochondral ossification front on the metaphysis side, which is responsible for longitudinal bone growth, there is a second ossification front on the epiphysis side, which might be responsible for subchondral bone plate formation[76] and modeling of the mammillary processes on the epiphyseal border.

The final stages of growth involve the process of epiphyseal fusion which was described by Parfitt[79] as the formation of two bony plates following the cessation of growth. One bony plate is what we refer to in this review as the subchondral bone plate which arises first and lies at the border of the reserve zone; at a later point in time a second bony plate forms at the border of the hypertrophic zone "arising from compaction of new trabeculae that are lying horizontally rather than vertically"[79]. The time between the formation of the first and second bone plates may vary with species and skeletal sites. In the bovine proximal tibial epiphysis, we have observed the presence of the subchondral bone plate at the reserve zone as early as 4-5 months and the absence of formation of the second plate at the metaphyseal border even as late as 12-18 months. The age of epiphyseal union varies for different species. Even for the same species, the epiphyseal union order is not the same for all long bones[80]. It is known that fusion occurs earlier in females[81] and is influenced by hormones. Estrogen is the principal hormone stimulating growth in puberty for both sexes; however, in late adolescence, estrogen promotes growth plate fusion[36,80,82,83]. Lower levels of estrogen stimulates bone growth, while higher levels promote epiphyseal fusion[83].

Haines et al.[78] found small cartilage nodules close to the subchondral bone including closely packed cells in a young and still growing dog model following completion of the epiphyseal growth from the secondary center. These cartilage nodules were located between the bone marrow and subchondral epiphyseal bone and suggest the formation of new cartilage from bone marrow[78]. Similar evidence can be seen in histology studies of the authors' laboratory for a yearling bovine calf (Fig. 2.5), in which there are some neocartilage cells in the reserve zone-subchondral bone interface. Neocartilage cells, proposed by Haines et al.[78], seem to be larger than chondrocytes existing in the reserve zone. They are closely packed

in a basophilic matrix, which suggests the formation of new cartilage from epiphyseal bone marrow that might participate in subsequent epiphyseal subchondral bone formation and further development of mamillary processes. Their basophilic matrix suggests that these cells are differentiating. The neocartilage cells may be chondroblast or osteoblast precursor cells.

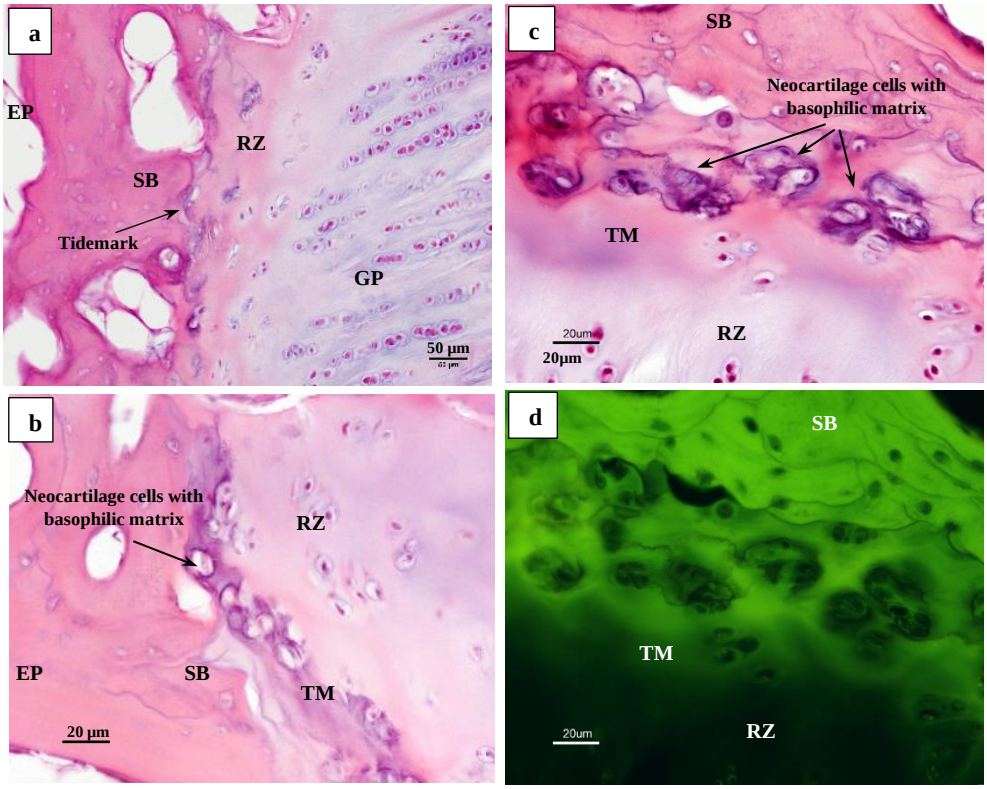

Fig. 2.5. a,b,c) Histology images of a yearling proximal tibial bovine growth plate, stained by H&E. d) Fluorescence image of RZ-SB interface. GP = Growth Plate, RZ = Reserve Zone, TM = Tide Mark, SB = Subchondral Bone, EP = Epiphyseal Bone. (from the authors' laboratory).

At the earlier developmental stage, before the formation of the subchondral bone plate when the secondary center of ossification (SCO) is still developing, there are larger cells in the reserve zone-epiphyseal bone interface of the SCO. These large cells are hypertrophic cells related to the growth of the SCO which are similar to those at the metaphyseal bone border of the primary center of ossification. Farnum & Wilsman[40] found such cells near the reserve zone-epiphyseal bone interface in their histology study of 4-week-old Yucatan pig (see Fig. 1.a, in ref.[40]). A narrow-calcified cartilage plate near the epiphyseal bone plate, which sometimes included a few hypertrophic cells, was also reported by Hansson

et al.[13]. Candela et al.[19] used immunohistochemistry labeling by thymidine analog 5-ethynyl-2′-deoxyuridine (EdU) to trace the "slow cycle" cells within the articular and growth plate cartilage of mice. EdU labeled cells were found in a narrow region within the superficial and reserve zone of articular and growth plate cartilage, respectively. These slow cycle cells are mostly stem or progenitor cells, which are able to differentiate to provide new chondrocytes[19].

Alkaline phosphate (ALP) localization within different zones of articular and growth plate cartilage has been used to reveal bone formation sites[84]. In articular cartilage, ALP is localized in the matrix of the deep zone and mature chondrocytes. Histology images of the growth plate (see Fig. 2c & d in ref.[84]) showed an increase in the ALP secretion from the proliferative to hypertrophic zones reaching the highest values in the hypertrophic zone. In these images ALP can also be seen to be localized in the reserve zone-subchondral bone interface, which could be a sign of bone formation[84]. Furthermore, an earlier study had reported finding a layer of calcified cartilage between the bone plate and reserve zone[9]. These aforementioned studies and observations show that there is a likely possibility for bone formation at the reserve zone-subchondral bone plate interface that could explain the mechanism of subchondral bone plate formation and mammillary process development. This hypothesis requires more studies and experiments to be fully explored.

2.4. Chondro-osseous junctions' chemical properties

2.4.1 Elemental distribution across the articular chondro-osseous junction

Bone has a dynamic structure that remodels continuously. Cartilage and bone structural and biomechanical properties are determined by compositional and biochemical variables. Alterations in biochemical properties in the cartilage zones may in part account for the varying zonal mechanical properties[85,86]. The measurement of the elemental and ion distributions in healthy and non-healthy tissue can be used as a diagnostic tool in clinical studies. One example is the evaluation of the chemical composition of calcified cartilage and subchondral bone in studies of degenerative joint disease or osteoarthritis (OA). There is some evidence that early OA is accompanied by alterations in elemental

composition[2]. Pathological changes in the major elemental distributions and the balance of the cartilage components may contribute to structural alteration in the collagen network, which can change mechanical properties and subsequently initiate cartilage degradation[87]. For instance, the local concentration of Pb as a toxic metal in the skeleton targets osteoblast and osteocyte activities, inhibits fracture healing, and results in osteopenia. Therefore, tracing Pb is of considerable interest in cartilage pathology. This toxic element mostly accumulates in the transition zone between the non-calcified cartilage and calcified cartilage (tidemark)[88,89].

Cartilage extracellular matrix (ECM) is composed of fluid and a small percentage of macromolecules[2], which control ECM turnover. Growth factors and enzymes, including matrix metalloproteinases (MMPs) and ALP have a key role in collagen formation, cartilage degeneration, and bone remodeling. ALP is involved in cartilage mineralization and bone formation and is produced by osteoblasts. ALP is also produced by chondrocytes in the deep zone of articular cartilage and the growth plate hypertrophic chondrocytes[90]. However, to function, these enzymes require bound metal ions of certain elements such as Ca, P, Zn and K, known as co-factors[2,87-89,91-94]. Among all co-factors, the divalent cation, Zn^{2+}, at the active site of the tidemark, plays a fundamental role in the growth and degeneration process of OA[88,95-98]. ALP is known as a Zn-dependent enzyme. Although Zn is considered as an essential element for normal skeletal growth and is concentrated at the site of new bone formation[96,97], its accumulation within the tidemark and transition zone suggest increased activity of cartilage degrading enzymes[2,87,94]. Accumulations of other co-factors at the bone-cartilage interface also indicate a raised activity of cartilage degrading enzymes. Therefore, elemental features are expected to provide a good estimation of changes in enzymatic activities, occurring in OA[2,94,95].

Elemental analysis has demonstrated that Ca and P reach their maximum values at the calcification front to participate in hydroxyapatite crystal formation. In addition to Ca and P, the presence of Zn is also essential for bone calcification[93]. Localization of S in articular cartilage relates to its contribution in matrix proteoglycans, while its level is decreased within bone[93]. Chemical studies of all essential elements in the articular cartilage-subchondral bone plate interface show a gradient in elemental

concentration from cartilage to bone, which might provide a mechanical transition zone between the two different tissues of cartilage and bone with very different mechanical properties. Calcified cartilage may function as such a transition zone. Elemental studies of the articular cartilage-subchondral bone interface using various techniques are summarized in Table 2.1.

Table 2.1. Summary of elemental analysis studies of the articular cartilage-subchondral bone interface.

	Tissue/Species	Technique	Essential element in cartilage-bone interface
Bradley et al. (2007)[77]	Metacarpophalangeal joint /Horse	XRF[a]	Zn, Sr, Ca
Zoeger et al. (2008)[88]	Femoral head, Patella/Human	SRm-XRF[b]	Ca, Zn, Sr, Pb
Kaabar et al. (2008)[2]	Femoral head, normal and OA/Human	PIXE[c] SAXS[d] RBS[e]	Ca, P, K, S, Zn
Kaabar et al. (2009)[95]	Femoral head, OA/ Human	μ-PIXE[f] RBS	Si, P, S, K, Ca, Fe, Cu, Zn
Kaabar et al. (2010)[94]	Femoral head, OA/Human	μ-PIXE SAXS	Si, P, S, K, Ca, Fe, Zn
Bradley et al. (2010)[87]	Femoral head, Normal and OA/Human	μ-SXRF[g] μ-PIXE RBS	Zn, Ca, P, S, K
Kaabar et al. (2011)[93]	Femoral head, normal and OA/Human	μ-PIXE PIGE[h]	Ca, P, K, S, Zn

a = Synchrotron X-Ray Fluorescence, b = Synchrotron-Radiation-induced micro X-Ray Fluorescence,
c = Proton Induced X-Ray Emission, d = Small-Angle X-Ray, e = Rutherford Backscattering, f = Micro-Proton Induced X-Ray Emission, g = Micro-Synchrotron X-Ray Fluorescence, h = Proton Induced Gamma-ray Emission.

2.4.2 Elemental distribution within the growth plate

In contrast to the aforementioned studies on the elemental analysis of the articular cartilage subchondral bone interface, to our knowledge, there is no such study of the reserve zone-subchondral bone interface. There have been studies on the elemental distribution across the growth plate and close to the metaphyseal bone border. One of the earliest elemental analyses of the growth plate was reported by Boyde and Shapiro[99]. They studied isolated chondrocytes (extracted from each of the GP zones) and ECM in different growth plate zones for four species; pig, rabbit, rat and guinea pig[99]. Their results show that the Ca and P content reached their highest values in the cells and ECM of the hypertrophic zone[99-101]. The higher concentration of P and Ca in the hypertrophic zone is related to their roles as precursors to phospholipid biosynthesis and hydroxyapatite formation ($Ca_{10}(PO_4)_6(OH)_2$)[101]. During remodeling, septoclasts solubilize the cartilage ECM and the dissolution of proteins in the matrix, releasing high local levels of ions, peptides, and glycans and secreted matrix metalloproteins. Some of these can act as potent

apoptogens of chondrocytes[39]. In addition, the higher concentration of Ca in the hypertrophic zone is associated with extracellular lymph within the cartilage matrix and chondroitin sulfate or other matrix acid mucopolysaccharides. Phosphorus is mostly stored in hydroxyapatite, extracellular lymph, and intracellular organic and inorganic phosphate and matrix polyphosphates[102].

In comparison with Ca and P, S content decreases in the hypertrophic zone, where chondrocytes no longer synthesize sulfated proteoglycans to provide more space for deposition of hydroxyapatite. Localization of S in non-calcified cartilage zones is needed for matrix proteoglycans negative chains that bind large amounts of water [99,100,103-105]. Potassium (K) and chloride (Cl) are present in all cells in different cartilage zones[99]. By evaluating the weight ratio of trace elements to Ca the percentage of Ca, S, K, Cl, Ni, Cu, Zn and Sr could be determined in each zone of growth plate[105]. In addition to these elements, C, N, O, Na, Mg, Si, Fe, Sn and Pb have been detected within the ovine scapula growth plate[92]. Higher percentages of C, N and O in cartilage are related to protein synthesis[92]. Mg and Cl are involved in cell physiology[106]. Comparing the distribution of the main elements of Mg, P, S, Cl, K, Na and Ca in the proliferative, pre-hypertrophic, hypertrophic and calcification zones showed that S and Cl decreased from proliferative zone to the zone of early calcification. Similarly, the value of Na dropped from the proliferative zone to early hypertrophic zone and then remained constant. While Mg and K stayed the same over all zones[106]. Table 2.2 summarizes the elemental studies on different zones of the growth plate using various techniques.

Table 2.2. Summary of elemental analysis studies of the growth plate.

	Tissue	Technique	Studied regions of growth plate
Howell et al. (1960)[102]	Costal cartilage, calf	X-ray Spectrophotometry	PZ, HZ
Howell et al. (1968)[103]	Costal cartilage, tibial cartilage, calf	X-ray Spectrophotometry	PZ, HZ
Takata et al. (1974)[101]	Upper tibia of puppies	EDX	RZ, PZ, HZ
Boyde et al. (1980)[99]	Femora of pig, rabbit, rat and young guinea pig	EDX	Dissected chondrocyte from RZ, PZ, HZ
Shapiro et al. (1984)[100]	Normal and rachitic chicks	EDX	Dissected chondrocytes and matrix cells of PZ, HZ
Hargest et al. (1985)[106]	Tibia, commercial broiler chicks	Electron probe analysis	PZ, PHZ, HZ, CZ
Vittur et al. (1992)[105]	Scapula, calf	SRIXE	RZ, HZ, CZ
Gangadhar et al. (2015)[92]	Scapula, sheep	EDX	Various locations of ovine scapula

EDX = energy Dispersive X-ray spectroscopy; SRIXE = Synchrotron radiation induced X-ray emission
RZ = Resting Zone, PZ = Proliferative Zone, HZ = Hypertrophic Zone, PHZ = Pre-Hypertrophic Zone, CZ = Calcification Zone.

2.5 Chondro-osseous junction permeability

Cartilage may be viewed as a poroelastic material with a porous solid phase and a mobile fluid phase. Permeability is measured by how fast the fluid phase can move through the solid phase when subjected to a pressure gradient. A tissue with relatively low permeability (resistance to fluid flow) builds up hydrostatic pressure under compressive loading, which helps articular cartilage support joint loads and avoid collapse of the solid matrix and prolongs the time to reach equilibrium[107]. In addition to hydraulic permeability as a material property, to evaluate the fluid flow throughout an irregular structure like the chondro-osseous junction, it is useful to also look at the hydraulic conductance as a structural property of the tissue[107]. Table 2.3 shows how the main material and structural properties of the articular unit, which affect the fluid flow, change with cartilage degeneration. Fluid flow and solute transport across the cartilage-bone interface are likely to be key factors in cartilage-bone crosstalk for maintaining normal physiology[108]. Cartilage is, in general, an anisotropic and inhomogeneous tissue and its permeability depends on collagen arrangement, fiber orientation and fiber volume fraction[109]. It has been shown that under compression, the permeability of articular cartilage is different between the axial and transverse direction and it is measured to be greater in the transverse direction[110-114]. Fluid exchange across the joint is also influenced by tissue vascular channels, microcracks, porosity, and subchondral bone thickness. The porosity of human articular subchondral bone has been measured to be 5.8 ± 1.8% [115]. The average pore diameters of the articular calcified cartilage and subchondral bone plate have been measured as 10.7

± 6.5 nm and 39.1 ± 26.2 nm, respectively[116]. In a healthy joint, the articular subchondral bone plate thickness is highly variable relative to the region of the joint surface. The thickness is a function of joint loading and stress distribution[73].

The subchondral bone plate is a highly vascular tissue. It has cavities of various sizes and shapes. The largest irregular cavities (more than 100 μm wide) relate to marrow containing spaces, while more cylindrical-shaped canals (30-70 μm in diameter) contain marrow cells and blood vessels. The smallest pores (less than 30 μm) are vascular canals, which hold one or two blood vessels[68]. The vessels enter calcified cartilage from subchondral bone to provide cartilage nutrition[117]. These arteries contribute to the remodeling of the calcified cartilage and subchondral bone plate and affect tissue permeability[118]. It has been shown that there is an increase in the vessels invading the calcified cartilage and tidemark with OA, which may explain the increase of tissue permeability[117,119,120]. Although the mineralization of cartilage in calcified regions acts as a barrier to molecular transport, its non-mineralized patches are considered as molecular pathways for small solutes[121]. The uncalcified cartilage helical patches/prolongations, dipping through the calcified cartilage to subchondral bone marrow spaces, affect chondro-osseous junction permeability and support tissue nutrition[54]. Furthermore, an in vivo study in humans using intravenous injection revealed that gadolinium diethylenetriaminepentaacetic acid ($Gd(DTPA)^{2-}$) penetrated through the subchondral bone into the articular cartilage[122]. The tidemark and mineralized cartilage are permeable to low molecular weight solutes, however, their diffusivity is lower than in uncalcified cartilage[108,123]. Depth-dependent cartilage diffusivity could be explained by various GAGs distribution, water content, collagen orientation, and other macromolecules through the cartilage[123-125]. Molecular transport through the chondro-osseous junction depends on the morphological and microstructural features of calcified cartilage, and subchondral bone[115,123]. It has been shown that there is a link between the diffusion behavior of the neutral solute and the micro-architecture of the subchondral plate/calcified cartilage[115].

Table 2.3. Effects of articular cartilage material and structural properties on fluid flow with OA progression.

Tissue	**Effect of OA progression**		
	Hydraulic conductance	Hydraulic permeability	Thickness
Articular cartilage	Increase[107]	Increase[107,126-128]	Decrease *[117,129,130]
Calcified cartilage	Increase[107]	Increase[119,131]	Increase *[107,129,130]
Subchondral bone plate	Increase[107]	Increase[126]	Increase*[107,117,129,130,132,133]
Chondro-osseous junction	Increase[107]	Increase[107,119,126]	-

*In healthy tissue, articular cartilage and subchondral bone plate thickness did not change with age for either women or men. However, the calcified cartilage thickness is age-dependent for women and doubles between age 20 and 80[134].

In contrast to these qualitative and quantitative studies on articular cartilage-subchondral bone permeabilities, little is known about the growth plate cartilage-bone interfaces. Cohen et al.[135] investigated bone-physis-bone permeability using numerical modeling of compressive stress relaxation experiments. They considered three different boundary conditions for the chondro-osseous junction permeability; permeable epiphyseal and metaphyseal, permeable metaphysis/impermeable epiphysis and finally, impermeable epiphysis and metaphysis. The best fit to their experimental stress relaxation data was obtained using a permeable metaphysis and impermeable epiphysis boundary condition. Another study investigated the time-dependent volume change of epiphysis-growth plate cartilage-metaphysis interfaces under cyclic compressive loading using MRI imaging[136]. The results showed that the time constants for physeal cartilage consolidation and recovery were 12 to 30% of the corresponding values for articular cartilage. It was hypothesized that this could be explained by a more permeable cartilage-metaphyseal border since the physeal cartilage-epiphyseal interface is similar to the articular cartilage-epiphyseal interface. It required less time to reach equilibrium and provided less hydrostatic pressure than cyclic compression of the articular cartilage[136].

2.6. Chondro-osseous junctions' mechanical properties

Physiological loading is essential for the maintenance of the composition and structure of normal cartilage[137]. Mechanical loading also modulates processes related to endochondral bone formation, such as mineral deposition and cartilage calcification[42]. Dynamic loads can also affect solute transport in cartilage extracellular matrix by pumping out the solutes from blood vessels and has a key role in the nutrition of avascular tissues for maintaining their cellular metabolic activities[138]. Many experimental and

computational studies have explored the mechanical behavior of growth plate regions at macro and microscale levels under physiological loads[19,139-144]. Although some of the mechanisms of mechano-transduction of the growth plate are known today, there are certainly many others still unrevealed, specifically in the chondro-osseous junction of both articular and growth plate cartilage. Understanding the mechanical and structural features of this junction can give us insights useful for engineering tissue interfaces and help to design and develop biomaterial replacements for the treatment of joint disease and lost tissue[145].

The chondro-osseous interface plays a crucial role in maintaining the integrity of the joint and the successful attachment of two mechanically dissimilar tissues. In comparison with articular cartilage, the higher impact energy absorbing and greater shock absorbing ability of subchondral bone is an advantage[146]. Higher energy absorption by subchondral bone can protect the overlying cartilage from further damage and in the long term, any microcracks/microfractures resulting from high-stress level can be remodeled because of the greater ability of bone for healing[146].

Physiological loads are transmitted through the junction of cartilage and the comparatively rigid subchondral bone. This material mismatch along the interface of two structurally and mechanically different tissues contributes to stresses likely to result in debonding unless mitigated by modifications in the surrounding tissue properties or in the nature of the bond between the dissimilar materials. The bone-cartilage interface is capable of resisting the static and dynamic loads of everyday activities by features that warrant further investigation[82]. In a study comparing the shock-absorbing ability of articular cartilage and subchondral bone, the reported impact-induced microcracks at the cartilage-bone interface under a dynamic load, presented in three samples out of ten, may be associated with the shock-absorbing ability mismatch between articular cartilage and subchondral bone[146]. Tensile and shear testing of the growth plate has produced failure planes through different zones of the growth plate, but not at the subchondral bone/reserve zone interface[24,147-149].

2.6.1. Mechanical properties of the articular chondro-osseous junction

Despite the importance of the chondro-osseous junction, there are few published studies on the mechanical properties of the articular cartilage-bone interface[150,151]. Ferguson et al. reported values for the human femoral head articular calcified cartilage (ACC) Young modulus of 19.01 ± 3.9 GPa by nanoindentation technique; however, Mente et al. measured it as 0.16 ± 0.09 and 0.58 ± 0.19 GPa for the bovine patella and femur, respectively, using three-point bending[150,152]. Campbell et al. mapped the elastic modulus of articular cartilage across the chondro-osseous interface using atomic force microscopy (AFM) and nanoindentation tests[153]. They revealed that there is a transition zone between the soft tissue and hard tissue with a width of 2.3 ± 1.2 μm for the rabbit femoral head. Gupta et al. evaluated the mechanical properties and mineral content of the cartilage-bone interface to address how the mineralized matrix of ACC remains attached to subchondral bone without debonding[154]. They reported an interface width of 20-40 μm using AFM technique, although their results were affected by sample dehydration. As a biphasic tissue, the interaction between the solid and fluid phases gives cartilage its viscous mechanical properties. Dehydration can result in tissue shrinkage, reduced toughness and increased strength and stiffness[155]. A study of age-related biochemical and biomechanical alterations across the articular cartilage-subchondral bone unit revealed that cartilage thickness decreased with growth, paralleled by a structural condensation of the underlying subchondral bone due to endochondral ossification[156]. Subchondral bone thickness and mineral density increase, and porosity decrease during skeletal development[157]. Table 2.4 summarizes research studies on the mechanical properties of the articular cartilage-bone interface.

Table 2.4. Summary of studies of mechanical properties of the articular cartilage-subchondral bone interface during growth.

	Species/location	Age	Method/equipment	E (GPa) for AC*/ACC*	E (GPa) for SB*	Transition zone width (μm)
Mente et al. (1994)[150]	Bovine/Patella&Femur	–	Three-point bending	-/0.32±0.25	5.7±1.9	–
Ferguson et al. (2003)[152]	Human/Femoral head	55-89 years	Nano-indentation, qBSE*	-/19.01	19.05	–
Gupta et al. (2005)[154]	Human/Patella	39-54 years	Nano-indentation, qBSE*	-/13-17	15-20	20-40
Doube et al. (2010)[151]	Horse/Distal condyle of metacarpal bone	12-18 months	Nano-indentation, qBSE*	-/12.90±1.66	14.57±1.76	–
Campbell et al. (2012)[153]	New Zealand white rabbit/Femoral head	6 months	AFM*, Nano-indentation	5.7±1/-	22.8±1.8	2.3±1.2

*AC = Articular Cartilage, ACC = Articular Calcified Cartilage, SB = Subchondral Bone Plate. E= Young's Modulus, qBSE = Quantitative Back-Scattered Electron Microscopy, AFM = Atomic Force Microscopy

2.6.2. Mechanical properties of the growth plate chondro-osseous junction

Although there have been studies investigating mechano-transduction and characterizing the biochemical properties of the growth plate, we have been unable to find any studies on the mechanical properties of the growth plate-subchondral bone interface, even though it plays a significant role in maintaining growth plate tissue integrity and strength. Most of the research has focused on measuring the biomechanical behavior of the growth plate zones, which are briefly mentioned here. The different zones of the growth plate vary in composition; therefore, each zone behaves mechanically differently under physiological loading conditions. Growth plate cartilage and articular cartilage are similar in that they have a mechanical gradient along their zones, and in both, growth starts with an increase in cell numbers and volumes[158]. The mechanical properties of the zones vary with stage of development and skeletal location. Chondrocytes respond differently depending on the frequency and amplitude and duration of loading[159]. Congdon et al. revealed that articular cartilage and growth plate cartilage respond differently to mechanical stimuli[160].

Using AFM to compare the Young modulus of the interterritorial matrix (ITM) and pericellular matrix (PCM) surrounding the chondrocytes showed that these elastic modulus values were greater for the ITM which has a more solid phase relative to those for the PCM with its more fluid phase. This might be related to their nanostructure, collagen type and concentration. Growth plate nanostructural and nanomechanical properties may have implications in nutrient diffusion and fluid dynamics, which are

vital for cartilage health and function[161]. The indentation-derived Young modulus measured in small (2 x 2 μm) areas of the ECM increases from 0.57 MPa in the reserve zone to 1.44 MPa in the zone of calcifying cartilage measured in the longitudinal direction employing AFM[158]. The growth plate is anisotropic with different values for Young's modulus along longitudinal and transverse directions[158]. An unconfined compression study of 0.4 mm diameter plugs of newborn swine (ulna) growth plate demonstrated[162] that the macroscopic (ECM + cells) Young's modulus of the reserve zone is double that of the proliferative/hypertrophic zone along the longitudinal direction, in agreement with the study by Cohen[163], while it is three times the value in the transverse direction. Tensile properties evaluated by testing 8-week-old rabbit distal radial and ulnar growth plate after excising the perichondrial ring, but otherwise intact, showed that the reserve zone is about 75% stiffer than other two zones[164]. These mechanical property values depend on test methods (micro-indentation vs macroscopic tension or compression), species, location and growth plate developmental stage. The macroscopic tensile Young's modulus is an order of magnitude greater than the compressive Young's modulus and aggregate modulus[163].

2.7 Summary and conclusion

The chondro-osseous junction in articular cartilage consists of non-calcified cartilage and calcified cartilage layers, a tidemark and a subchondral bone plate. The mechanical and structural properties of this junction play a key role in skeletal joint diseases like OA. It has been observed that a similar interface exists at the growth plate reserve zone-epiphysis junction which includes the cartilage reserve zone, calcified cartilage, tidemark region, and subchondral bone plate. Therefore, the growth plate may be considered to consists of two ossification fronts, one at the hypertrophic zone-metaphysis interface and another at the reserve zone-subchondral bone epiphysis interface. In this paper, we reviewed the biochemical, histological and mechanical literature on the chondro-osseous junctions of articular cartilage and growth plate cartilage. Our focus was on the reserve zone-subchondral bone region which has received comparatively less attention than articular cartilage. It is hypothesized that there is a gradual

mechanical and chemical transition between the soft reserve zone and the stiff epiphyseal subchondral bone plate, which would enable a stable interface similar to the articular cartilage-subchondral bone interface. In histological preparations of the growth plate, clusters of neocartilage cells have been observed in this transition zone[78,165]. These neocartilage cells have not been reported in the tidemark region of articular cartilage. The neocartilage clusters in the reserve zone-epiphysis junction could provide insight into the mechanism of subchondral bone formation. This study highlights a need for an improved understanding of chondro-osseous junction of the growth plate-epiphyseal bone to enable new tissue engineering strategies to be explored for osteochondral defect treatment. The study of the growth plate reserve zone chondro-osseous junction development can also help us understand the mechanism of mammillary process formation and how the undulations on the epiphyseal side continues to match those on the metaphyseal side long after the formation of a compact epiphyseal bone plate.

References

[1]. Eggli PS, Herrmann W, Hunziker EB, Schenk RK. Matrix compartments in the growth plate of the proximal tibia of rats. The Anatomical Record. 1985;211:246-257.

[2]. Kaabar W, Gundogdu O, Bradley DA, Bunk O, Pfeiffer F, Farquharson MJ, *et al*. Compositional studies at the Bone-Cartilage interface using PIXE, RBS and cSAXS techniques. Egypt, IX Radiation Physics & Protection Conference. 2008.

[3]. Byers S, Van Rooden JC, Foster BK. Structural changes in the large proteoglycan, aggrecan, in different zones of the ovine growth plate. Calcified tissue international. 1997;60:71-78.

[4]. Alexopoulos LG, Setton LA, Guilak F. The biomechanical role of the chondrocyte pericellular matrix in articular cartilage. Acta biomaterialia. 2005;1:317-325.

[5]. Shao YY, Wang L, Welter JF, Ballock RT. Primary cilia modulate Ihh signal transduction in response to hydrostatic loading of growth plate chondrocytes. Bone. 2012;50:79-84.

[6]. Seeger-Nukpezah T, Golemis EA. The extracellular matrix and ciliary signaling. Current opinion in cell biology. 2012;24:652-661.

[7]. Zhang Z. Chondrons and the pericellular matrix of chondrocytes. Tissue Engineering Part B: Reviews. 2014;21:267-277.

[8]. Poole CA, Flint MH, Beaumont BW. Chondrons in cartilage: ultrastructural analysis of the pericellular microenvironment in adult human articular cartilages. Journal of orthopaedic research. 1987;5:509-522.

[9]. Trueta J, Little K. The vascular contribution to osteogenesis: II. Studies with the electron microscope. The Journal of bone and joint surgery. 1960;42:367-376.

[10]. Brighton CT. Structure and function of the growth plate. Clinical Orthopaedics and Related Research. 1978;136:22-32.

[11]. Brighton CT. The growth plate. The orthopedic clinics of North America. 1984;15:571-595.

[12]. Hunziker EB. Mechanism of longitudinal bone growth and its regulation by growth plate chondrocytes. Microscopy research and technique. 1994;28:505-519.

[13]. Hansson LI. Daily Growth in Length of Diaphysis Measured by Oxytetracycline in Rabbit Normally. Acta Orthopaedica Scandinavica. 1967;38:3-199.

[14]. Buckwalter JA, Mower D, Schafer J, Ungar RO, Ginsberg BA, Moore K. Growth-plate-chondrocyte profiles and their orientation. The Journal of bone and joint surgery. 1985;67:942-955.

[15]. Trueta J, Morgan JD. The vascular contribution to osteogenesis: I. Studies by the injection method. The Journal of bone and joint surgery. 1960;42:97-109.

[16]. Schrier L, Ferns SP, Barnes KM, Emons JA, Newman EI, Nilsson O, *et al*. Depletion of resting zone chondrocytes during growth plate senescence. Journal of Endocrinology. 2006;189:27-36.

[17]. Ohlsson C, Nilsson A, Isaksson O, Lindahl A. Growth hormone induces multiplication of the slowly cycling germinal cells of the rat tibial growth plate. Proceedings of the National Academy of Sciences. 1992;89:9826-9830.

[18]. Abad V, Meyers JL, Weise M, Gafni RI, Barnes KM, Nilsson O, *et al*. The role of the resting zone in growth plate chondrogenesis. Endocrinology. 2002;143:1851-1857.

[19]. Candela ME, Cantley L, Yasuaha R, Iwamoto M, Pacifici M, Enomoto-Iwamoto M. Distribution of slow-cycling cells in epiphyseal cartilage and requirement of β-catenin signaling for their maintenance in growth plate. Journal of Orthopaedic Research. 2014;32:661-668.
[20]. Amini S, Veilleux D, Villemure I. Three-dimensional in situ zonal morphology of viable growth plate chondrocytes: a confocal microscopy study. Journal of Orthopaedic Research. 2011;29:710-717.
[21]. Amini S, Veilleux D, Villemure I. Tissue and cellular morphological changes in growth plate explants under compression. Journal of biomechanics. 2010;43:2582-2588.
[22]. Benninghoff A., Ueber den functionellen Bau des Knorpels. Journal of Anatomischer Anzeiger. 1922;55:250-267.
[23]. Poole CA. Articular cartilage chondrons: form, function and failure. The Journal of Anatomy. 1997;191:1-3.
[24]. Williams JL, Do PD, Eick JD, Schmidt TL. Erratum to "Tensile properties of the physis vary with anatomic location, thickness, strain rate and age" [Journal of Orthopaedic Research 2001;1043-1048]. Journal of Orthopaedic Research. 2002;4:894.
[25]. Morgan JD. Blood supply of growing rabbit's tibia. J Bone Joint Surg, B. 1959;41:185-203.
[26]. Irving MH. The blood supply of the growth cartilage in young rats. Journal of anatomy. 1964;98:631-639.
[27]. Von Pfeil D.J.F., DeCamp CE. The epiphyseal plate: physiology, anatomy, and trauma. Compend. Contin. Educ. Vet. 2009;31:E1-11.
[28]. Harris W.R., Martin R, Tile M. Transplantation of epiphyseal plates: an experimental study. The journal of bone and joint surgery. 1965;47:897-914.
[29]. Dodds GS. Row formation and other types of arrangement of cartilage cells in endochondral ossification. The Anatomical Record. 1930;46:385-399.
[30]. Morales TI. Chondrocyte moves: clever strategies? Osteoarthritis and Cartilage. 2007 Aug 1;15(8):861-871.
[31]. Kember NF. Comparative patterns of cell division in epiphyseal cartilage plates in the rabbit. Journal of anatomy. 1985;142:185-190.
[32]. Kember NF. Cell division in endochondral ossification: a study of cell proliferation in rat bones by the method of tritiated thymidine autoradiography. The Journal of bone and joint surgery. 1960;42:824-839.
[33]. Hunziker EB, Schenk RK, Cruz-Orive LM. Quantitation of chondrocyte performance in growth-plate cartilage during longitudinal bone growth. Journal of bone and joint surgery. 1987;69:162-173.
[34]. Howlett CR. The fine structure of the proximal growth plate of the avian tibia. Journal of anatomy. 1979;128:377-399.
[35]. Hunziker EB, Schenk RK. Physiological mechanisms adopted by chondrocytes in regulating longitudinal bone growth in rats. The Journal of physiology. 1989;414:55-71.
[36]. Emons J, Chagin AS, Sävendahl L, Karperien M, Wit JM. Mechanisms of growth plate maturation and epiphyseal fusion. Hormone research in paediatrics. 2011;75:383-391.
[37]. Duesterdieck-Zellmer K, Semevolos S, Kinsley M, Riddick T. Age-related differential gene and protein expression in postnatal cartilage canal and osteochondral junction chondrocytes. Gene Expression Patterns. 2015;17:1-10.

[38]. Ballock RT, O'Keefe RJ. The biology of the growth plate. The Journal of bone and joint surgery. 2003;85:715-726.

[39]. Shapiro IM, Adams CS, Freeman T, Srinivas V. Fate of the hypertrophic chondrocyte: microenvironmental perspectives on apoptosis and survival in the epiphyseal growth plate. Birth Defects Research Part C: Embryo Today: Reviews. 2005;75:330-339.

[40]. Farnum CE, Wilsman NJ. Morphologic stages of the terminal hypertrophic chondrocyte of growth plate cartilage. The Anatomical Record. 1987;219:221-232.

[41]. Park J, Gebhardt M, Golovchenko S, Perez-Branguli F, Hattori T, Hartmann C, *et al*. Dual pathways to endochondral osteoblasts: a novel chondrocyte-derived osteoprogenitor cell identified in hypertrophic cartilage. Biology open. 2015;4:608-621.

[42]. Klein-Nulend J, Veldhuijzen JP, Burger EH. Increased calcification of growth plate cartilage as a result of compressive force in vitro. Arthritis & Rheumatism: Official Journal of the American College of Rheumatology. 1986;29:1002-1009.

[43]. Alini M, Matsui Y, Dodge GR, Poole AR. The extracellular matrix of cartilage in the growth plate before and during calcification: changes in composition and degradation of type II collagen. Calcified tissue International. 1992;50:327-335

[44]. Zheng Q, Zhou G, Morello R, Chen Y, Garcia-Rojas X, Lee B. Type X collagen gene regulation by Runx2 contributes directly to its hypertrophic chondrocyte–specific expression in vivo. The Journal of cell biology. 2003;162:833-842.

[45]. Lerner AL, Kuhn JL. Characterization of regional and age-related variations in the growth of the rabbit distal femur. Journal of orthopaedic research. 1997;15:353-361.

[46]. Lerner AL, Kuhn JL, Hollister SJ. Are regional variations in bone growth related to mechanical stress and strain parameters? Journal of biomechanics. 1998;31:327-335.

[47]. Gao J, Williams JL, Roan E. On the state of stress in the growth plate under physiologic compressive loading. Open Journal of Biophysics. 2014;4:13-21.

[48]. Morris WZ, Li RT, Liu RW, Salata MJ, Voos JE. Origin of cam morphology in femoroacetabular impingement. The American journal of sports medicine. 2018;46:478-486.

[49]. Broom ND, Poole CA. A functional-morphological study of the tidemark region of articular cartilage maintained in a non-viable physiological condition. Journal of anatomy. 1982;135:65-82.

[50]. Speer DP. Collagenous architecture of the growth plate and perichondrial ossification groove. The Journal of bone and joint surgery. 1982;64:399-407.

[51]. Speer DP, Dahners L. The collagenous architecture of articular cartilage. Correlation of scanning electron microscopy and polarized light microscopy observations. Clinical orthopaedics and related research. 1979;139:267-275.

[52]. Dallek M, Jungbluth KH, Holstein AF. Studies on the arrangement of the collagenous fibers in infant epiphyseal plates using polarized light and the scanning electron microscope. Archives of orthopaedic and traumatic surgery. 1983;101:239-245.

[53]. Zambrano NZ, Montes GS, Shigihara KM, Sanchez EM, Junqueira LC. Collagen arrangement in cartilages. Cells Tissues Organs. 1982;113:26-38.
[54]. Lyons TJ, McClure SF, Stoddart RW, McClure J. The normal human chondro-osseous junctional region: evidence for contact of uncalcified cartilage with subchondral bone and marrow spaces. BMC musculoskeletal disorders. 2006;7:1-8.
[55]. Lyons TJ, Stoddart RW, McClure SF, McClure J. The tidemark of the chondro-osseous junction of the normal human knee joint. Journal of molecular histology. 2005;36:207-215.
[56]. Madry H, van Dijk CN, Mueller-Gerbl M. The basic science of the subchondral bone. Knee surgery, sports traumatology, arthroscopy. 2010;18:419-433.
[57]. McFadyen I, Field J, McCann P, Ward J, Nicol S, Curwen C. Should unstable extra-articular distal radial fractures be treated with fixed-angle volar-locked plates or percutaneous Kirschner wires? A prospective randomised controlled trial. Injury. 2011;42:162-166.
[58]. Anderson DD, Brown TD, Radin EL. The influence of basal cartilage calcification on dynamic juxtaarticular stress transmission. Clinical orthopaedics and related research. 1993;286:298-307.
[59]. Thambyah A, Broom N. On new bone formation in the pre-osteoarthritic joint. Osteoarthritis and cartilage. 2009;17:456-463.
[60]. Hwang J, Kyubwa EM, Bae WC, Bugbee WD, Masuda K, Sah RL. In vitro calcification of immature bovine articular cartilage: formation of a functional zone of calcified cartilage. Cartilage. 2010;1:287-297.
[61]. Fawns HT, Landells JW. Histochemical Studies of Rheumatic Conditions: I. Observations on the Fine Structures of the Matrix of Normal Bone and Cartilage. Annals of the rheumatic diseases. 1953;12:105.
[62]. Thambyah A, Broom N. On how degeneration influences load-bearing in the cartilage–bone system: a microstructural and micromechanical study. Osteoarthritis and cartilage. 2007;15:1410-1423.
[63]. Redler IR, Mow VC, Zimny ML, Mansell JO. The ultrastructure and biomechanical significance of the tidemark of articular cartilage. Clinical orthopaedics and related research. 1975;112:357-362.
[64]. Mansfield JC, Peter Winlove C. A multi-modal multiphoton investigation of microstructure in the deep zone and calcified cartilage. Journal of anatomy. 2012;220:405-416.
[65]. Lane LB, Bullough PG. Age-related changes in the thickness of the calcified zone and the number of tidemarks in adult human articular cartilage. The Journal of bone and joint surgery. 1980;62:372-375.
[66]. Bonde HV, Talman ML, Kofoed H. The area of the tidemark in osteoarthritis–a three-dimensional stereological study in 21 patients. Apmis. 2005;113:349-352.
[67]. Hoemann CD, Lafantaisie CH, Lascau V, Chen G, Guzmán J. The cartilage-bone interface. The journal of knee surgery. 2012;25:85-98.
[68]. Clark JM. The structure of vascular channels in the subchondral plate. Journal of anatomy. 1990;171:105-115.
[69]. Broom ND, Thambyah A. The soft-hard tissue junction: structure, mechanics and function. United Kingdom. Pa; Cambridge University Press. 2018.
[70]. Wang F, Ying Z, Duan X, Tan H, Yang B, Guo L, Chen G, Dai G, Ma Z, Yang L. Histomorphometric analysis of adult articular calcified cartilage zone. Journal of structural biology. 2009;168:359-365.

[71]. Duncan HO, Jundt J, Riddle JM, Pitchford W, Christopherson T. The tibial subchondral plate. A scanning electron microscopic study. The Journal of bone and joint surgery. 1987;69:1212-1220.
[72]. Clark JM, Huber JD. The structure of the human subchondral plate. The Journal of bone and joint surgery. 1990;72:866-873.
[73]. Mila S, Putz R. Quantitative morphology of the subchondral plate of the tibial plateau. Journal of anatomy. 1994;185:103-110.
[74]. Findlay DM, Kuliwaba JS. Bone–cartilage crosstalk: a conversation for understanding osteoarthritis. Bone research. 2016;4:1-12.
[75]. Amin AK, Huntley JS, Simpson AH, Hall AC. Chondrocyte survival in articular cartilage: the influence of subchondral bone in a bovine model. The Journal of bone and joint surgery. 2009;91:691-699.
[76]. Delgado MJ, Fernández AT, Canillas F, Quintana B, del Riego SS, Delgado E, *et al*. Does the epiphyseal cartilage of the long bones have one or two ossification fronts? Medical hypotheses. 2013;81:695-700.
[77]. Bradley DA, Moger CJ, Winlove CP. Zn deposition at the bone–cartilage interface in equine articular cartilage. Nuclear Instruments and Methods in Physics Research Section A: Accelerators, Spectrometers, Detectors and Associated Equipment. 2007;580:473-476.
[78]. Haines RW. The histology of epiphyseal union in mammals. Journal of anatomy. 1975;120:1-25.
[79]. Parfitt AM. Misconceptions (1): epiphyseal fusion causes cessation of growth. Bone. 2002;30:337-339.
[80]. Dawson AB. The age order of epiphyseal union in the long bones of the albino rat. The Anatomical Record. 1925;31:1-7.
[81]. Bokariya P, Chowdhary DS, Tirpude BH, Kothari R, Waghmare JE, Tarnekar A. A review of the chronology of epiphyseal union in the bones at knee and ankle joint. Journal of Indian Academy of Forensic Medicine. 2011;33:258-260.
[82]. Weise M, De-Levi S, Barnes KM, Gafni RI, Abad V, Baron J. Effects of estrogen on growth plate senescence and epiphyseal fusion. Proceedings of the National Academy of Sciences. 2001;98:6871-6876.
[83]. Juul A. The effects of oestrogens on linear bone growth. Human Reproduction Update, 2001;7:303-313.
[84]. Miao D, Scutt A. Histochemical localization of alkaline phosphatase activity in decalcified bone and cartilage. Journal of Histochemistry & Cytochemistry. 2002;50:333-340.
[85]. Kaviani R, Londono I, Parent S, Moldovan F, Villemure I. Changes in growth plate extracellular matrix composition and biomechanics following in vitro static versus dynamic mechanical modulation. Journal of musculoskeletal & neuronal interactions. 2018;18:81-91.
[86]. Buddhachat K, Klinhom S, Siengdee P, Brown JL, Nomsiri R, Kaewmong P, *et al*. Elemental analysis of bone, teeth, horn and antler in different animal species using non-invasive handheld X-ray fluorescence. PloS one. 2016;11:1-21.
[87]. Bradley DA, Farquharson MJ, Gundogdu O, Al-Ebraheem A, Ismail EC, Kaabar W, *et al*. Applications of condensed matter understanding to medical tissues and disease progression: Elemental analysis and structural integrity of tissue scaffolds. Radiation Physics and Chemistry. 2010;79:162-175.

[88]. Zoeger N, Streli C, Wobrauschek P, Jokubonis C, Pepponi G, Roschger P, *et al*. Determination of the elemental distribution in human joint bones by SR micro XRF. X-Ray Spectrometry: An International Journal. 2008;37:3-11.
[89]. Zöger N, Roschger P, Hofstaetter JG, Jokubonis C, Pepponi G, Falkenberg G, *et al*. Lead accumulation in tidemark of articular cartilage. Osteoarthritis and cartilage. 2006;14:906-913.
[90]. Ayodele BA, Mirams M, Pagel CN, Mackie EJ. The vacuolar H^+ ATPase V0 subunit D2 is associated with chondrocyte hypertrophy and supports chondrocyte differentiation. Bone reports. 2017;7:98-107.
[91]. Carter DR, Wong M. The role of mechanical loading histories in the development of diarthrodial joints. Journal of Orthopaedic Research. 1988;6:804-816.
[92]. Gangadhar R, Jaleeli KA, Ahmad A. Energy dispersive x-ray analysis of ovine scapular cartilage. International Journal of Science, Environment and Technology. 2015;4:1195-1198.
[93]. Kaabar W, Daar E, Bunk O, Farquharson MJ, Laklouk A, Bailey M, *et al*. Elemental and structural studies at the bone–cartilage interface. Nuclear Instruments and Methods in Physics Research Section A: Accelerators, Spectrometers, Detectors and Associated Equipment. 2011;652:786-790.
[94]. Kaabar W, Gundogdu O, Laklouk A, Bunk O, Pfeiffer F, Farquharson MJ, *et al*. μ-PIXE and SAXS studies at the bone–cartilage interface. Applied Radiation and Isotopes. 2010;68:730-734.
[95]. Kaabar W, Daar E, Gundogdu O, Jenneson PM, Farquharson MJ, Webb M, *et al*. Metal deposition at the bone–cartilage interface in articular cartilage. Applied Radiation and Isotopes. 2009;67:475-479.
[96]. Gomez S, Rizzo R, Pozzi-Mucelli M, Bonucci E, Vittur F. Zinc mapping in bone tissues by histochemistry and synchrotron radiation–induced x-ray emission: correlation with the distribution of alkaline phosphatase. Bone. 1999;25:33-38.
[97]. Nishi Y. Zinc and growth. Journal of the American College of Nutrition. 1996;15:340-344.
[98]. Kim JH, Jeon J, Shin M, Won Y, Lee M, Kwak JS, *et al*. Regulation of the catabolic cascade in osteoarthritis by the zinc-ZIP8-MTF1 axis. Cell. 2014;156(4):730-43.
[99]. Boyde A, Shapiro IM. Energy dispersive X-ray elemental analysis of isolated epiphyseal growth plate chondrocyte fragments. Histochemistry. 1980;69:85-94.
[100]. Shapiro IM, Boyde A. Microdissection-elemental analysis of the mineralizing growth cartilage of the normal and rachitic chick. Metabolic Bone Disease and Related Research. 1984;5:317-326.
[101]. Takata K, Yamamoto K, Ohmori S, Watanabe T. Scanning Electron Microscopic Study and Elemental Analysis of the Epiphyseal Growth Plate in Normal Puppies. Orthopedics & Traumatology. 1974;23:44-47.
[102]. Howell DS, Delchamps E, Riemer W, Kiem I. A profile of electrolytes in the cartilaginous plate of growing ribs. The Journal of clinical investigation. 1960;39:919-929.
[103]. Howell DS, Carlson L. Alterations in the composition of growth cartilage septa during calcification studied by microscopic x-ray elemental analysis. Experimental cell research. 1968;51:185-195.
[104]. Reinert T, Reibetanz U, Schwertner M, Vogt J, Butz T, Sakellariou A. The architecture of cartilage: Elemental maps and scanning transmission ion microscopy/tomography. Nuclear Instruments and Methods in Physics Research Section B: Beam Interactions with Materials and Atoms. 2002;188:1-8.

[105]. Vittur F, Tuniz C, Psoletti S, Rizzo R, Jones KW. Elemental analysis of growth plate cartilage by synchrotron-radiation-induced X-ray emission (SRIXE). Biochemical and biophysical research communications. 1992;188:1010-1017.

[106]. Hargest TE, Gay CV, Schraer HA, Wasserman AJ. Vertical distribution of elements in cells and matrix of epiphyseal growth plate cartilage determined by quantitative electron probe analysis. Journal of Histochemistry & Cytochemistry. 1985;33:275-286.

[107]. Hwang J, Bae WC, Shieu W, Lewis CW, Bugbee WD, Sah RL. Increased hydraulic conductance of human articular cartilage and subchondral bone plate with progression of osteoarthritis. Arthritis & Rheumatism: Official Journal of the American College of Rheumatology. 2008;58:3831-3842.

[108]. Arkill KP, Winlove CP. Solute transport in the deep and calcified zones of articular cartilage. Journal of osteoarthritis and cartilage. 2008;16:708-14.

[109]. Federico S, Herzog W. On the anisotropy and inhomogeneity of permeability in articular cartilage. Biomechanics and modeling in mechanobiology. 2008;7:367-378.

[110]. Higginson GR, Litchfield MR, Snaith J. Load-displacement-time characteristics of articular cartilage. International Journal of Mechanical Sciences. 1976;18:481-486.

[111]. Oloyede A, Broom ND. The generalized consolidation of articular cartilage: an investigation of its near-physiological response to static load. Journal of connective tissue research. 1994;31:75-86.

[112]. Quinn TM, Dierickx P, Grodzinsky AJ. Glycosaminoglycan network geometry may contribute to anisotropic hydraulic permeability in cartilage under compression. Journal of biomechanics. 2001;34:1483-1490.

[113]. Reynaud B, Quinn TM. Anisotropic hydraulic permeability in compressed articular cartilage. Journal of biomechanics. 2006;39:131-137.

[114]. Federico S, Herzog W. On the anisotropy and inhomogeneity of permeability in articular cartilage. Biomechanics and modeling in mechanobiology. 2008;7:367-378.

[115]. Pouran B, Arbabi V, Bleys RL, van Weeren PR, Zadpoor AA, Weinans H. Solute transport at the interface of cartilage and subchondral bone plate: effect of micro-architecture. Journal of biomechanics. 2017;52:148-154.

[116]. Pouran B. Multi-scale physico-chemical phenomena in articular cartilage and subchondral bone. Netherland. Utrecht University. 2017.

[117]. Oegema TR, Carpenter RJ, Hofmeister F, Thompson RC. The interaction of the zone of calcified cartilage and subchondral bone in osteoarthritis. Microscopy research and technique. 1997;37:324-332.

[118]. Lane LB, Villacin AQ, Bullough PG. The vascularity and remodelling of subchondrial bone and calcified cartilage in adult human femoral and humeral heads. An age-and stress-related phenomenon. The Journal of bone and joint surgery. 1977;59:272-278.

[119]. Pan J, Wang B, Li W, Zhou X, Scherr T, Yang Y, *et al.* Elevated cross-talk between subchondral bone and cartilage in osteoarthritic joints. Bone. 2012;51:212-7.

[120]. Botter SM, Van GJ, Clockaerts S, Waarsing JH, Weinans H, van Leeuwen JP. Osteoarthritis induction leads to early and temporal subchondral plate porosity in the tibial plateau of mice: an in vivo microfocal computed tomography study. Arthritis & Rheumatism. 2011;63:2690-2699.

[121]. Pan J, Zhou X, Li W, Novotny JE, Doty SB, Wang L. In situ measurement of transport between subchondral bone and articular cartilage. Journal of Orthopaedic Research. 2009;27:1347-1352.
[122]. Bashir A, Gray ML, Boutin RD, Burstein D. Glycosaminoglycan in articular cartilage: in vivo assessment with delayed Gd $(DTPA)^{2-}$ enhanced MR imaging. Radiology. 1997;205:551-558.
[123]. Pouran B, Arbabi V, Zadpoor AA, Weinans H. Isolated effects of external bath osmolality, solute concentration, and electrical charge on solute transport across articular cartilage. Medical engineering & physics. 2016;38:1399-1407.
[124]. Leddy HA, Guilak F. Site-specific molecular diffusion in articular cartilage measured using fluorescence recovery after photobleaching. Annals of biomedical engineering. 2003;31:753-760.
[125]. Kokkonen HT, Mäkelä J, Kulmala KA, Rieppo L, Jurvelin JS, Tiitu V, *et al*. Computed tomography detects changes in contrast agent diffusion after collagen cross-linking typical to natural aging of articular cartilage. Osteoarthritis and cartilage. 2011;19:1190-1198.
[126]. Stender ME, Regueiro RA, Ferguson VL. A poroelastic finite element model of the bone–cartilage unit to determine the effects of changes in permeability with osteoarthritis. Computer methods in biomechanics and biomedical engineering. 2017;20:319-331.
[127]. Herzog W, Diet S, Suter E, Mayzus P, Leonard TR, Müller C, Wu JZ, Epstein M. Material and functional properties of articular cartilage and patellofemoral contact mechanics in an experimental model of osteoarthritis. Journal of Biomechanics. 1998;31:1137-1145.
[128]. Knecht S, Vanwanseele B, Stüssi E. A review on the mechanical quality of articular cartilage–Implications for the diagnosis of osteoarthritis. Clinical biomechanics. 2006;21:999-1012.
[129]. Finnilä MA, Thevenot J, Aho OM, Tiitu V, Rautiainen J, Kauppinen S, *et al*. Association between subchondral bone structure and osteoarthritis histopathological grade. Journal of orthopaedic research. 2017;35:785-792.
[130]. Yuan XL, Meng HY, Wang YC, Peng J, Guo QY, Wang AY, *et al*. Bone–cartilage interface crosstalk in osteoarthritis: potential pathways and future therapeutic strategies. Osteoarthritis and cartilage. 2014;22:1077-1089.
[131]. Wu JZ, Herzog W, Epstein M. Joint contact mechanics in the early stages of osteoarthritis. Medical engineering & physics. 2000;22:1-12.
[132]. Findlay DM, Kuliwaba JS. Bone–cartilage crosstalk: a conversation for understanding osteoarthritis. Bone research. 2016;4:1-2.
[133]. Burr DB. The importance of subchondral bone in osteoarthrosis. Current opinion in rheumatology. 1998;10:256-262.
[134]. Nielsen AW, Klose-Jensen R, Hartlev LB, Boel LW, Thomsen JS, Keller KK, *et al*. Age-related histological changes in calcified cartilage and subchondral bone in femoral heads from healthy humans. Bone. 2019;129:115037.
[135]. Cohen B, Chorney GS, Phillips DP, Dick HM, Mow VC. Compressive stress-relaxation behavior of bovine growth plate may be described by the nonlinear biphasic theory. Journal of orthopaedic research. 1994;12:804-813.
[136]. Song Y, Lee D, Shin CS, Carter DR, Giori NJ. Physeal cartilage exhibits rapid consolidation and recovery in intact knees that are physiologically loaded. Journal of biomechanics. 2013;46:1516-1523.

[137]. Villemure I, Stokes IA. Growth plate mechanics and mechanobiology. A survey of present understanding. Journal of biomechanics. 2009;42:1793-1803.
[138]. Albro MB, Banerjee RE, Li R, Oungoulian SR, Chen B, Del Palomar AP, Hung CT, Ateshian GA. Dynamic loading of immature epiphyseal cartilage pumps nutrients out of vascular canals. Journal of biomechanics. 2011;44:1654-1659.
[139]. Gao J, Roan E, Williams JL. Regional variations in growth plate chondrocyte deformation as predicted by three-dimensional multi-scale simulations. PloS one. 2015;10:e0124862.
[140]. Gao J, Williams JL, Roan E. Multiscale modeling of growth plate cartilage mechanobiology. Biomechanics and modeling in mechanobiology. 2017;16:667-679.
[141]. Vendra BB, Roan E, Williams JL. Chondron curvature mapping in growth plate cartilage under compressive loading. Journal of the mechanical behavior of biomedical materials. 2018;84:168-177.
[142]. Kaviani R, Londono I, Parent S, Moldovan F, Villemure I. Growth plate cartilage shows different strain patterns in response to static versus dynamic mechanical modulation. Biomechanics and modeling in mechanobiology. 2016;15:933-946.
[143]. Shefelbine SJ, Carter DR. Mechanobiological predictions of growth front morphology in developmental hip dysplasia. Journal of Orthopaedic Research. 2004;22:346-352.
[144]. M. Kazemi and J. Williams, Chondrocyte and pericellular matrix deformation and strain in the growth plate cartilage reserve zone under compressive loading. Springer. In Press 2020.
[145]. Seidi A, Ramalingam M, Elloumi-Hannachi I, Ostrovidov S, Khademhosseini A. Gradient biomaterials for soft-to-hard interface tissue engineering. Acta biomaterialia. 2011;7:1441-1451.
[146]. Malekipour F, Whitton C, Oetomo D, Lee PV. Shock absorbing ability of articular cartilage and subchondral bone under impact compression. Journal of the mechanical behavior of biomedical materials. 2013;26:127-135.
[147]. Williams JL, Vani JN, Eick JD, Petersen EC, Schmidt TL. Shear strength of the physis varies with anatomic location and is a function of modulus, inclination, and thickness. Journal of orthopaedic research. 1999;17:214-222.
[148]. Cohen B, Chorney GS, Phillips DP, Dick HM, Buckwalter JA, Ratcliffe A, Mow VC. The microstructural tensile properties and biochemical composition of the bovine distal femoral growth plate. Journal of Orthopaedic Research. 1992;10:263-275.
[149]. Moen CT, Pelker RR. Biomechanical and histological correlations in growth plate failure. Journal of pediatric orthopedics. 1984;4:180-184.
[150]. Mente PL, Lewis JL. Elastic modulus of calcified cartilage is an order of magnitude less than that of subchondral bone. Journal of Orthopaedic Research. 1994;12:637-647.
[151]. Doube M, Firth EC, Boyde A, Bushby AJ. Combined nanoindentation testing and scanning electron microscopy of bone and articular calcified cartilage in an equine fracture predilection site. European Cells and Materials. 2010;19:242-251.
[152]. Ferguson VL, Bushby AJ, Boyde A. Nanomechanical properties and mineral concentration in articular calcified cartilage and subchondral bone. Journal of Anatomy. 2003;203:191-202.

[153]. Campbell SE, Ferguson VL, Hurley DC. Nanomechanical mapping of the osteochondral interface with contact resonance force microscopy and nanoindentation. Acta biomaterialia. 2012;8:4389-4396.
[154]. Gupta HS, Schratter S, Tesch W, Roschger P, Berzlanovich A, Schoeberl T, *et al*. Two different correlations between nanoindentation modulus and mineral content in the bone–cartilage interface. Journal of structural biology. 2005;149:138-148.
[155]. Bushby AJ, Ferguson VL, Boyde A. Nanoindentation of bone: Comparison of specimens tested in liquid and embedded in polymethylmethacrylate. Journal of Materials Research. 2004;19:249-259.
[156]. Hamann N, Zaucke F, Dayakli M, Brüggemann GP, Niehoff A. Growth-related structural, biochemical, and mechanical properties of the functional bone–cartilage unit. Journal of anatomy. 2013;222:248-259.
[157]. Ren P, Niu H, Gong H, Zhang R, Fan Y. Morphological, biochemical and mechanical properties of articular cartilage and subchondral bone in rat tibial plateau are age related. Journal of anatomy. 2018;232:457-471.
[158]. Radhakrishnan P, Lewis NT, Mao JJ. Zone-specific micromechanical properties of the extracellular matrices of growth plate cartilage. Annals of biomedical engineering. 2004;32:284-291.
[159]. Kaviani R, Londono I, Parent S, Moldovan F, Villemure I. Compressive mechanical modulation alters the viability of growth plate chondrocytes in vitro. Journal of Orthopaedic Research. 2015;33:1587-1593.
[160]. Congdon KA, Hammond AS, Ravosa MJ. Differential limb loading in miniature pigs: a test of chondral modeling theory. Journal of Experimental Biology. 2012;215:1472-1483.
[161]. Allen DM, Mao JJ. Heterogeneous nanostructural and nanoelastic properties of pericellular and interterritorial matrices of chondrocytes by atomic force microscopy. Journal of structural biology. 2004;145:196-204.
[162]. Sergerie K, Lacoursière MO, Lévesque M, Villemure I. Mechanical properties of the porcine growth plate and its three zones from unconfined compression tests. Journal of biomechanics. 2009;42:510-516.
[163]. Cohen B, Lai WM, Mow VC. A transversely isotropic biphasic model for unconfined compression of growth plate and chondroepiphysis. Journal of biomechanical engineering. 1998;120:491-496.
[164]. Fujii T, Takai S, Arai Y, Kim W, Amiel D, Hirasawa Y. Microstructural properties of the distal growth plate of the rabbit radius and ulna: biomechanical, biochemical, and morphological studies. Journal of orthopaedic research. 2000;18:87-93.
[165]. Kazemi M., Williams JL. Elemental and histological study of the growth plate reserve zone-subchondral bone interface. Orthopaedic Research Society Annual Meeting (ORS), 2018.

Chapter 3

On the role of the reserve zone and mechano-regulatory stimuli in the development and maturation of the growth plate: Observations and models.

3.1 Introduction

The development and growth of much of the vertebrate skeleton, and especially the long bones, proceeds via endochondral bone formation, the process by which a cartilage precursor is gradually replaced by bone. In brief, a rudimentary cartilaginous model (anlage) of the future bone initially forms from primordial cells. The proliferating chondrocytes in the center of this anlage then differentiate and become hypertrophic after which their matrix is resorbed by invading hematopoetic and osteoblast precursor cells, forming trabecular bone and bone marrow to become the primary ossification center. This primary center expands by a complex process as the fetus grows. Somewhat later, secondary centers of ossification develop at one or both of the joint ends, which form the epiphyseal bone and articular cartilage layers. Growth cartilage gradually becomes entrapped between the expanding primary and secondary centers resulting in the formation of the epiphyseal growth plate. This layer of growth plate cartilage subsequently develops a lamellar bone plate on the epiphyseal side between the trabecular bone of the epiphysis and the growth plate reserve zone, while the metaphyseal interface continues to produce and calcify cartilage in preparation for replacement by trabecular bone. As growth continues, the shape of the epi- and meta-physeal interfaces with the growth cartilage begin to evolve three-dimensional convex or concave surfaces which in large animals become increasingly more convoluted as growth continues. These interdigitations, termed mammillary processes, have been observed at various scales, as primary, secondary and tertiary mammillary processes (Cohen et al,1992; Williams et al, 1999). The mammillary processes provide an interlocking joint consisting of hills and valleys that continues to evolve during

skeletal maturity. Such undulations also help orient the growth plate perpendicularly to directions of local principal compressive stresses to reduce tensile and shear stresses across the interfaces and provide biomechanical stability to the joint (Gao et al, 2014; Smith, 1962). It is conceivable that deficiencies in the development of the subchondral bone plate and mammillary processes may result in weakening of the interface and could contribute to conditions such as slipped capital femoral epiphysis (SCFE). SCFE is characterized by a non-traumatic displacement of the femoral metaphysis with respect to the capital femoral epiphysis through failure of the physis and is believed to have a multifactorial etiology involving biomechanical, biochemical and endocrine and developmental factors (Barrios et al., 2005; Hosseinzadeh et al. 2020; Liu et al. 2013; Loder, 1998; Manoff et al., 2005).

Although the mechanism by which the growth plate subchondral bone plate and mammillary processes develop is not known, it has been noted that the undulating pattern of newly formed bone on the metaphyseal side is matched by that of the epiphyseal subchondral bone (SB) plate at the growth plate reserve zone (RZ) border (Gao et al, 2014; Lerner and Kuhn, 1997; Lerner et al., 1998). This suggests that modeling and remodeling of the SB plate continues throughout development as axial skeletal growth proceeds at the metaphyseal border. While little is known about the interface between the reserve zone and SB, histologically it resembles the osteochondral interface between articular cartilage and SB (Kazemi and Williams, 2018). Articular SB has a functionally graded interlayer through which collagen fibers traverse from the deep zone of cartilage into a calcified cartilage layer (Speer and Dahners, 1979); the calcified cartilage consists of a series of undulating and interdigitating tidemarks that provide a mechanical interlock between the uncalcified cartilage and added layers of calcified cartilage (Broom and Poole, 1982; Speer, 1982). Articular SB has a chemical transition zone providing a gradient in elements associated with mineralization that may help provide a buffer zone to transmit stresses across this bi-material interface. We hypothesized that a similar mechanism might exist at the osteochondral interface between the epiphyseal subchondral bone and the growth cartilage RZ.

It is known that besides biological factors the dynamic mechanical environment also provides signals to chondrocytes that are necessary for normal development and growth. The observations of

Hueter and Volkmann (Hueter, 1863; Volkmann, 1862) that increasing and decreasing physiological levels compression across the growth plate can modulate the growth process, have led to various mechano-regulatory concepts and growth theories to explain more quantitatively how the mechanical environment may stimulate or inhibit cartilage and bone growth (Carter and Wong, 1988; Frost, 1990; Hueter, 1863; Pauwels, 1960; Volkmann, 1862). The effect of intermittently applied loading on tissue differentiation has been explained by a combination of two scalar components of the stress tensor, the octahedral shear (deviatoric stress) and hydrostatic stress (volumetric or dilatational stress). Hydrostatic compressive stress is believed to promote the formation of cartilage while octahedral shear stress provides a driving force for bone formation (Carter and Beaupré, 2007; Claes and Heigele, 1999). Chondrocytes play a central role in the process of endochondral ossification. Their behavior is regulated by circulating hormones, local growth factors and components of the extracellular matrix. A recent multiscale model (Gao et al, 2017) has shown that the stresses and strains in chondrocytes in the proliferative and hypertrophic zones are consistent with the tissue level stresses and strains in fracture healing (Claes and Heigele, 1999) in terms of these mechanobiology theories of bone growth. However, the role of the reserve zone (RZ) in all of this has largely been overlooked until recently. An emerging model of endochondral bone growth postulates that the RZ plays an important role in the development and growth of endochondral bones and contains a niche of skeletal stem cells. In one of the proposed schemes these RZ cells become self-renewing when stimulated by conditions in the local environment (Lui, 2020).

In the present study we examined the microstructural and chemical properties across the epiphyseal bone-cartilage interface at three stages of mammillary processes development to determine if a transition zone of graded properties and a layer of mineralized cartilage with tidemarks also exists in the SB of the growth plate. We employed histology and energy dispersive x-ray spectroscopy (EDX) to analyze proximal femoral growth plate samples of domestic pigs in three age groups. EDX, a qualitative and quantitative microanalytical technique used for the identification of the elemental composition of a specimen (d'Alfonso et al., 2010; Wollman et al. 1997), has been used to investigate the elemental characteristics of the different growth plate zones (Boyde and Shapiro, 1984 ; Gangadhar et al., 2015;

Shapiro and Boyde, 1984; Takata at al., 1974), but it has not been applied to the interface at the epiphyseal-reserve zone border. We also developed a series of multiscale finite element models of growth plate cartilage to relate the mechano-regulatory concepts at the tissue and cell level in the reserve zone with the histology and EDX observations. We addressed two questions: 1) whether our histological and elemental observations at the SB interface support the hypothesis of a secondary but slower bone growth front that shapes the mammillary processes at the epiphyseal interface, and 2) whether the mechanical milieu of chondrocytes within the reserve zone is consistent with the observations of a secondary growth front in the light of prevailing quantitative mechanobiological concepts and the discovery of a niche of chondroprogenitor stem cells that can differentiate into multiple cell types including osteoblasts.

3.2 Materials and method

3.2.1 Sample preparation

Femurs were collected post-mortem from 20-, 35- and 480-day-old mixed-breed pigs (5 female and 1 male) after the completion of another study approved by the University of Memphis institutional animal care and use committee. Table 3.1 shows the gender and weight (kg) of the subjects in each age group. Pigs in the 20 and 480-day-old group were not subjected to any prior experimental treatment. Pigs in the 35-day-old group were used in a prior study to examine the short-term effects of methotrexate (MTX) chemotherapy on the kidneys. MTX was injected at two time points: 14 days (4 g/kg) and 4 days (2g/kg) before sacrifice. Although MTX chemotherapy at a high dose may cause bone growth defects in growing bones, these side effects are dosage- and duration-dependent (Cavalcanti et al., 2014; Fan et al., 2009; Van et al., 2003; Xian et al., 2007) and we did not observe any obvious adverse effects of this treatment on the development of the growth plate in this study. All samples were sectioned along the plane bisecting the femoral neck and shaft using a low-speed bone saw (IsoMet 1000).

Table 3.1. Subject details for each age group.

Age group	subject number	sex	limb	Weight (kg)
20 days old	1	Female	Right hindlimb	3.158
	2	Male	Right hind limb	2.598
35days old	1	Female	Right hindlimb	5.760
	2	Female	Right hindlimb	5.400
	3	Female	Left hindlimb	4.971
480 days old	1	Female	Left hindlimb	204.1

3.2.2 Histology studies

Formalin-fixed tissues were decalcified in formic acid for 7 days, embedded in paraffin, cut into 6-µm thick slices using a microtome, and stained with hematoxylin and eosin (H&E) and with Masson's Trichrome. The microstructures of the cartilage-bone interface were examined by stereo- (Olympus SZX16, Japan), bright-field- (Nikon DXM1200F, Japan), differential interference contrast (DIC) optical- (Olympus DP80, Japan) and fluorescence- microscopies. Bright-field and dark-field images were obtained at each magnification and at each image session to remove background noise (ImageJ, V1.50i, NIH) (Schneider et al., 2012). Two-dimensional cell areas near the reserve zone-epiphysis/subchondral bone (RZ-EP/SB) interface were measured using ImageJ. Higher magnification (40x) images from the interface were acquired for this purpose. The chondrocytes chosen to compute cell areas were selected from the H&E image among those which had stronger basophilic staining nuclei (dark purple).

3.2.3 Scanning Electron microscopy and EDX

All samples were prepared following a standard protocol of tissue fixation in 2.5% glutaraldehyde in 0.1M Na/K Tousimis-Sorensen buffer, tissue dehydration in a graded series of increasing ethanol concentrations (33, 67, 85, 95, and 100% ethanol), critical point drying, and eventually sputter-coated with a 5-nm layer of Au/Pd. Chemical and elemental studies were conducted by EDX attached to the scanning electron microscopy (SEM, NOVA NANOSEM650, Japan). Elemental line scans and map scans were obtained at a low accelerating voltage of 15 kV, a working distance of 5 mm, a low beam current of 370 pA, a spot size of 3 and an image scan size of 2048 pixels. Lower values of accelerating voltage, probe current and scan time were used to limit any further surface damage of the cartilage tissue

(Lešer et al., 2010). The acquisition time was set to scan 500 points per line scan during data acquisition. Backscatter images (BE) and EDX line- and map-scans were acquired across the cartilage-bone interface to trace the major elements including Ca, P and C and characterize spatial changes in elemental composition. At least 5 scans were collected for each age group. To remove noise and minimize spectral artifacts from line profiles and also smoothen the line profiles, a Gaussian filter was employed using a signal analyzer (MATLAB R2019a).

3.2.4 Statistical analyses

The widths of the elemental transition zones between age groups were analyzed using one-way ANOVA followed by post-hoc two-tailed student t-tests. Variations in the morphological parameters of chondrocytes in the RZ-EP/SB interface were evaluated using the cumulative distribution function (CDF) for each age group. The normality of cell area distributions was checked with the Shapiro-Wilk test. Due to the non-normalized distribution of the data, the nonparametric Kolmogorov-Smirnov test (KS test) was applied to compare cell areas in the RZ-EP/SB interface with those within the reserve zone within each age group. Descriptive statistics for the cell areas were calculated by log transformation to normalize the data, followed by back transformation to obtain geometric means and 95% confidence intervals. The KS test was performed with the statistical significance reported at the 95% confidence level.

3.2.5 Finite element analysis

To determine how mechanical stimuli regulate ossification, we modeled the growth plate during early growth as the growth plate thickness (or width) decreased from 6 mm to 1 mm between the ages of 20 to 35 days. A series of multiscale axisymmetric large deformation models were developed with ABAQUS/CAE 2019. Details of the finite element model have been published elsewhere (Kazemi and Williams, 2019, Kazemi and Williams 2021). Isotropic linearly elastic material properties were assigned to all regions of the models: epiphyseal trabecular bone (EP), calcified cartilage at the RZ border (CC), RZ, proliferative/hypertrophic zone (PZ/HZ), and calcified cartilage beyond the border of the HZ (provisional calcification, PC) and metaphysis (MP), as well as the cells and PCM (Table 3.2). Each

region of macroscale model was meshed with four-node bilinear axisymmetric quadrilateral, hybrid, constant pressure (CAX4H) elements. We developed three microscale models of cells in three different locations of the RZ to study how macroscale loads are transferred to the RZ chondrocytes and their PCM to produce cell-level mechano-regulatory signals. All cells were enveloped in a thin shell of pericellular matrix (PCM). Cell 1 represented a hypertrophic chondrocyte at 20 days in age or a large cell associated with neocartilage tissue at 35 and 480 days, located 1 mm away from the RZ-EP border as observed in our histology study. Cell 2 was placed 20 μm away from Cell 1, along the axisymmetry axis, to represent the next closest chondrocyte to Cell 1. Cell 3 represented a chondrocyte located near the RZ-PZ/HZ border. Higher-order elements (CAX8H) were used to mesh the cells and PCMs, while CAX3H elements were employed for the rest of the geometry. The cylindrical growth plate model was free to expand radially while being compressed by 15% of the overall original growth plate cartilage (GP) width or thickness, along the long axis (Y) of the bone. A mesh convergence study for the microscale model was performed until further mesh refinement produced changes in the volume-average hydrostatic cell stress of 3%. Due to the assumption of a short time scale of loading, representing peak joint loading during gait, the effect of fluid flow was ignored. To explore the tissue and cell response with respect to mechano-regulatory concepts, the volume-averaged hydrostatic compressive stress was calculated, as described in more detail elsewhere (Kazemi and Williams, 2019). Similarly, the volume-averaged octahedral shear stress and maximum principal tensile strains (logarithmic strain LE) of each cell were evaluated. The cell-averaged hydrostatic stresses and maximum principal tensile strains were used to create a quantitative tissue differentiation phase diagram similar to those proposed at the tissue macroscale level for bone fracture healing (Claes and Heigele, 1999) and at the microscale cell level for the proliferative and hypertrophic zones of the growth plate (Gao et al. 2017).

Table 3.2. Material properties and dimensions of the growth plate components used in the multi-scale models.

Layer	E (MPa)	Poisson's ratio	Thickness (T) in mm Radius (R) in μm
Trabecular bone at both ends of the growth cartilage	400	0.3	T 6
Calcified cartilage at the RZ border	100 (Stevens et al., 1999)	0.3	T 0.4*
Calcified cartilage at the HZ border	50	0.3	T 0.8*
RZ	0.98 (Gao et al., 2015)	0.47 (Gao et al., 2015)	T 4, 3, 1, 0.5 $^{+}$
PZ/HZ	0.49 (Gao et al., 2015)	0.47 (Gao et al., 2015)	T 2, 1, 1, 0.5 $^{+}$
Hypertrophic cell within RZ-EP border (Cell 1)/ PCM	0.002 (Gao et al., 2015, 2017) /0.265 (Allen and Mao, 2004)	0.4999 ((Gao et al., 2015, 2017) /0.45 (Allen and Mao, 2004)	R 10*/15$^{\#}$
Cell within RZ (Cell 2)/ PCM	0.002 (Gao et al., 2015, 2017) /0.265 (Allen and Mao, 2004)	0.4999 (Gao et al., 2015, 2017) /0.45 (Allen and Mao, 2004)	R 5*/7.5$^{\#}$
Cell in RZ-PZ/HZ border (Cell 3)/ PCM	0.002 (Gao et al., 2015, 2017) /0.265 (Allen and Mao, 2004)	0.4999 (Gao et al., 2015, 2017)/0.45 (Allen and Mao, 2004)	R 5* /7.5$^{\#}$

* Based on the histology of a 20-day piglet femoral head. $^{+}$ Total GP thicknesses (RZ + PZ/HZ) are 6, 4, 2 and 1mm.
# PCM shell thickness = 0.5 x Cell radius (Guilak et al., 1995). RZ = Reserve zone, PZ = Proliferative zone, HZ = Hypertrophic zone.

3.3 Results

Evidence of the formation of the capital femoral tubercle appeared by 20 days while the secondary ossification center was still expanding toward metaphysis and before any evidence of a subchondral bone plate appeared (Figs. 3.1A &D). At 20 days there were two active growth fronts producing bone on the epiphyseal and metaphyseal sides of the growth cartilage. Fifteen days later, by 35 days, the secondary ossification center had completed most if its lengthwise growth and a thin subchondral bone plate began to form on the epiphyseal side above the RZ (Figs. 3.1 B& E). By 35 days a prominent capital femoral tubercle had developed, which at this age may be considered a primary mammillary process (Fig. 3.1 B); smaller secondary mammillary processes, also began to form (arrow to the left of the tubercle). At this stage, the undulations of the epiphyseal bone – reserve zone border can be seen to closely match those of the hypertrophic zone – metaphyseal bone border. By 480 days both primary and secondary mammillary processes (black arrow and arrowhead in Fig.1C) had developed even further and the metaphyseal and epiphyseal undulations continued to be matched, maintaining a nearly uniform thickness of the growth plate cartilage (Fig. 3.1F).

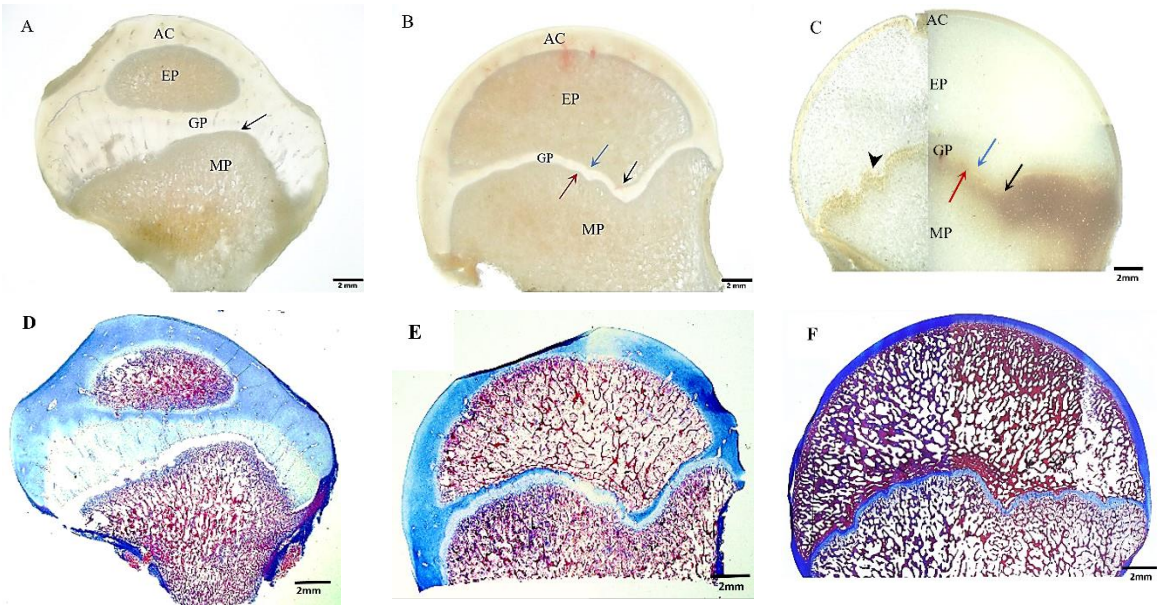

Fig. 3.1. A, B and C are stereo-microscopy images of a pig femoral head for three different age groups, unstained sections, which show the development of mammillary processes with age. A, B and C are thin sections of the middle of the femoral head (cut along a plane in which the caput-collum-diaphysis angle is measured) for a 20-, 35- and 480-day-old pig, respectively. The different contrast between right and left sides of C is due to varying slice thicknesses. D, E and F are sections stained with Masson's Trichrome adjacent to those of A, B, and C, respectively. AC=Articular cartilage, GP=Growth Plate cartilage, EP=Epiphysis, MP=Metaphysis. Black arrows indicate the undulation of the tubercle in the femoral head; red arrows denote the metaphyseal mammillary process and blue arrows point to the epiphyseal mammillary process. Arrowhead marks secondary mammillary processes. The scale bar is 2 mm.

3.3.1 Histology of the RZ-EP/SB interface

At 20 days, hypertrophic cells could be seen within the border of the RZ, belonging to the secondary center of ossification and performing similar functions to the hypertrophic cells at the metaphyseal side of the growth plate cartilage, producing calcified cartilage scaffolding to be converted later into primary spongiosa. At 20 days the growth fronts at both epi- (Fig. 3.2A) and meta-physeal (Fig. 3.2B&C) borders of the cartilage contained hypertrophic chondrocytes, but they were fewer in number at the epiphyseal border and lacked any evidence of a columnar zone as seen at the metaphyseal border (Fig. 3.2A,D&G). By 35 days, a plate-like structure of condensed bone appeared between the RZ and the epiphyseal trabecular bone (Fig. 3.2B, E&H). At the RZ-SB interface, clusters of cells varying in size and associated with neocartilage along the developing subchondral bone plate, accumulated near the bone marrow and tidemark (Fig. 3.2H&I). Eventually, by 480 days, a thick plate of subchondral bone had

developed, the tidemark had advanced and clusters of cells associated with neocartilage increased in size and number, mostly near the bone marrow becoming entrapped between multiple tidemarks (Fig. 3.2C,F&I). DIC microscopy afforded a clear indication of the tissue structural texture throughout cartilage-bone interface and sharply delineated the advancing tidemarks (Fig. 3.3). The tidemark became sharper/darker and developed a more irregular wave-shape line. The higher intensity region of tidemark is more visible in oldest age group (Fig. 3.3B&C).

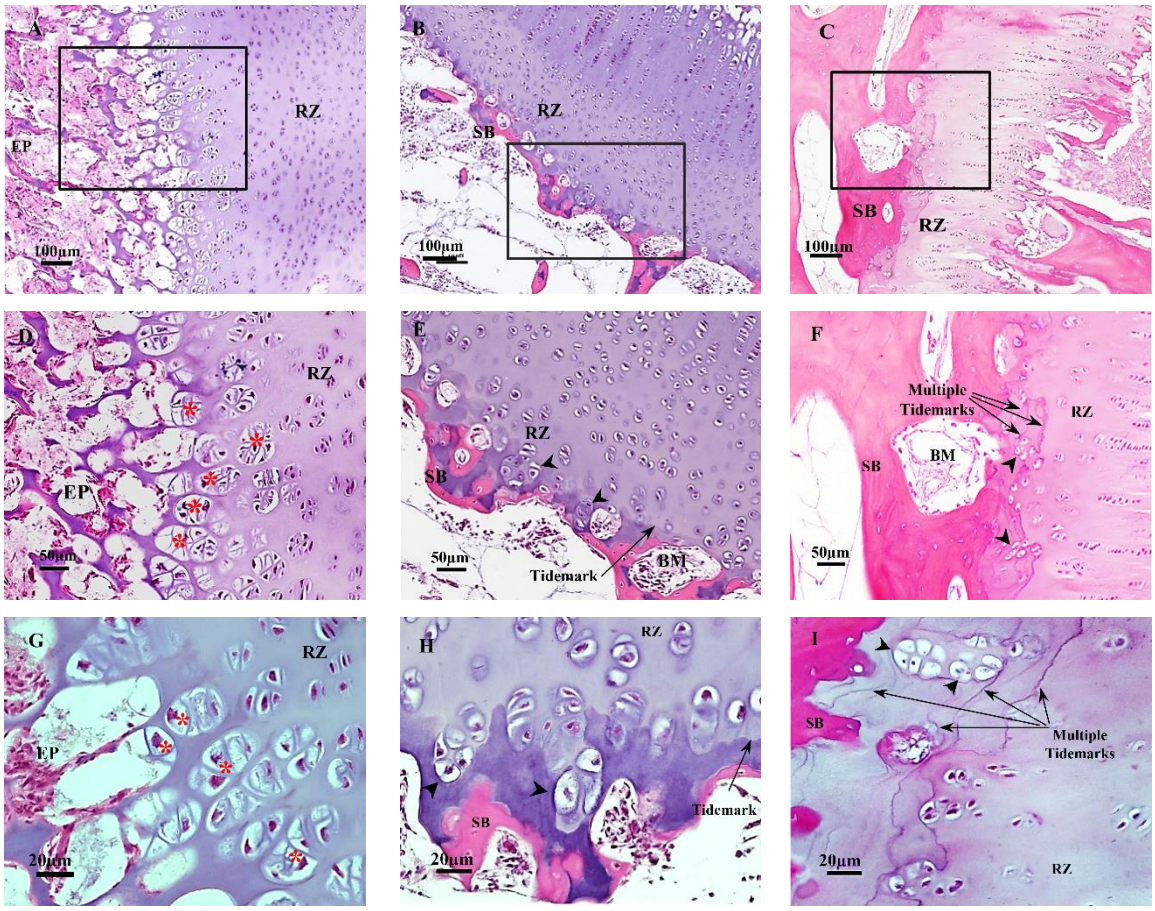

Fig. 3.2. Histology images of reserve zone-epiphysis/subchondral bone (RZ-EP/SB) interface, stained with H&E, for the femoral head of A) 20-, B) 35- C) 480-days-old pig. D, E and F are magnified images of black rectangular in A, B and C respectively. G, H and I indicate cell features in RZ-EP/SB interface for 20-,35- and 480-days old pig. Red asterisks denote hypertrophic cells and black arrowhead point to cells associated with neocartilage. EP=Epiphyseal bone, RZ=Reserve Zone, SB= Subchondral Bone, BM= Bone Marrow.

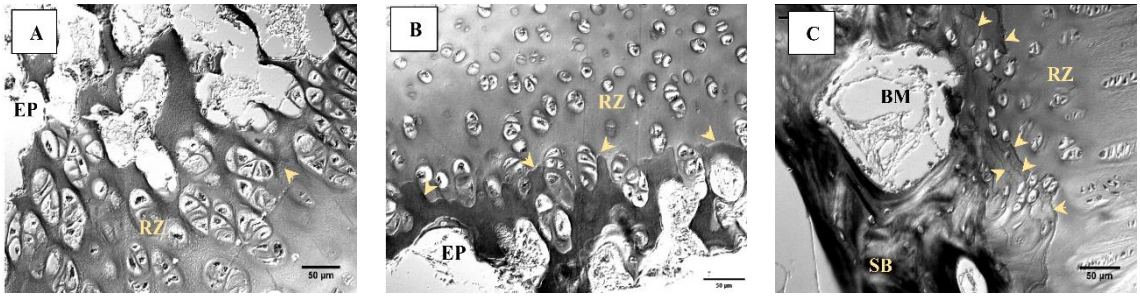

Fig. 3.3. Differential interference contrast images of reserve zone-epiphysis/subchondral bone (RZ-EP/SB) interface by differential interference contrast (DIC) optical microscopy, from the femoral head of A) 20-, B) 35- C) 480-day-old pig. Yellow arrowheads point to tidemark. EP=Epiphyseal bone, RZ=Reserve Zone, SB= Subchondral Bone, BM= Bone Marrow.

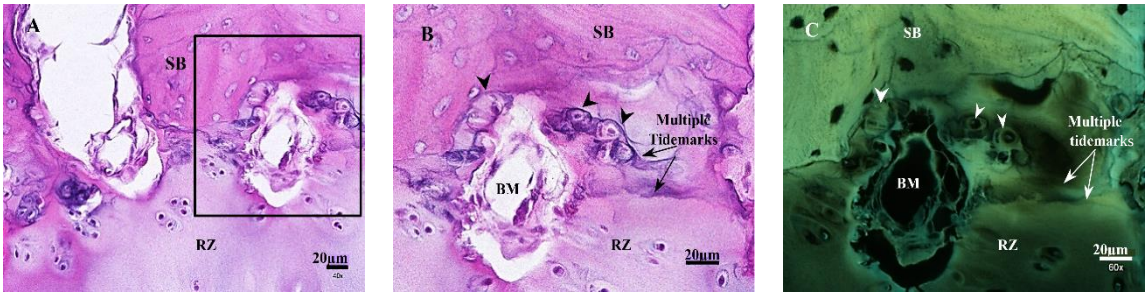

Fig. 3.4. A) Histology images of the reserve zone-subchondral bone (RZ-SB) interface of the proximal tibial growth plate of yearling bovine calf, stained with H&E, B) magnified image of black rectangular in A, C) fluorescence image of B by light microscope (Keyence, BZ-X710). Arrowheads point to neocartilage cells. RZ=Reserve Zone, SB= Subchondral Bone.

To further document the existence cells that appeared at locations of neocartilage within the RZ-SB interface, we looked for evidence of these in the proximal tibial growth plate of a yearling bovine calf, following the same tissue preparation protocol (Kazemi and Williams, 2018). The EDX and histology (Fig. 3.4) results of the bovine samples were consistent with those of the porcine growth plate. The line profile of the bovine transition zone between RZ and SB extended over 20-50 µm. The H&E stained tissue also revealed multiple tidemarks and many neocartilage nodules with closely packed cells between the epiphyseal bone marrow and growth plate reserve zone (Fig. 3.4A&B). Fluorescence microscopy of H&E stained sections showed light regions indicative of bone tissue in the SB (Fig. 3.4C) and evidence of tidemark regions corresponding to the eosinophilic tissues seen in Fig. 3.4B.

The RZ-EP/SB interface appeared to contain cells of various sizes, some larger than cells within the RZ proper (Table 3.3). By 20 days, the hypertrophic cell areas in the RZ-EP interface were about four

times larger than those of reserve zone chondrocytes. For two other age groups, in which subchondral bone were present, the cell areas of cells around neocartilage nodules were double those of the RZ chondrocytes. The distribution of cell areas within the RZ-EP/SB interface followed the same pattern for all age groups (Fig. 3.5). However, statistical analysis (KS test) indicated a significant difference for all age groups between the two groups of larger cells; one group being the hypertrophic cells at 20 days and cells associated with neocartilage at 35 and 480 days, found within the interface; and the other group consisting of the chondrocytes within the RZ proper.

Table 3.3. The results of cell area measurement (geometric mean (95% CI)) for three age groups using ImageJ.

Age group	**Cell area (μm^2)**	
	Hypertrophic cell/cell near neocartilage in RZ-EP/SB interface	RZ cell close to RZ-EP/SB interface
20 days old	173.2 (92.3, 324.4), n=42	37.13 (73.55, 18.54), n=49
35 days old	93.53 (159.015, 54.54), n=54	39.55 (62.11, 25.02), n=54
480 days old	66.92 (106.96, 40.85), n=78	29.10 (49, 15.99), n=80

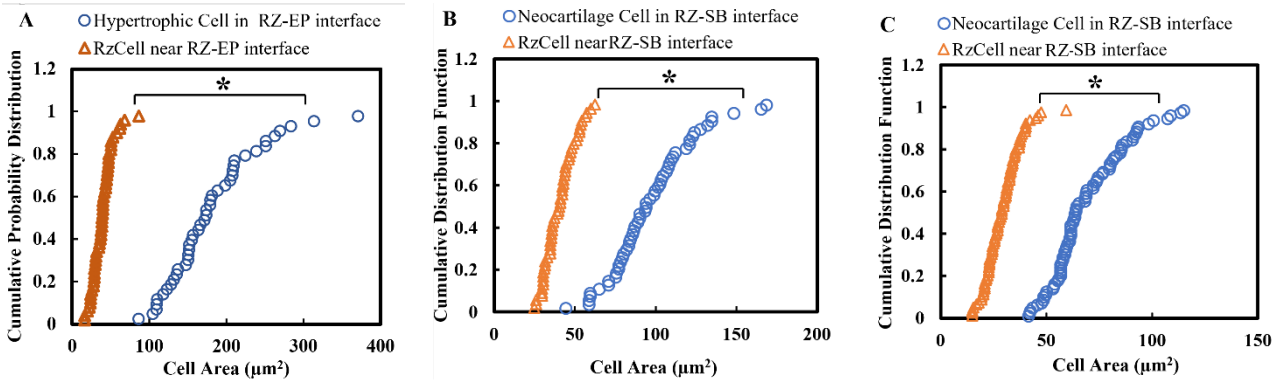

Fig. 3.5. The distribution of cell areas near/within the cartilage-bone interface for A) 20- , B) 35- and C) 480-day-old pig. *Hypertrophic/neocartilage cells are significantly larger than the reserve zone cell (RzCell) (P-value<0.05).

3.3.2 Scanning Electron microscopy and EDX

Using Energy dispersive x-ray spectroscopy (EDX), we traced the distributions of some essential elements, over the areas of cartilage and bone, as well as the interfacial regions between bone and the RZ. The results of line scans of the key elements revealed an enhanced intensity of C (Fig. 3.6) and S (not shown) within the RZ. There was also a significant accumulation of Ca and P in the EP/SB region. The

line profiles drawn across the cartilage-bone interface presented a chemical gradient of Ca, P and C across the RZ-EP/SB interface (Fig. 3.6). The average width of the gradient decreased with age so that at 480 days it was on average half the value at 20 days (Table 3.5 and Fig. 3.7). The gradient transition region between the RZ and EP/SB is demarcated by two red dash-lines in Fig.6. The start and endpoints of the transition zone were delineated based on the backscatter electron (BE) images and the individual smoothed line profiles of the major elements (Ca, P and C) within the RZ-EP/SB interface, across which Ca/P gradually increased toward the bone side as C decreased (Fig. 3.6 D,E&F). Backscatter electron (BE) microscopy signals are proportional to the atomic numbers of the scan area; bright gray levels in the BE images indicate mineralized regions with a high concentration of Ca, whereas dark grey levels reflect areas with lower mineral density (Fig. 3.6A,B&C) (Bradley et al., 2010).

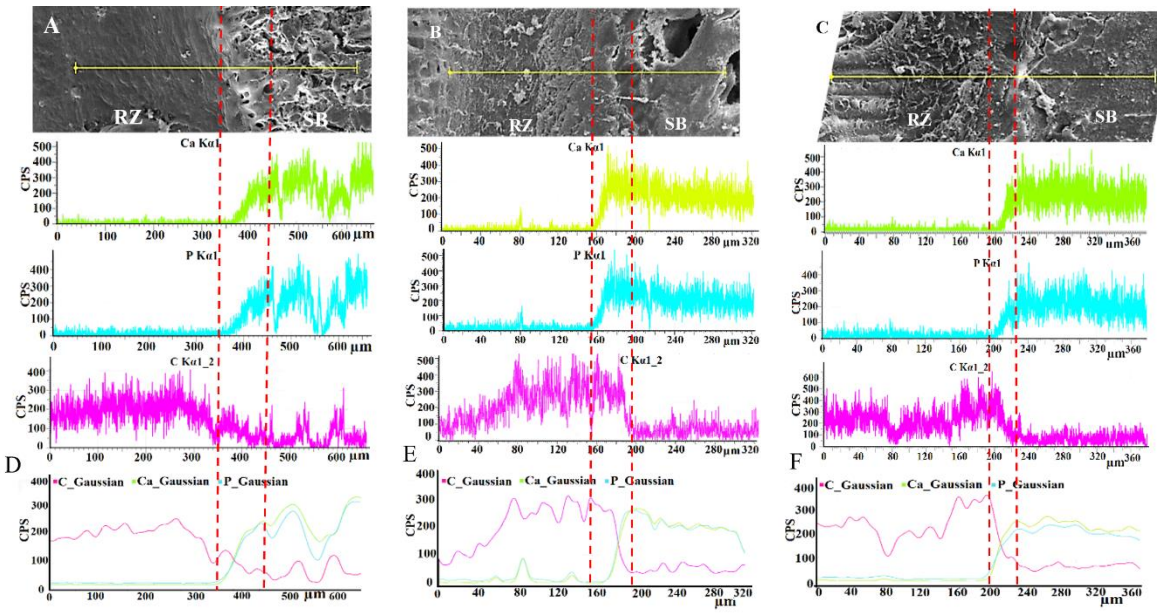

Fig. 3.6. Line profiles taken by EDX across the reserve zone-epiphysis/subchondral bone (RZ-EP/SB) interface for A) 20-, B) 35- and C) 480-day-old pigs. Vertical red dash lines denote the transition zone between cartilage and bone. The transition zone is determined based on the backscatter image and the EDX line profiles of maximum and minimum values of major elements (Ca, P and C). D, E and E are the smoothed data of A, B and C, respectively, using a Gaussian filter. CPS= count per second.

Table 3.4. The results of several line-scans across the RZ-EP/SB interface detected by EDX.

Age group / parameter	The measured chemical transition zone, μm	The width of the transition zone, μm*	Number of pixels per scanned line
20 days old	38.7	39.6±19.0	317
	35.5		291
	25.8		204
	72.2		99
	26.0		68
35 days old	24.0	29.0±14.3	43
	26.0		213
	17.0		212
	54.0		55
	24.0		100
480 days old	22.0	18.4±4.3	184
	16.0		183
	18.4		151
	16.5		135
	12.9		106
	25.0		86

* Mean value ± Std, error from a pooled estimate of error variance.

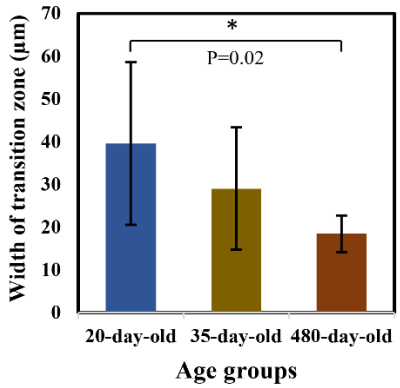

Fig. 3.7. The mean value (±Std) of the width of the transition zone between the reserve zone and epiphysis/subchondral bone plate for each age group. *The width of the transition zone at 20 days is significantly larger than that at 480 days (P-value=0.02).

3.3.3 Finite element model results

The histology results revealed fundamental changes in the piglet growth plates between 20 and 35 days of age in terms of subchondral bone development and cell morphology at the RZ border. When corresponding 20 to 35 day old finite element models were subjected to compression of 15% of the original growth plate thickness, the results showed a depth-dependent distribution of cell-averaged hydrostatic stresses and maximum principal strains for growth plate (GP) thickness (or widths) values ranging from 1 to 6 mm (Fig. 3.8). The cell-averaged hydrostatic stress at all locations in the RZ increased threefold as the GP thickness decreased from 6 to 1 mm but changed little with cell location

within the RZ (Fig. 3.8A). As the GP thickness decreased, the cell-averaged maximum tensile strain decreased seven-fold or more at the cell location near the border of the proliferative zone (cell 3) but changed only slightly at the other cell locations within the RZ (Fig. 3.8B).

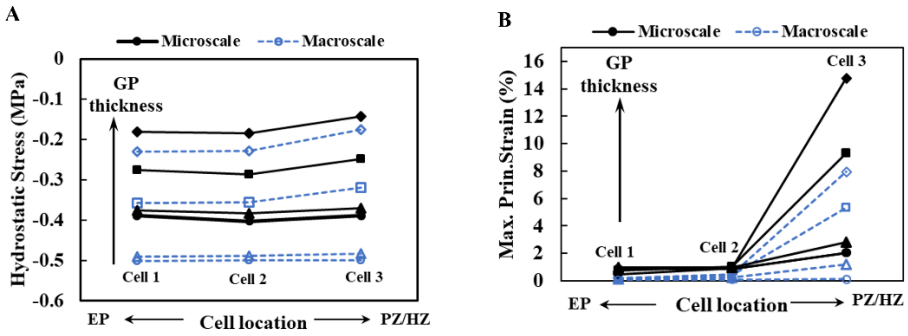

Fig 3.8. The distribution of depth-dependent A) cell-averaged hydrostatic stress and B) maximum principal strain within each cell location for the microscale model and the macroscale model in which there are no cells.

For growth plate thicknesses of 4- and 6-mm the cell-averaged maximum tensile strain for cell 3 increased by about 9 and 15 times, respectively, compared with cells 2 and 1 (Fig. 3.8B). Comparing results at different GP thicknesses, cells in a thicker GP experienced lower magnitude of hydrostatic stress and higher maximum principal strain at every location compared with thinner growth plates (Fig. 3.8A). Cells near the PZ border in the thickest cartilage had about 63% lower hydrostatic stress than those in the thinnest cartilage. Similar trends were observed for the macroscale model where the cell volumes were assigned to have the same Young's modulus and Poisson's ratio as the surrounding RZ matrix.

Pauwels (Pauwels, 1960) hypothesized that deviatoric stresses provide a stimulus for differentiation into bone or fibrous connective tissue, and that hydrostatic stresses provide mechanical signals to stimulate the formation of cartilage tissue. In previous modeling studies, which with one exception (Gao et al., 2017) were all conducted at the tissue level, the proposed stimulus for bone or fibrous connective tissue has sometimes been examined using deviatoric stress (Carter and Beaupré, 2007) and at other times using maximum principal strain (Claes and Heigele, 1999). To examine which of these two parameters at the cell level should be evaluated as possible stimuli for bone formation we

plotted the relationship between cell volume-averaged maximum principal strains and deviatoric (octahedral shear) stresses for both the micro- and macro-scale models in Fig. 3.9. As can be seen in both the macro- and micro-scale models that deviatoric (or octahedral) shear stress is accompanied by maximum tensile strain, which demonstrates that even at the cell level Pauwels' hypothesis can be explored using either deviatoric stress or maximum tensile strain.

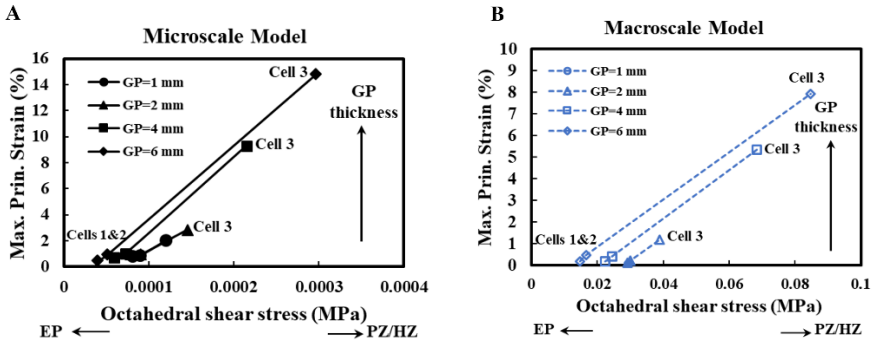

Fig 3.9. Cell-averaged octahedral shear stress vs maximum principal tensile strain for cells in different locations within the reserve zone moving from epiphysis (EP) to proliferative zone (PZ) subjected to 15% compression of the growth plate cartilage for A) microscale model and B) macroscale model in which the material properties of ECM was defined for cell geometry.

We plotted the combination of the cell-level mechano-regulatory factors on a tissue differentiation phase diagram to determine if the results are consistent, in qualitative and quantitative terms, with the observed and presumed role of the chondrocytes within the RZ (Fig. 3.10). The combinations of cell volume-averaged mechano-regulatory signals for four different growth plate thickness representing thinning of the cartilage with aging, all fell within the region of the diagram that is consistent with endochondral bone formation as shown previously for chondrocytes in the proliferative and hypertrophic zones (Gao et al., 2017).

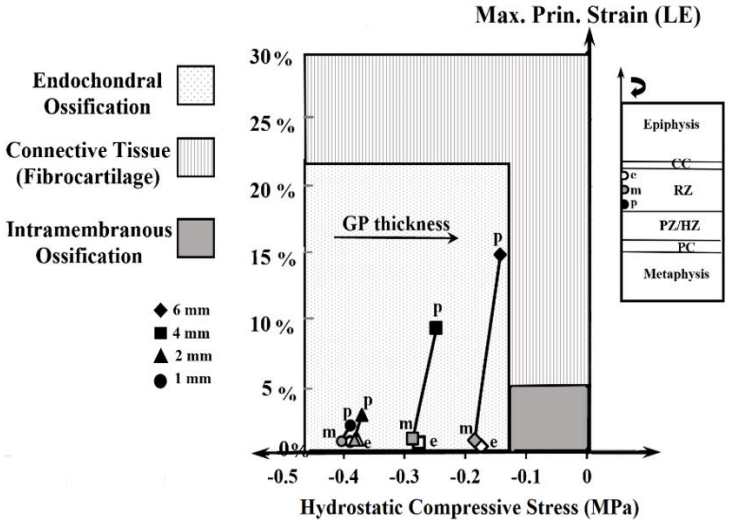

Fig. 3.10. Cell-averaged hydrostatic stress and maximum principal (tensile) strain in reserve zone chondrocytes when the model is subjected to 15% nominal compression. The tissue differentiation phase diagram is similar to one proposed for fracture healing at the tissue macroscale level [35] and for the proliferative and hypertrophic chondrocytes of the growth plate at the cell level (23).

3.4. Discussion

In this study we investigated the hypothesis of a secondary bone growth front at the epiphyseal border of the growth plate that begins after the secondary center of ossification near completion and that continues into adolescence to form bone in the development of the subchondral bone plate and the mammillary processes. We found a well-developed calcified cartilage layer at the SB/RZ interface with multiple tidemarks and groups of cells at the edge of the calcified border associated with neocartilage and that appeared to become encased in calcified cartilage and occasionally could be seen in proximity to epiphyseal marrow at perforations in the SB plate. These cells bear a resemblance to the chondroprogenitor stem cells that have recently been identified in this location in the reserve zone (Fig. 6 b and Fig. 8 g in Newton et al., 2019) and that can transdifferentiate into multiple cell types including osteoblasts. We showed the existence of a chemical transition zone across the subchondral bone layer between uncalcified cartilage and bone with a gradient in Ca and P indicating the preparation of a calcified cartilage scaffold for subsequent replacement by bone. The width of this transition zone decreased with age as the subchondral bone plate developed ever more undulating patterns to form

secondary mammillary processes. Taken together these histological and elemental studies suggest that bone continues to be actively formed at this interface to provide interlocking mammillary processes by a process of endochondral bone formation wherein cartilage is calcified in thin layers that serve as templates for replacement by bone. It also provides evidence that RZ cells calcify the matrix adjacent to the SB and that RZ stem cells may participate in converting this layer into bone. We developed finite element models to show that the mechanical milieu in the RZ is consistent with prevailing quantitative mechanobiological concepts in providing a combination of stress and strain stimuli relevant to endochondral bone formation at both the tissue and cell levels.

3.4.1 Histology of the RZ/EP interface

At 20 days after birth, hypertrophic cells could be seen at the interface between the RZ cartilage and the chondroepiphysis. At this stage these large cells are part of the mini growth plate belonging to the secondary ossification center (Farnum and Wilsman, 2018; Hansson et al., 1972). In our results, such hypertrophic cells were found only in the earliest age group, before the completion of growth from the secondary center of ossification and before the formation of the subchondral bone plate. These cells perform a similar function as the cells in the hypertrophic zone near the metaphyseal interface. They disappeared after the SB plate was in the early stages of forming, when a different type of cell was observed, arranged in clusters near nodules of newly formed cartilage (neocartilage). We believe these cells may be stem cells. Between 20 and 35 days the thickness (width) of the RZ decreased dramatically indicating depletion of non-regenerating reserve zone chondrocytes as they are recruited into the proliferative zone. By 35 and 480 days, after the SB plate began to develop, clusters of cells could be observed, which were closely packed in a basophilic matrix within the RZ-SB interface. These clusters of cells (Haines, 1975) were mostly localized between the tidemarks and bone marrow, which suggests the formation of new cartilage from cells derived either from epiphyseal bone marrow or more likely from stem cells in the RZ that participate in subsequent epiphyseal subchondral bone formation and further development of mamillary processes. The basophilic network of matrix suggests that these cells are

differentiating. It has been proposed that such cells could be osteoblast progenitor cells derived from bone marrow (Parfitt, 2002). Based on recent studies we might presume that these could also be RZ stem cells, changing their phenotype into osteoblasts to participate in forming an ossification front (Abad et al., 2002; Hallett et al., 2019; Hammond et al., 2010; Killion et al., 2017; Lui, 2020; Matsushita et al., 2020; Newton et al., 2019; Parfitt, 2002). Quantification of the cell areas within the RZ-EP/SB interface for all age groups, also indicated the hypertrophic cells and the cells associated with neocartilage nodules found close to the interface are significantly larger than the areas of RZ chondrocytes more distant from the interface. Our 2D cell area values for cells in locations 2 and 3 are consistent with a previous study (Amini et al. 2011, 2010). The measured cell radius values, based on the 2D cell area and assuming cells to be circular in shape, are also compatible with a previous study (Amini et al., 2011).

The appearance of a tidemark by 35 and 480 days indicates that cartilage calcification occurs along the reserve zone border. At 480 days there was evidence of advancing tidemarks which is a sign of a slow ossification front at the RZ/SB interface. Tidemarks along the border of the reserve zone have been noted in a few studies (Haines, 1975; Hoemann et al., 2012; Parfitt, 2002). Alkaline phosphate (ALP) localization studies have shown the highest values of the ALP secretion to occur at both ends of growth plate cartilage (Miao and Scutt, 2002). During active bone growth, the higher value of ALP found at the hypertrophic end of the growth plate is expected. However, localization of ALP at the border of the RZ could be also a further sign of an ossification front. This suggests that the RZ plays a role in the formation of the mammillary processes. Clusters of cells, either arising from the marrow or from the reserve zone are associated with calcified cartilage that appears over time to entrap these cells. The appearance of multiple tidemarks indicates that this is an ongoing process and suggests that it enables the continued evolution of secondary mammillary processes after the initial creation of a subchondral bone plate.

3.4.2 Elemental gradient at the RZ/EP interface

The SEM/EDX results for the main elemental distribution through the RZ-EP/SB interface were similar in all age groups. In all cases, the concentration of P and Ca, required for hydroxyapatite crystal

formation, gradually increased across the cartilage-bone interface, reaching maximum values within the bone region. Conversely, C and S decreased, as expected, from their peak values in cartilage, where C is an essential element for proteoglycan synthesis and C and S are required for collagen/protein production. These results are consistent with previous studies on articular (Kaabar et al., 2008, 2009, 2010, 2011) and growth plate cartilages (Althoff et al., 1982; Boyde and Shapiro, 1980; Shapiro IM, Boyde, 1984; Takata et al., 1974; Vittur et al., 1992). The gradient of chemical elements associated with mineralization suggests that there is a graded transition in tissue modulus between the stiffer bone tissue and softer cartilage tissue, providing a stress reduction mechanism to the attachment between two structurally and mechanically different tissues. This chemical gradient may also facilitate the transport of small solutes by diffusion thereby enabling crosstalk between calcified cartilage and subchondral bone (Arkill and Winlove, 2008; Gribbon et al., 1998). Such a mechanical transition zone has been reported for the interface between the articular cartilage (AC) and subchondral bone (SB) which has a similar chemical element gradient ranging from 10 to 30 μm in width (Campbell et al., 2012; Gupta et al., 2005) as reviewed elsewhere (Kazemi and Williams, 2020). Our results indicate that the width of the chemical transition zone decreases with age. This age-dependent decrease in the width of the transition zone in the growth plate SB coincides with thinning of the growth cartilage as longitudinal growth slows; and it is accompanied by the formation of secondary mammillary processes that interdigitate across the interface and help reduce the stress concentration. These developments may indicate the beginning stages of eventual epiphyseal fusion when chondrocyte proliferation ceases and another bone plate is formed at the metaphyseal border eventually leading to the replacement of the growth cartilage by well-calcified bone (Parfitt, 2002). Similarities in the EDX results and histology patterns between bovine and porcine samples suggests that a dual ossification front exists in many vertebrates including humans.

3.4.3 Finite element models

We related the mechano-regulatory parameters to the emerging evidence that chondrocytes in the resting zone have two distinct functions: stem cell-like properties as well as the ability to coordinate the

orderly differentiation into proliferative and hypertrophic chondrocytes (Abad et al., 2002; Hallett et al., 2019; Killion et al., 2017; Lui, 2020; Mizuhashi et al., 2018; Newton et al., 2019). Recent studies (Hallett et al., 2019) provide evidence of a stem cell niche of cells in the reserve zone near the proliferative zone giving rise to chondrocytes that line up and enter the proliferative zone; In addition to biological factors (Hallett et al., 2019) the mechanical environment in and around these stem cells may influence the propensity for recruitment of cells from this stem cell niche. The thickness of the reserve zone decreases with age and this in turn alters the mechanical environment of the RZ cells, including those near the chondroepiphysis border and those adjacent to the proliferative zone. Cell 3 (at the PZ border) experienced higher magnitudes of maximum principal strain and lower magnitudes of hydrostatic stress (Figs. 3.8 and 3.9) in thicker cartilage, conditions more favorable for proliferation, compared with thinner cartilage. This is consistent with the observation that the rate of bone growth slows with aging (programmed senescence) as the growth plate thickness decreases until growth ceases and cartilage fusion occurs (Haines, 1975; Parfitt, 2002).

When viewed on a tissue differentiation phase diagram (Fig. 3.10) for each of the four growth plate thickness values the results indicate that the cell-level hydrostatic stress and maximum tensile strain values for all RZ cells fall within the region associated with endochondral ossification (greater than 0.15 MPa of compressive hydrostatic pressure and principal tensile strain values less than 15% strain, as was shown previously at the cell level for cells in the PZ and HZ (Gao et al., 2017)). Higher maximum principal strain (occurring primarily in the direction perpendicular to column formation) and lower hydrostatic stress, provide a favorable environment for chondrocyte division and this occurs for the cells located closest to the PZ (cell 3). RZ chondrocytes near the PZ border provide new cells that enter the proliferative zone and this mechanical environment may be favorable for stimulating either non-self-renewing or self-renewing RZ cells into becoming part of or dividing and contributing cells to the proliferative zone in early stages of growth when the growth plate is relatively thick. When the results for Cell 3 in the 6-mm thick growth plate are plotted on a tissue differentiation phase diagram along with the results for cells in the PZ and HZ from a previous study (Gao et al., 2017) on a 0.67-mm thick growth

plate it can be seen that the maximum principal strain for RZ Cell 3 is similar to that for the first chondrocyte in the PZ (P in Fig.3.11), while the hydrostatic pressure is less than that in proliferative cells. With aging the growth plate gets thinner and the maximum principal strains decrease while hydrostatic stresses increase (Fig. 3.10) creating conditions to keep the cells in a quiescent state unless they are in the proximity of a blood supply. It can also be observed that Cell 1, located at the RZ/SB interface, has a low maximum principal strain and low hydrostatic pressure in the 6-mm thick growth plate. This is similar to conditions for cells at the end of the HZ (H in Fig.3.11). This suggests that these mechanical conditions may be favorable not only for calcifying cartilage but for stimulating skeletal stem cells to transdifferentiate into osteoblasts at either the HZ/metaphysis or RZ/SB interfaces in the presence of an adequate source of blood.

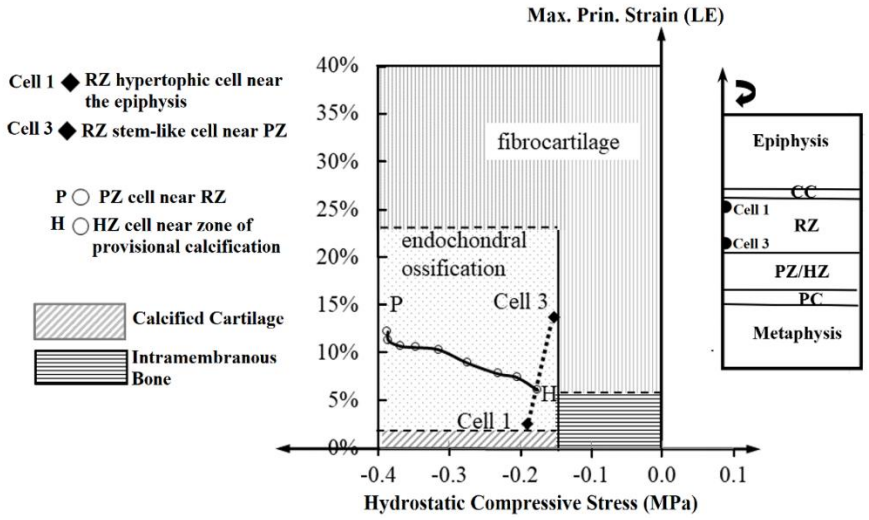

Fig. 3.11. Tissue differentiation diagram showing data from the current study for cells in the RZ under 15% compression of the original growth plate thickness for a 6-mm thick growth plate, along with data from a previous study on cells in the proliferative (P) and hypertrophic (H) zones in a 0.67-mm thick growth plate model subjected to 20% compression. Cell 1 represents a cell at the SB/RZ interface and Cell 3 is a RZ chondrocyte at the border of the PZ. P is a cell at the top of the proliferative zone and H is a cell at the bottom of the hypertrophic zone.

Our cell-level results indicate that the combination of maximum principal strains and hydrostatic stresses in RZ chondrocytes could predict depth-dependent cell responses. Our results are consistent with tissue level theories in which the combination of mechano-regulatory factors predict tissue differentiation

in a tissue differentiation phase diagram of the kind proposed at the tissue level for fracture healing (Claes and Heigele, 1999) and for the proliferative and hypertrophic zones at the cell level (Gao et al., 2017). All the aforementioned evidence suggests that growth plate cartilage has two ossification fronts and two chondro-osseous junctions, one at the HZ border and the other at RZ border with bone. The growth front at the RZ border is responsible for forming the SB plate and either directly or indirectly shaping the mammillary processes. Thus, there may be a third role for the RZ. In addition to providing a niche of stem cells and coordinating the formation of the PZ and HZ, the RZ also appears to actively form the SB plate and may be responsible for forming a robust interdigitating interface with a uniform thickness of growth cartilage.

3.5. Limitations

One of the limitations of this study is our sample size per age group. A larger population would enhance the results. The second limitation concerns the gap in continuity between the 35- and 480-days old samples, which does not provide us with data on how mammillary processes develop within this age gap. Third, the 35-day-old pigs received MTX, a drug used in chemotherapy. This was administered at 14 days and at 4 days before sacrifice. Only the middle age group, the 35-day-old group, was given MTX injections, which could affect bone formation and growth plate thickness depending on the treatment dosage and duration (Fan et al., 2009; Cavalcanti et al., 2014). Changes in GP thickness, cell apoptosis and length of tibia have been shown to return to normal at 14 days after injection (Xian et al., 2007). In this study the effect of MTX on the bone and cartilage is not clear as we did not have a similar age control group for comparison. However, the histology results showed normal appearing growth plate zones. We believe that although the growth rate may possible have been temporarily interrupted, the data for this group still provide data relevant to an animal with an age between 20 and 480 days old, which is consistent with the aim of this study. Finally, the tissues were stored at -20 °C until use and therefore not suitable for histochemistry studies on the cells at the RZ-SB interface.

References

Abad V, Meyers JL, Weise M, Gafni RI, Barnes KM, Nilsson O, Bacher JD, Baron J. The role of the resting zone in growth plate chondrogenesis. Endocrinology. 2002 May 1;143(5):1851-7. https://doi.org/10.1210/endo.143.5.8776.

Allen DM, Mao JJ. Heterogeneous nanostructural and nanoelastic properties of pericellular and interterritorial matrices of chondrocytes by atomic force microscopy. Journal of structural biology. 2004 Mar 1;145(3):196-204. https://doi.org/10.1016/j.jsb.2003.10.003.

Althoff J, Quint P, Krefting ER, Höhling HJ. Morphological studies on the epiphyseal growth plate combined with biochemical and X-ray microprobe analyses. Histochemistry. 1982 Dec 1;74(4):541-52.

Amini S, Veilleux D, Villemure I. Three-dimensional in situ zonal morphology of viable growth plate chondrocytes: a confocal microscopy study. Journal of Orthopaedic Research. 2011 May;29(5):710-7. https://doi.org/10.1002/jor.21294.

Arkill KP, Winlove CP. Solute transport in the deep and calcified zones of articular cartilage. Osteoarthritis and Cartilage. 2008 Jun 1;16(6):708-14. https://doi.org/10.1016/j.joca.2007.10.001.

Barrios C, Blasco MA, Blasco MC, Gascó J. Posterior sloping angle of the capital femoral physis: a predictor of bilaterality in slipped capital femoral epiphysis. Journal of Pediatric Orthopaedics. 2005 Jul 1;25(4):445-9. https://doi.org/10.1097/01.bpo.0000158811.29602.a5.

Boyde A, Shapiro IM. Energy dispersive X-ray elemental analysis of isolated epiphyseal growth plate chondrocyte fragments. Histochemistry. 1980 Jan 1;69(1):85-94.

Bradley DA, Farquharson MJ, Gundogdu O, Al-Ebraheem A, Ismail EC, Kaabar W, Bunk O, Pfeiffer F, Falkenberg G, Bailey M. Applications of condensed matter understanding to medical tissues and disease progression: Elemental analysis and structural integrity of tissue scaffolds. Radiation Physics and Chemistry. 2010 Feb 1;79(2):162-75. https://doi.org/10.1016/j.radphyschem.2008.12.007.

Broom ND, Poole CA. A functional-morphological study of the tidemark region of articular cartilage maintained in a non-viable physiological condition. Journal of anatomy. 1982 Aug;135(Pt 1):65.

Campbell SE, Ferguson VL, Hurley DC. Nanomechanical mapping of the osteochondral interface with contact resonance force microscopy and nanoindentation. Acta biomaterialia. 2012 Dec 1;8(12):4389-96. https://doi.org/10.1016/j.actbio.2012.07.042.

Carter DR, Wong M. Mechanical stresses and endochondral ossification in the chondroepiphysis. Journal of orthopaedic research. 1988 Jan;6(1):148-54. https://doi.org/10.1002/jor.1100060120.

Carter DR, Beaupré GS. Skeletal function and form: mechanobiology of skeletal development, aging, and regeneration. Cambridge university press; 2007 Aug 25.

Cavalcanti SC, Corrêa L, Mello SB, Luz JG. The effect of methotrexate on the bone healing of mandibular condylar process fracture: An experimental study in rats. Journal of Cranio-Maxillofacial Surgery. 2014 Oct 1;42(7):1133-9. https://doi.org/10.1016/j.jcms.2014.01.044.

Claes LE, Heigele CA. Magnitudes of local stress and strain along bony surfaces predict the course and type of fracture healing. Journal of biomechanics. 1999 Mar 1;32(3):255-66. https://doi.org/10.1016/S0021-9290(98)00153-5.

Cohen B, Chorney GS, Phillips DP, Dick HM, Buckwalter JA, Ratcliffe A, Mow VC. The microstructural tensile properties and biochemical composition of the bovine distal femoral growth plate. Journal of Orthopaedic Research. 1992 Mar;10(2):263-75. https://doi.org/10.1002/jor.1100100214.

d'Alfonso AJ, Freitag B, Klenov D, Allen LJ. Atomic-resolution chemical mapping using energy-dispersive x-ray spectroscopy. Physical Review B. 2010 Mar 8;81(10):100101. https://doi.org/10.1103/PhysRevB.81.100101.

Fan C, Cool JC, Scherer MA, Foster BK, Shandala T, Tapp H, Xian CJ. Damaging effects of chronic low-dose methotrexate usage on primary bone formation in young rats and potential protective effects of folinic acid supplementary treatment. Bone. 2009 Jan 1;44(1):61-70. https://doi.org/10.1016/j.bone.2008.09.014.

Farnum CE, Wilsman NJ. Morphologic stages of the terminal hypertrophic chondrocyte of growth plate cartilage. Anat Rec. 1987 Nov 1 ;219(3):221–32. https://doi.org/10.1002/ar.1092190303

Frost HM. Skeletal structural adaptations to mechanical usage (SATMU): 3. The hyaline cartilage modeling problem. The Anatomical Record. 1990 Apr;226(4):423-32. https://doi.org/10.1002/ar.1092260404.

Gao J, Williams JL, Roan E. On the state of stress in the growth plate under physiologic compressive loading. Open Journal of Biophysics. 2014 Jan 6;2014. https://doi.org/10.4236/ojbiphy.2014.41003.

Gao J, Roan E, Williams JL. Regional variations in growth plate chondrocyte deformation as predicted by three-dimensional multi-scale simulations. PloS one. 2015 Apr 17;10(4):e0124862. https://doi.org/10.1371/journal.pone.0124862.

Gao J, Williams JL, Roan E. Multiscale modeling of growth plate cartilage mechanobiology. Biomechanics and modeling in mechanobiology. 2017 Apr 1;16(2):667-79. https://doi.org/10.1007/s10237-016-0844-8.

Gangadhar R, Jaleeli KA, Ahmad A. Energy dispersive x-ray analysis of ovine scapular cartilage. International Journal of Science, Environment and Technology. 2015;4(4):1195-8.

Guilak F, Ratcliffe A, Mow VC. Chondrocyte deformation and local tissue strain in articular cartilage: a confocal microscopy study. Journal of Orthopaedic Research. 1995 May;13(3):410-21. https://doi.org/10.1002/jor.1100130315.

Gribbon PM, Maroudas A, Parker KH, Winlove CP. Water and solute transport in the extracellular matrix: physical principles and macromolecular determinants. Wenner green international series. 1998:95-124.

Gupta HS, Schratter S, Tesch W, Roschger P, Berzlanovich A, Schoeberl T, Klaushofer K, Fratzl P. Two different correlations between nanoindentation modulus and mineral content in the bone–cartilage interface. Journal of structural biology. 2005 Feb 1;149(2):138-48. https://doi.org/10.1016/j.jsb.2004.10.010.

Haines RW. The histology of epiphyseal union in mammals. Journal of anatomy. 1975 Sep;120(Pt 1):1.

Hallett SA, Ono W, Ono N. Growth plate chondrocytes: Skeletal development, growth and beyond. International journal of molecular sciences. 2019 Jan;20(23):6009. https://doi.org/10.3390/ijms20236009.

Hammond AS, Ning J, Ward CV, Ravosa MJ. Mammalian limb loading and chondral modeling during ontogeny. The Anatomical Record: Advances in Integrative Anatomy and Evolutionary Biology. 2010 Apr;293(4):658-70. https://doi.org/10.1002/ar.21136.

Hansson LI, Menander-Sellman K, Stenstrsm A, Thorngren K-G. Rate of Normal Longitudinal Bone Growth in the Rat. Vol. 10, Calm Tiss. Res. Springer-Verlag; 1972.

Hoemann CD, Lafantaisie-Favreau CH, Lascau-Coman V, Chen G, Guzmán-Morales J. The cartilage-bone interface. The journal of knee surgery. 2012 Jun;25(02):085-98. http://dx.doi.org/ 10.1055/s-0032-1319782.

Hosseinzadeh S, Kiapour AM, Maranho DA, Emami SA, Portilla G, Kim YJ, Novais EN. The metaphyseal fossa surrounding the epiphyseal tubercle is larger in hips with moderate and severe slipped capital femoral epiphysis than normal hips. Journal of Children's Orthopaedics. 2020 May 20;14(0):1-6. https://doi.org/10.1302/1863-2548.14.200010.

Hueter C. Anatomische Studien an den Extremitätengelenken Neugeborener und Erwachsener. Arch für Pathol Anat und Physiol und für Klin Med. 1863 Sep;26 (5–6):484–519.

Kaabar W, Gundogdu O, Bradley DA, Bunk O, Pfeiffer F, Farquharson MJ, Webb M, Jeynes C. Compositional studies at the Bone-Cartilage interface using PIXE, RBS and cSAXS techniques.2008.

Kaabar W, Daar E, Gundogdu O, Jenneson PM, Farquharson MJ, Webb M, Jeynes C, Bradley DA. Metal deposition at the bone–cartilage interface in articular cartilage. Applied Radiation and Isotopes. 2009 Mar 1;67(3):475-9. https://doi.org/10.1016/j.apradiso.2008.06.019.

Kaabar W, Daar E, Bunk O, Farquharson MJ, Laklouk A, Bailey M, Jeynes C, Gundogdu O, Bradley DA. Elemental and structural studies at the bone–cartilage interface. Nuclear Instruments and Methods in Physics Research Section A: Accelerators, Spectrometers, Detectors and Associated Equipment. 2011 Oct 1;652(1):786-90. https://doi.org/10.1016/j.nima.2010.09.095.

Kaabar W, Gundogdu O, Laklouk A, Bunk O, Pfeiffer F, Farquharson MJ, Bradley DA. μ-PIXE and SAXS studies at the bone–cartilage interface. Applied Radiation and Isotopes. 2010 Apr 1;68(4-5):730-4. https://doi.org/10.1016/j.apradiso.2009.09.038.

Kazemi, M, Williams, JL. Elemental and histological study of the growth plate reserve zone–subchondral bone interface. Paper presented at: Orthopaedic Research Society Annual Meeting (ORS); March 10-13, 2018; New Orleans, LA.

Kazemi M, Williams JL. Chondrocyte and pericellular matrix deformation and strain in the growth plate cartilage reserve zone under compressive loading. InInternational Symposium on Computer Methods in Biomechanics and Biomedical Engineering 2019 Aug 14 (pp. 526-538). Springer, Cham.

Kazemi M, Williams JL. Properties of Cartilage–Subchondral Bone Junctions: A Narrative Review with Specific Focus on the Growth Plate. Cartilage. 2020 May 27. https://doi.org/10.1177/1947603520924776.

Kazemi M, Williams JL. Depth and strain rate-dependent mechanical response of chondrocytes in reserve zone cartilage subjected to compressive loading. Biomechanics and Modeling in Mechanobiology . 2021 April. https://doi.org/10.1007/s10237-021-01457-1.

Killion CH, Mitchell EH, Duke CG, Serra R. Mechanical loading regulates organization of the actin cytoskeleton and column formation in postnatal growth plate. Molecular biology of the cell. 2017 Jul 7;28(14):1862-70. https://doi.org/10.1091/mbc.e17-02-0084.

Lerner AL, Kuhn JL. Characterization of regional and age-related variations in the growth of the rabbit distal femur. Journal of orthopaedic research. 1997 May;15(3):353-61. https://doi.org/10.1002/jor.1100150307.

Lerner AL, Kuhn JL, Hollister SJ. Are regional variations in bone growth related to mechanical stress and strain parameters? Journal of biomechanics. 1998 Apr 1;31(4):327-35. https://doi.org/10.1016/S0021-9290(98)00015-3.

Lešer V, Milani M, Tatti F, Tkalec ŽP, Štrus J, Drobne D. Focused ion beam (FIB)/scanning electron microscopy (SEM) in tissue structural research. Protoplasma. 2010 Oct 1;246(1-4):41-8. https://doi.org/10.1007/s00709-010-0118-8.

Liu RW, Armstrong DG, Levine AD, Gilmore A, Thompson GH, Cooperman DR. An anatomic study of the epiphyseal tubercle and its importance in the pathogenesis of slipped capital femoral epiphysis. JBJS. 2013 Mar 20;95(6):e34. https://doi.org/10.2106/JBJS.L.00474.

Loder RT. Slipped capital femoral epiphysis. American family physician. 1998 May 1;57(9):2135.

Lui JC. Home for a rest: stem cell niche of the postnatal growth plate. Journal of Endocrinology. 2020 Jul 1;246(1):R1-1. https://doi.org/10.1530/JOE-20-0045.

Manoff EM, Banffy MB, Winell JJ. Relationship between body mass index and slipped capital femoral epiphysis. Journal of Pediatric Orthopaedics. 2005 Nov 1;25(6):744-6. https://doi.org/10.1097/01.bpo.0000184651.34475.8e.

Matsushita Y, Ono W, Ono N. Growth plate skeletal stem cells and their transition from cartilage to bone. Bone. 2020 Apr 7:115359. https://doi.org/10.1016/j.bone.2020.115359.

Miao D, Scutt A. Histochemical localization of alkaline phosphatase activity in decalcified bone and cartilage. Journal of Histochemistry & Cytochemistry. 2002 Mar;50(3):333-40. https://doi.org/10.1177/002215540205000305.

Mizuhashi K, Ono W, Matsushita Y, Sakagami N, Takahashi A, Saunders TL, Nagasawa T, Kronenberg HM, Ono N. Resting zone of the growth plate houses a unique class of skeletal stem cells. Nature. 2018 Nov;563(7730):254-8. https://doi.org/10.1038/s41586-018-0662-5.

Newton PT, Li L, Zhou B, Schweingruber C, Hovorakova M, Xie M, Sun X, Sandhow L, Artemov AV, Ivashkin E, Suter S. A radical switch in clonality reveals a stem cell niche in the epiphyseal growth plate. Nature. 2019 Mar;567(7747):234-8. https://doi.org/10.1038/s41586-019-0989-6.

Parfitt AM. Misconceptions (1): epiphyseal fusion causes cessation of growth. Bone (New York, NY). 2002;30(2):337-9.

Pauwels F. Eine neue Theorie über den Einfluß mechanischer Reize auf die Differenzierung der Stützgewebe. Zeitschrift für Anatomie und Entwicklungsgeschichte. 1960 Nov 1;121(6):478-515.

Schneider CA, Rasband WS, Eliceiri KW. NIH Image to ImageJ: 25 years of image analysis. Nature methods. 2012 Jul;9(7):671-5.

Shapiro IM, Boyde A. Microdissection-elemental analysis of the mineralizing growth cartilage of the normal and rachitic chick. Metabolic Bone Disease and Related Research. 1984 Jan 1;5(6):317-26. https://doi.org/10.1016/0221-8747(84)90019-5.

Smith JW. The relationship of epiphysial plates to stress in some bones of the lower limb. Journal of anatomy. 1962 Jan;96(Pt 1):58.

Speer DP, Dahners L. The collagenous architecture of articular cartilage: correlation of scanning electron microscopy and polarized light microscopy observations. Clinical Orthopaedics and Related Research®. 1979 Mar 1(139):267-75.

Speer DP. Collagenous architecture of the growth plate and perichondrial ossification groove. JBJS. 1982 Mar 1;64(3):399-407.

Stevens SS, Beaupré GS, Carter DR. Computer model of endochondral growth and ossification in long bones: biological and mechanobiological influences. Journal of Orthopaedic Research. 1999 Sep;17(5):646-53. https://doi.org/10.1002/jor.1100170505.

Takata K, Yamamoto K, Ohmori S, Watanabe T. Scanning electron microscopic study and elemental analysis of the epiphyseal growth plate in normal puppies. Orthopedics & Traumatology. 1974 Jun 8;23(1):44-7. https://doi.org/10.5035/nishiseisai.23.44.

Van Leeuwen BL, Verkerke GJ, Hartel RM, Sluiter WJ, Kamps WA, Jansen HW, Hoekstra HJ. Chemotherapy decreases epiphyseal strength and increases bone fracture risk. Clinical Orthopaedics and Related Research®. 2003 Aug 1;413:243-54. https://doi.org/10.1097/01.blo.0000073348.50837.f2.

Vittur F, Tuniz C, Psoletti S, Rizzo R, Jones KW. Elemental analysis of growth plate cartilage by synchrotron-radiation-induced X-ray emission (SRIXE). Biochemical and biophysical research communications. 1992 Nov 16;188(3):1010-7. https://doi.org/10.1016/0006-291X(92)91332-K.

Volkmann R. Chirurgische erfahrungen uber knochenverbiegungen und knochenwachsthum. Arch f Path Anat Physiol u Klin Med. 1862;24:512–41.

Williams JL, Vani JN, Eick JD, Petersen EC, Schmidt TL. Shear strength of the physis varies with anatomic location and is a function of modulus, inclination, and thickness. Journal of orthopaedic research. 1999 Mar;17(2):214-22. https://doi.org/10.1002/jor.1100170210.

Wollman DA, Irwin KD, Hilton GC, Dulcie LL, Newbury DE, Martinis JM. High-resolution, energy-dispersive microcalorimeter spectrometer for X-ray microanalysis. Journal of Microscopy. 1997 Dec;188(3):196-223. https://doi.org/10.1046/j.1365-2818.1997.2670824.x.

Xian CJ, Cool JC, Scherer MA, Macsai CE, Fan C, Covino M, Foster BK. Cellular mechanisms for methotrexate chemotherapy-induced bone growth defects. Bone. 2007 Nov 1;41(5):842-50. https://doi.org/10.1016/j.bone.2007.07.021.

Chapter 4

Chondrocyte and pericellular matrix deformation and strain in the growth plate cartilage reserve zone under compressive loading

4.1 Introduction

The growth plate or physis consists of a thin layer of hyaline cartilage sandwiched between epiphyseal and metaphyseal bone; it is responsible for most of the longitudinal bone growth by an endochondral ossifcation mechanism. Growth plate cartilage consists of three main regions: a highly cellular region of proliferative and hypertrophic chondrocytes located in tubular structures aligned with the bone long axis and a region that is more sparsely populated by chondrocytes called the resting zone, or reserve zone, which is located adjacent to the epiphyseal bone [1]. Blood vessels pass through the subchondral bone plate and reserve zone ending at the beginning of the proliferative zone [2, 3], but the RZ itself has no blood supply. In each location throughout the growth plate every chondrocyte is surrounded by an extracellular matrix (ECM). Generally, chondrocytes are responsible for making, maintaining and repairing extracellular matrix in response to mechanical loading. It has been shown that mechanical loading modulates chondrocyte metabolic activities [4]. However, we have a limited understanding of how biomechanical signals are sensed by the cell and what the relevant molecular pathways are. Chondrocyte behavior is partly regulated by the stress-strain state in and around the cell [4–6]. The morphology and mechanical properties of the growth plate have been measured at the cell and tissue level by confocal microscopy/fluorescent labeling techniques [7, 8] and atomic force microscopy (AFM) [9, 10]. These studies have revealed differences in the structural and mechanical properties between the zones of the cartilage [9]. It has been shown that the chondrocytes are surrounded by a narrow region of pericellular matrix (PCM) [11, 12].

Chondrocytes and their surrounding PCM and territorial matrix were described by Benninghof as the basic functional units of cartilage and named chondrons using the analogy of osteons in bone [11, 12, 15]. The PCM has been characterized by type IV collagen [13, 14]. Experimental and theoretical studies have reported the mechanical properties of the PCM and extracellular matrix (ECM) within articular cartilage by various techniques, such as micropipette aspiration and atomic force microscopy (AFM) [11, 12, 16, 17] and showed that the PCM mechanical and microstructural properties signficantly influence the biomechanical environment of chondrocytes [11, 18, 19]. In contrast to the nonuniformity and mechanical anisotropy of cartilage ECM, the PCM has zonal uniformity and constant mechanical properties at the microscale [20, 21]. There is a large difference between the elastic moduli of chondrocytes, PCM and ECM [4, 7, 22]. Therefore, the stress-strain fields within the cells are expected to differ from the surrounding matrix. Although several biomechanical studies have reported microscale models to study the stress-strain state around the chondrocytes and PCM within articular cartilage ECM, relatively few studies have been published on the deformation and strain of chondrocytes in different zones of growth plate cartilage [8, 23, 24] and to our knowledge none have examined the chondrocytes within the growth plate reserve zone.

The overall goal of this study was to explore the role of the PCM in modulating chondrocyte deformation and stress-strain state as a function of depth within the reserve zone under normal physiological loads. Specifically, we sought to answer the following three questions: (1) How do deformation, strain and stress within the chondrocyte and PCM vary through the depth of the reserve zone? (2) Does the PCM protect reserve zone chondrocytes from excessive stress? (3) Does the PCM amplify or reduce strains in the reserve zone chondrocytes?

4.2 Method

4.2.1 Model description

An axisymmetric elastic microscale model was developed in which circular chondrocytes were embedded within the RZ extracellular matrix (ECM) at four depths between the subchondral bone plate and the proliferative zone. The PCM wall thickness was set to be half of the chondrocyte radius (cell

radius = 10 μm, PCM thickness = 0.5 μm) [25][26]. Chondrocytes make up only about 10% of the reserve zone volume. Therefore, to simplify the model, we simulated four cells in the RZ in a finite element microscale model using ABAQUS/CAE 2019 (SIMULIA, USA). A chondrocyte was placed in four different locations of the RZ, starting with a location near the subchondral bone (SB) interface and moving along the symmetry axis to a location near the proliferative zone (PZ) interface. Homogeneous isotropic linearly elastic materials (Table 4.1) were used for all components. The cartilage was unconfined along the perichondrial periphery. This quasi-static elastic analysis represents a state during short duration loading (relative to stress relaxation time), such as heal strike in gait, during which the cartilage does not have time to undergo relaxation and creep and the influence of the fluid component is negligible.

Table 4.1. Material properties and dimensions.

	Young's Modulus (MPa)	**Poisson's Ratio**	**Thickness (mm)**	**Radius (mm)**
Chondrocyte	0.002 [27]	0.4999 [27]	-	0.01 [26]
PCM	0.265 [17]	0.45 [17]	0.005[26]	-
RZ (ECM)	0.98 [27]	0.47 [27]	0.94 [28]	-
PZ/HZ	0.49 [27]	0.47 [27]	0.4 [28]	-
PC	300 [29]	0.2 [30]	0.16*	-
SB	1100 [31]	0.3 [31]	0.5*	-

*Based on our histology of a 20-day piglet distal ulnar growth plate.

To account for large deformation, the effect of geometrical nonlinearity was considered by turning on NLGEOM. The idealized geometry of our model is shown in Fig. 4.1, in which a single cell is surrounded by a PCM and both are embedded in the ECM of the reserve zone along the symmetry axis of the axisymmetric model. The growth plate layer was partitioned into two sections to represent the reserve zone (RZ) and the proliferative/hypertrophic zones (PZ/HZ). The bottom of the model was fixed at the junction between the zone of provisional calcification (PC) and the metaphyseal cancellous bone; and the nodes at the subchondral bone plate surface were constrained to prevent translation in the horizontal direction and a vertical displacement was prescribed equal to 15 % of the overall growth plate thickness (height) representing normal physiological loading along the bone long axis (vertical axis). Bilinear axisymmetric quadrilateral hybrid elements (CAX4H) were used for all parts to avoid hour-glassing and

volumetric locking during analysis, which is caused by zero energy deformation modes because nearly incompressible material properties have been assigned for all regions. A mesh convergence study for the microscale model was done to optimize the mesh. The microscale model was run with all four cells and also with one cell at each depth individually which confirmed that there were no cell-cell interactions in the stress-strain field.

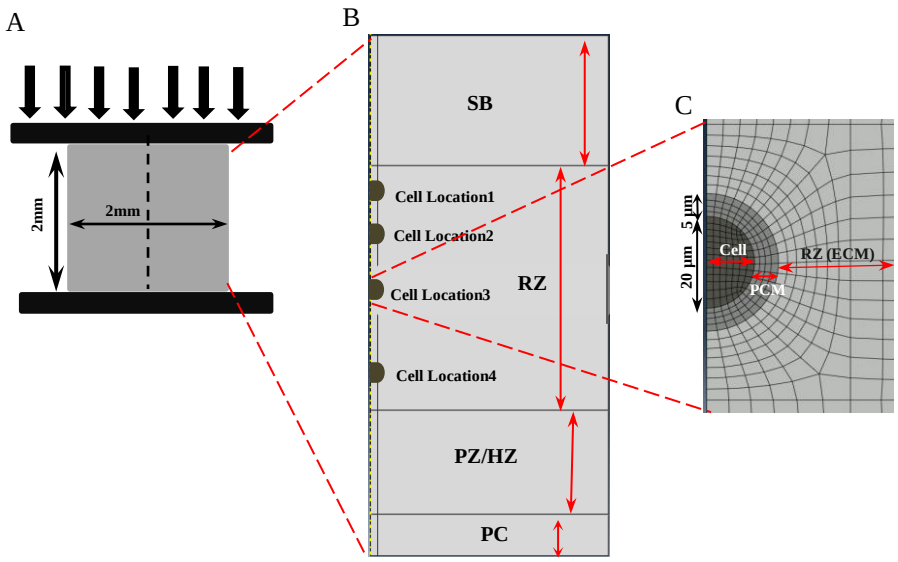

Fig. 4.1. Overview of the modeling approach. (A) Cross-section of a cylindrical plug of growth plate cartilage, subjected to a displacement of 15 % of the overall cartilage thickness. (B) Idealized axisymmetric model consisting of subchondral bone plate (SB), reserve zone (RZ), proliferative/hypertrophic zone (PZ/HZ), provisional calcification (PC). (C) Chondrocyte cell wrapped with a narrow region of pericellular matrix (PCM) embedded in extracellular matrix (ECM).

To evaluate the effect of the PCM on the stress-strain distribution in the chondrocytes, ECM material properties were assigned for the elements in the PCM region to compare it with the model in which chondrocyte, PCM and ECM material properties were defined to be different for each individual location. In addition, a 'macroscale' model without cells and PCM was analyzed to evaluate the volume-averaged stresses and strains in the same four cell/PCM locations within the reserve zone by assigning material properties of the ECM to the regions otherwise occupied by the cells and PCM. This allowed for

comparisons of stresses and strains over the same cell and PCM regions of the mesh in the microscale cell model as the macroscale cell model devoid of cells and PCM.

4.2.2 Stress-strain measurement

To analyze the interaction between cell and matrix and study the local stress-strain state of the cell, hydrostatic stresses and maximum tensile principal strains of the cells were calculated as the main key mechanobiological factors. The volume averaged hydrostatic compressive stress (volumetric or dilatational stress) and principal tensile strain (related to octahedral shear stress) of the cells and PCM were calculated according to equations (1) and (2), respectively.

$$\text{Average cellular stress}=\sum_{i=1}^{n} \sigma i\text{Evol}i/\sum_{i=1}^{n} \text{Evol}i \quad (1)$$

where i represent the element number, N is total number of the elements for the cell, Evol_i refers to the element volume and σ_i is hydrostatic stress for the i^{th} element.

$$\text{Average cellular strain}= \sum_{i=1}^{n} \varepsilon i/n \quad (2)$$

where i is the element number, ε_i represents the maximum tensile principal strain for each element within the cell and n is the total number of elements for each chondrocyte.

In this paper, the maximum principal strain was used as a substitute for octahedral shear stress since the maximum principal (tensile) strains in the cells and PCM of the reserve zone were found to vary by location in a very similar manner to the octahedral shear stresses. The maximum principal strain results were extracted in terms of logarithmic strains.

Cell height and width engineering strains were calculated based on the change in the horizontal diameter and vertical radius of the cell, respectively before and after compression. PCM height and width strains were also defined as the change in the vertical and horizontal wall thickness, respectively, of the PCM divided by the original wall thickness. This was also done for the reserve zone macroscale model which had no cells or PCM, by using the same mesh used for the microscale model in which cells and

PCM were present, but in which the reserve zone was homogenous (assigned Young's modulus and Poisson's ratio of the ECM).

4.3 Results

The results revealed a highly non-homogenous and depth-dependent strain field within and around the cells for the model that included the PCM and the model that excluded the PCM. Fig. 4.2 shows the contour plots of maximum principal tensile strain (logarithmic strain) distribution within and around the cell at different locations within the growth plate reserve zone. The magnitudes of the cell-averaged hydrostatic stresses and maximum principal tensile strains change throughout the depth of RZ as we move our viewpoint from close to the epiphyseal subchondral bone (cell location 1) to near the PZ/HZ interface (cell location 4) (Fig. 4.2).

4. 3.1 Influence of cell location within the reserve zone on chondrocyte stress and strain

When the PCM was included in the model, the cell-averaged maximum principal tensile strains within the chondrocytes increased in magnitude from a value of 6 % strain near the epiphyseal subchondral bone (SB) to 22 % near the proliferative zone (PZ) interface, representing a nearly 4-fold increase (Fig. 4.3A). Cellular height and width strains followed a similar trend (Fig. 4.3C). However, the opposite pattern was observed for the cell hydrostatic compressive stresses which decreased from a value 0.12 near the SB to 0.09 MPa near the PZ, an approximate location-dependent decline of 26 %. Fig. 4.2 represents how the presence of the PCM changes the stress-strain state around and within the cell.

The height and width strains of the matrix within the cell locations in macroscale model in which there were no cells within the matrix, are compared with the microscale model in which cells and PCM were present in Fig. 4.4.

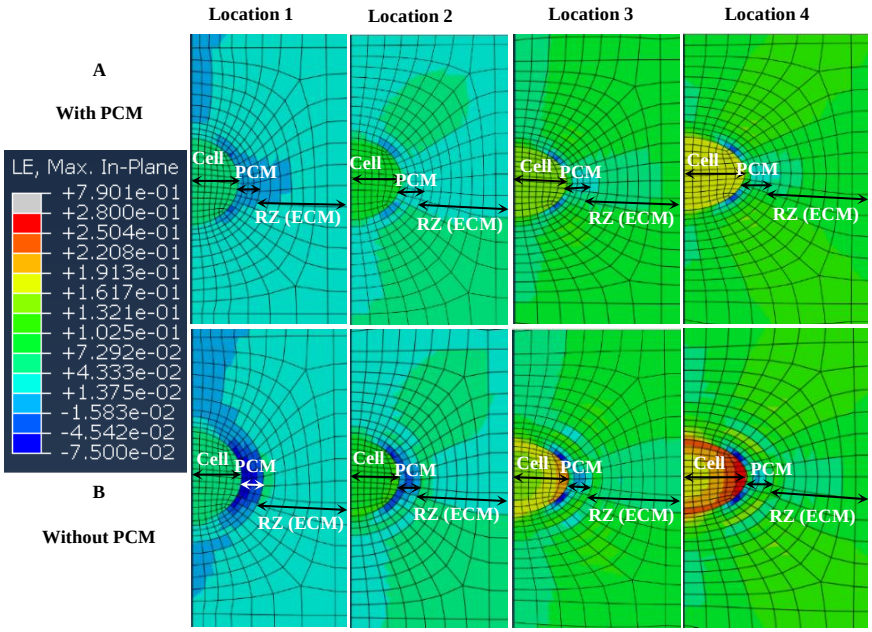

Fig. 4.2. Distribution of maximum principal strains around and within the cell for models (A) with PCM and (B) without PCM (when material properties of ECM are assigned to the PCM, i.e. PCM=ECM), for different locations of the cell within the reserve zone, moving from subchondral bone to proliferative zone, subjected to 15 % compression and using CAX4H elements.

4.3.2 Influence of the pericellular matrix on chondrocyte stress and strain

The presence of the pericellular matrix (PCM) resulted in an approximate 20 % increase in the cell-averaged maximum principal strains in reserve zone locations 2, 3 and 4 and in a 10 -12 % decrease in cell-averaged hydrostatic pressure. The influence of the PCM on strains was greatest for the cell located near the SB border where the presence of the PCM amplified the cell-averaged maximum principal strains by 45 % (Fig. 4.3B). Likewise, cellular height strain of the cell closer to the SB was most influenced by the presence of the PCM (Fig. 4.3D), while the influence of the PCM on cell width strains appeared not to vary much with cell location (Fig. 4.3D).

The height and width strains of the PCM followed similar trends to those for cell height and width (Fig. 4.5). Heights of both cells and PCM decreased under the compression, while their widths increased.

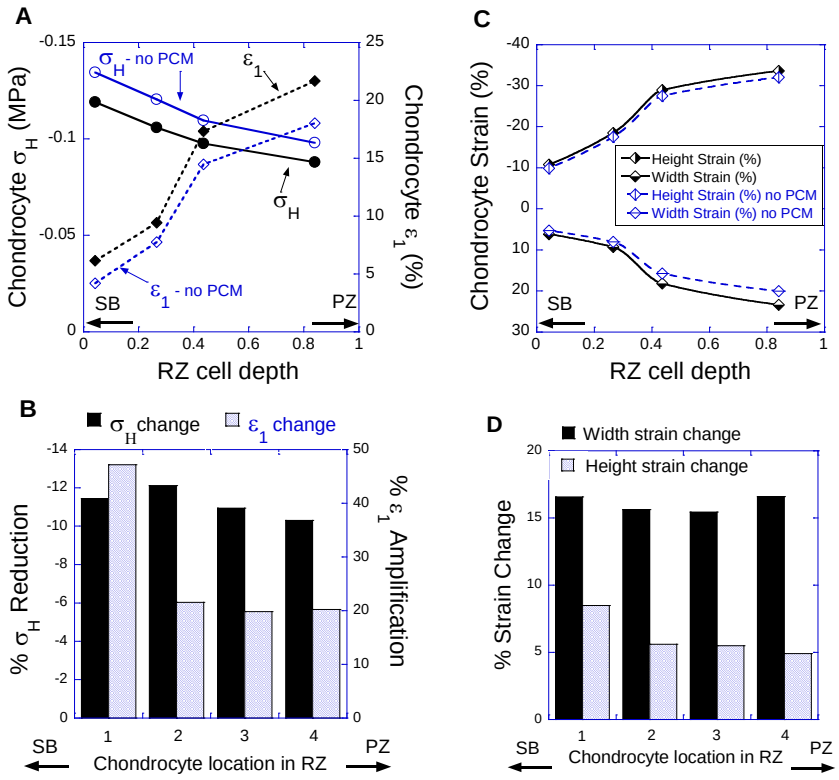

Fig. 4.3. (A) Cell-averaged hydrostatic stress and maximum principal tensile strain for cells in different locations within the reserve zone moving from subchondral bone (SB) to proliferative zone (PZ) subjected to 15% compression of the growth plate cartilage for two models (with/without PCM). (B) Changes in hydrostatic stress and maximum principal strain due to the presence of the PCM, (C) Chondrocyte height and width strains in locations 1-4, (D) Changes in width and height strains due to the presence of the PCM.

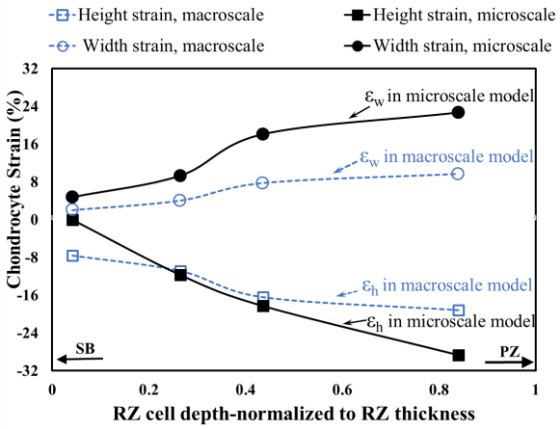

Fig. 4.4. Chondrocyte region height and width strains within each cell location moving from subchondral bone (SB) to proliferative zone (PZ) for: the microscale model in which cells and PCM are present; and the macroscale model in which there are no cells or PCM ('Chondrocyte Strain' in this case refers the ECM strain in the location of cell).

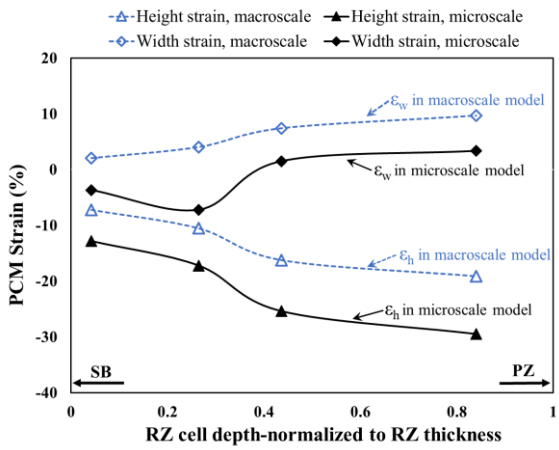

Fig. 4.5. PCM region height and width strains within each cell location moving from subchondral bone (SB) to proliferative zone (PZ) for: the microscale model in which cells and PCM are present; and the macroscale model in which there are no cells or PCM ('PCM Strain' in this case refers the ECM strain in the location of PCM).

4.4 Discussion and conclusion

We developed a computational model to simulate chondrocyte deformation and study chondrocyte–matrix interactions as a function of cell depth within the reserve zone of growth plate cartilage under physiological compression. The main objectives of the current study were to characterize the depth-dependent chondrocyte stress-strain distribution within the reserve zone and the influence of the microenvironment of the chondrocytes. Our findings indicate that the pericellular matrix (PCM) amplifies the cell's internal strains and the cell's height and width strains, while slightly reducing the cell's internal hydrostatic stress. The results showed that the state of stress and strain in the reserve zone chondrocytes are significantly depth dependent. The cell-averaged maximum principal strain increased from a minimum near the SB interface and reached maximum near the PZ interface. Cell height and width strains were also smallest at the SB border and greatest at the border with the PZ. This may play a role in preparing the reserve zone chondrocyte for cell alignment in the proliferative zone column of cells (chondron) and for the cells function as a daughter cell. In this study, the presence of PCM with a Young modulus value between that of the chondrocyte and ECM, decreased the cell-averaged hydrostatic stress, while it had the opposite effect on the cellular strains and acted as a strain amplifier, which is similar to the results reported for articular cartilage [4][11].

In particular, the cell-averaged maximum principal strains, cell height, and cell width strains all increased with cell location from the SB towards the PZ border where they reached maximal values. The addition of the PCM in the model further increased the maximum principal strains, width, and height strains near the PZ by about 20 %, 5 %, and 16.6 %, respectively. The most notable influence of the PCM in amplifying cellular strains occurred for the cell located near the subchondral bone, where cellular strains were at a minimum. This further suggests that the PCM may act as a mechano-transducer and serve as a transitional zone between cell and ECM. Our results revealed that PCM plays a more dominant role in regulating the micro-mechanical strain environment of chondrocytes near the interface with the much 'stiffer' subchondral bone.

Experimental and computational studies on PCM biological function and its chemical and mechanical properties, suggest that the PCM chemical composition, and physical and mechanical properties are directly proportional to one another [19]. The PCM can function as a thin barrier between the cell and ECM to filter molecules and regulate the biochemical environment of articular cartilage chondrocytes, and is hypothesized to have a prominent role in cartilage degeneration and osteoarthritis [12][32]. Computational studies of micromechanical environment of chondrocytes in different zones of articular cartilage imply that the PCM plays a dominant role in modifying the cellular stress-strain state; and any change in PCM properties with aging or cartilage abnormality can significantly affect the biophysical/biomechanical environment of the chondrocytes [18][33]. Computational modeling of articular cartilage has given rise to the idea that the PCM can act as a mechano-transducer between cells and ECM [4][11].

Generally, chondrocytes are responsible for making, maintaining and repairing extracellular matrix in response to mechanical loading. Despite the cited foregoing studies on cell-matrix interactions, it is not known how biomechanical signals are transmitted to the cell and transduced-exact molecular mechanisms and pathways are still unknown. One proposed general mechanism by which chondrocytes may sense mechanical signal variations, is through the alteration of cell shape and volume [6]. A confocal

microscopy study revealed that the micromechanical environment in articular cartilage is depth and zone dependent and causes an inhomogeneous and anisotropic deformation of the cells [6]. Other studies have proposed that primary cilia on the surface of the cell can act as mechanosensory organelles, which transduce mechanical forces into biological signals [34][35]. The PCM may function in conjunction with cilia to provide a feasible signal transducer [4][11]. In articular cartilage, the PCM reduces the local stress of the cell, providing a protective role for the PCM while amplifying the cellular strain [4][11]. The current study on growth plate cartilage reserve zone suggests a similar role for the PCM in the growth plate reserve zone. Understanding the sequence of events by which cells and ECM can communicate and convert the biomechanical and biochemical signals or signal transduction is still a challenge to investigators. Further evaluation how PCM components contribute to chondrocyte mechano-transduction in the reserve zone of growth plate cartilage may elucidate factors contributing growth abnormalities and disturbances and enhance our understanding of regulatory mechanical factors that modulate bone growth.

In the current model we have chosen to represent the reserve zone with a thickness slightly more than double the height or thickness of the proliferative and hypertrophic zones combined, based on our histological studies of twenty-day old mixed breed piglet distal ulnar growth plates. The relative thickness of each zone varies by age and location and may influence the reserve zone chondrocyte stress and strain magnitudes. We also chose to model a flat growth plate and need to explore the influence of mammillary processes on reserve zone cell stress and strain and the possible role that reserve zone cells might play in mammillary processes development.

Despite developing different macroscale models of the three zones of the growth plate for various loading conditions [24][36][37][27][38][39], to date there has been no model that includes chondrocytes in the reserve zone or of the interaction between reserve zone cells, PCM and ECM. Further computational studies of the Cell-PCM-ECM interaction in growth plate cartilage may generate new insight into the role of the micromechanical environment around chondrocytes in mechano-transduction

mechanisms in growth plate cartilage, which may be a key issue in in tissue engineering of bone and cartilage.

References

1. Abad, Veronica, Jodi L. Meyers, Martina Weise, Rachel I. Gafni, Kevin M. Barnes, Ola Nilsson, John D. Bacher, and Jeffrey Baron: The role of the resting zone in growth plate chondrogenesis. Endocrinology 143(4), 1851-1857 (2002).
2. Brighton, C. T.: The growth plate. The orthopedic clinics of North America 15(4), 571-595 (1984).
3. DeCamp, C. E.: The epiphyseal plate: physiology, anatomy, and trauma. Compendium (Yardley, PA) 31(8), 1-11 (2009).
4. Guilak, Farshid, and Van C. Mow: The mechanical environment of the chondrocyte: a biphasic finite element model of cell–matrix interactions in articular cartilage. Journal of biomechanics 33(12), 1663-1673 (2000).
5. Guilak, Farshid: Compression-induced changes in the shape and volume of the chondrocyte nucleus. Journal of biomechanics 28(12), 1529-1541 (1995).
6. Guilak, Farshid, Anthony Ratcliffe, and Van C. Mow: Chondrocyte deformation and local tissue strain in articular cartilage: a confocal microscopy study. Journal of Orthopaedic Research 13(3), 410-421 (1995).
7. Amini, Samira, Daniel Veilleux, and Isabelle Villemure: Three-dimensional in situ zonal morphology of viable growth plate chondrocytes: a confocal microscopy study. Journal of Orthopaedic Research 29(5), 710-717 (2011).
8. Amini, Samira, Daniel Veilleux, and Isabelle Villemure: Tissue and cellular morphological changes in growth plate explants under compression." Journal of biomechanics 43(13), 2582-2588 (2010).
9. Radhakrishnan, Priya, Naama T. Lewis, and Jeremy J. Mao: Zone-specific micromechanical properties of the extracellular matrices of growth plate cartilage." Annals of biomedical engineering 32(2), 284-291 (2004).
10. Campbell, Sara E., Virginia L. Ferguson, and Donna C. Hurley: Nanomechanical mapping of the osteochondral interface with contact resonance force microscopy and nanoindentation. Acta biomaterialia 8(12), 4389-4396 (2012).
11. Alexopoulos, Leonidas G., Lori A. Setton, and Farshid Guilak: The biomechanical role of the chondrocyte pericellular matrix in articular cartilage." Acta biomaterialia 1(3), 317-325 (2005).
12. Zhang, Zijun: Chondrons and the pericellular matrix of chondrocytes. Tissue Engineering Part B: Reviews 21(3), 267-277 (2014).
13. Alini, Mauro, Yasumoto Matsui, George R. Dodge, and A. Robin Poole: The extracellular matrix of cartilage in the growth plate before and during calcification: changes in composition and degradation of type II collagen." calcified tissue International 50(4), 327-335 (1992).

14. Alexopoulos, Leonidas G., Mansoor A. Haider, Thomas P. Vail, and Farshid Guilak: Alterations in the mechanical properties of the human chondrocyte pericellular matrix with osteoarthritis. Journal of biomechanical engineering 125(3), 323-333 (2003).
15. Poole, C. Anthony, T. T. Glant, and J. R. Schofield: Chondrons from articular cartilage (IV). Immunolocalization of proteoglycan epitopes in isolated canine tibial chondrons. Journal of Histochemistry & Cytochemistry 39(9), 1175-1187 (1991).
16. Ferguson, Virginia L., Andrew J. Bushby, and Alan Boyde: Nanomechanical properties and mineral concentration in articular calcified cartilage and subchondral bone. Journal of Anatomy 203(2), 191-202 (2003).
17. Allen, Daniel M., and Jeremy J. Mao: Heterogeneous nanostructural and nanoelastic properties of pericellular and interterritorial matrices of chondrocytes by atomic force microscopy. Journal of structural biology 145(3), 196-204 (2004).
18. Guilak, Farshid, Leonidas G. Alexopoulos, Mansoor A. Haider, H. Ping Ting-Beall, and Lori A. Setton: Zonal uniformity in mechanical properties of the chondrocyte pericellular matrix: micropipette aspiration of canine chondrons isolated by cartilage homogenization. Annals of biomedical engineering 33(10), 1312-1318 (2005).
19. Wilusz, Rebecca E., Johannah Sanchez-Adams, and Farshid Guilak: The structure and function of the pericellular matrix of articular cartilage. Matrix biology 39, 25-32 (2014).
20. McLeod, Morgan A., Rebecca E. Wilusz, and Farshid Guilak: Depth-dependent anisotropy of the micromechanical properties of the extracellular and pericellular matrices of articular cartilage evaluated via atomic force microscopy. Journal of biomechanics 46(3), 586-592 (2013).
21. Sanchez-Adams, Johannah, Holly A. Leddy, Amy L. McNulty, Christopher J. O'Conor, and Farshid Guilak: The mechanobiology of articular cartilage: bearing the burden of osteoarthritis. Current rheumatology reports 16(10), 451-460 (2014).
22. Alexopoulos, Leonidas G., Gregory M. Williams, Maureen L. Upton, Lori A. Setton, and Farshid Guilak: Osteoarthritic changes in the biphasic mechanical properties of the chondrocyte pericellular matrix in articular cartilage. Journal of biomechanics 38(3), 509-517 (2005).
23. Sergerie, Kim, Marc-Olivier Lacoursière, Martin Lévesque, and Isabelle Villemure: Mechanical properties of the porcine growth plate and its three zones from unconfined compression tests. Journal of biomechanics 42(4), 510-516 (2009).
24. Piszczatowski, Szczepan: Geometrical aspects of growth plate modelling using Carter's and Stokes's approaches. Acta of Bioengineering & Biomechanics 14(1), 93-106 (2012).
25. Maggiano, Corey: Confocal laser scanning microscopy as a tool for the investigation of tetracycline fluorescence in archaeological human bone, master thesis, university of Florida (2005).

26. Korhonen, Rami K., Petro Julkunen, Wouter Wilson, and Walter Herzog: Importance of collagen orientation and depth-dependent fixed charge densities of cartilage on mechanical behavior of chondrocytes. Journal of Biomechanical Engineering 130(2), 1-11 (2008).
27. Gao, Jie, Esra Roan, and John L. Williams: Regional variations in growth plate chondrocyte deformation as predicted by three-dimensional multi-scale simulations. PloS one 10(4), 1-18 (2015).
28. Vendra, Bhavya B., Esra Roan, and John L. Williams: Chondron curvature mapping in growth plate cartilage under compressive loading. Journal of the mechanical behavior of biomedical materials 84, 168-177 (2018).
29. Mente, P. L., and J. L. Lewis: Elastic modulus of calcified cartilage is an order of magnitude less than that of subchondral bone. Journal of Orthopaedic Research 12(5), 637-647 (1994).
30. Carter, D. R., B. Mikić, and Kevin Padian: Epigenetic mechanical factors in the evolution of long bone epiphyses. Zoological Journal of the Linnean Society 123(2), 163-178 (1998).
31. Wei, Hung-Wen, Shih-Sheng Sun, Shyh-Hua Eric Jao, Chiuan-Ren Yeh, and Cheng-Kung Cheng: The influence of mechanical properties of subchondral plate, femoral head and neck on dynamic stress distribution of the articular cartilage. Medical engineering & physics 27(4), 295-304 (2005).
32. Leddy, Holly A., Susan E. Christensen, and Farshid Guilak: Microscale diffusion properties of the cartilage pericellular matrix measured using 3D scanning microphotolysis. Journal of biomechanical engineering 130(6), 1-20 (2008).
33. Guilak, Farshid, Wendy R. Jones, H. Ping Ting-Beall, and Greta M. Lee: The deformation behavior and mechanical properties of chondrocytes in articular cartilage. Osteoarthritis and Cartilage 7(1), 59-70 (1999).
34. Shao, Yvonne Y., Lai Wang, Jean F. Welter, and R. Tracy Ballock: Primary cilia modulate Ihh signal transduction in response to hydrostatic loading of growth plate chondrocytes. Bone 50(1), 79-84 (2012).
35. Seeger-Nukpezah, Tamina, and Erica A. Golemis: The extracellular matrix and ciliary signaling. Current opinion in cell biology 24(5), 652-661 (2012).
36. Narváez-Tovar, Carlos A., and Diego A. Garzón-Alvarado: Computational modeling of the mechanical modulation of the growth plate by sustained loading. Theoretical Biology and Medical Modelling 9(1), 9-41 (2012).
37. Gao, Jie, John L. Williams, and Esra Roan: On the state of stress in the growth plate under physiologic compressive loading. Open Journal of Biophysics 4(1), 13-21 (2014).
38. Farzaneh, Solmaz, Oscar Paseta, and M. J. Gómez-Benito: Multi-scale finite element model of growth plate damage during the development of slipped capital femoral epiphysis. Biomechanics and modeling in mechanobiology 14(2), 371-385 (2015).

39. Gao, Jie, John L. Williams, and Esra Roan. "Multiscale modeling of growth plate cartilage mechanobiology. Biomechanics and modeling in mechanobiology 16(2), 667-679 (2017).

Chapter 5

Depth and strain-rate dependent mechanical response of chondrocytes in reserve zone cartilage subjected to compressive loading

5.1. Introduction

Growth plate cartilage consists of two main components: interstitial fluid consisting of water with dissolved solutes and a solid matrix comprised mainly of collagen and proteoglycans (Mow et al. 1980). Previous studies on articular cartilage have shown that cartilage behaves as a biphasic material and deformation of the tissue induces fluid flow through the solid matrix (Mow et al. 1980, 1990). Due to the high-water content of cartilage (~70%), the interstitial fluid plays a vital role in the tissue response to physiological loads (Lai et al, 1980). When cartilage is loaded at high strain rates with short time scales of the order of < 200 ms, such as during heel strike phase in gait, the interstitial fluid becomes trapped and has insufficient time to flow through the pores. The tissue then behaves as an incompressible, single-phase elastic material (Eberhardt et al.1990). Under conditions with longer time scales fluid can flow through the tissue and the behavior becomes time-dependent, in which case poroelastic or biphasic theories can be employed. Both elastic models (Gao et al. 2014, 2015, 2017; Kazemi and Williams 2019; Leipzig et al. 2008; Nguyen et al. 2010; Sylvestre et al. 2007) and poroelastic computational models (Cohen et al. 1994, 1998; Komeili et al. 2020; Lacroix et al. 2002; Sergerie et al. 2009; Wu et al. 1997, 2000) have been developed to investigate the response of articular, growth plate, and fracture healing tissues to compression. Multiscale elastic models of the growth plate that include chondrocytes arranged in zonal distribution patterns have also been developed (Sergerie et al. 2009; Gao et al. 2015, 2017; Kazemi and Williams 2019) to investigate the effects of forces applied across the growth plate on the mechanics at the cellular level.

Physiological loading modulates endochondral ossification and regulates cellular activity (Bries et al. 2012; Carter et al. 1998; Frost 1990; Song et al. 2013). The ability of chondrocytes to sense the mechanical environment is vital in the structural adaptation of cartilage to loading. Several mechanisms have been reported to explain signal transmission and consequent metabolic responses of chondrocytes. Cells may sense external stimuli by means of the stress-strain state produced at the cell boundary due to differences between matrix and cell mechanical properties. Cellular strains and fluid flow-induced shear stress, imposed during tissue compression, act as mechanical stimuli through a variety of possible mechanisms including integrin receptors and stretch-activated activated ion channels (Cancel et al. 2009; Alexopoulos et al. 2005; Guilak and Mow 2000). The pericellular matrix (PCM) may also serve as a possible signal transducer for cells (Kazemi and Williams 2019; Seeger and Golemis 2012; Shao et al. 2012) in conjunction with the primary cilia. The primary cilium can act as an antenna on the cell surface to sense biomechanical and biochemical signals within the matrix (Lacroix et al. 2002; Yellowley et al. 1997). In order to study the various mechanisms involved in the complex process of mechanical transduction, it is first necessary to precisely define the stress, strain, and fluid flow environments in the vicinity of the cartilage cell. A variety of studies have evaluated the mechanical properties and stress-strain distribution within growth plate cartilage either experimentally, using confined or unconfined compression (Cohen et al. 1994; Sergerie et al. 2009), tensile testing (Williams et al. 2001), nanoindentation (Radhakrishnan et al. 2004), image-based strain mapping (Wosu et al. 2012), or computational modeling (Cohen et al. 1998; Gao et al. 2015; Shefelbine and Carter 2004). Elastic models of growth plate cartilage have suggested that maximum principal strain, or distortional strain, and hydrostatic stress act as mechanoregulatory factors at the tissue level in the differentiation of cells to produce cartilage and bone (Carter and Wong 1988; Pauwels 1960). It has also been suggested that fluid-flow-induced shear stresses may provide a biophysical stimuli to regulate tissue differentiation in bone fracture healing (Lacroix et al. 2002). Multiscale elastic models have shown that these principles also apply at the cell level for chondrocytes in the proliferative and hypertrophic zones (Gao et al. 2015, 2017) and reserve zone (Kazemi and Williams 2019) of the growth plate. However, these multiscale models did

not consider the biphasic nature of the growth plate and cannot provide insight into any time-dependent and fluid-related mechanoregulatory factors. Furthermore, while the biochemical and physiological function of the proliferative and hypertrophic zones has been extensively studied the function of the reserve zone has long been unclear, as reserve zone cells appear to be in a quiescent state, but recent studies have shown that this zone contains a stem cell niche, which contributes cells to the columnar or proliferative zone and which we hypothesize may also contribute to subchondral bone formation in response to mechanoregulatory signals (Hallett et al. 2019; Kazemi and Williams 2018; Lui 2020; Matsushita et al. 2020).

The fluid flow boundary conditions at the two growth-plate chondro-osseous interfaces have been noted to be critical to the mechanical behavior of the cartilage (Cohen et al. 1994). By fitting computational biphasic model (Cohen et al. 1994) results to stress relaxation experiments, it was hypothesized that the interface of the epiphysis is more likely impermeable, while the large open marrow pores within the metaphysis is more permeable (Cohen et al. 1994). The relative permeability of articular and growth plate borders with bone was also investigated experimentally in an MRI study during simulated cyclic gait loading of sheep knee specimens (Song et al. 2013). The rate of consolidation and recovery of the articular cartilage was found to be slower than that of the growth plate cartilage, which was thought to be due to the open pore structure of the zone of provisional calcification and its border with metaphysis, whereas the dense subchondral bone underneath of articular cartilage limited the fluid exchange (Song et al. 2013). Beyond these studies, the question of the biomechanical effects of fluid exchange across the growth plate chondro-osseous junctions on the mechanical environment of chondrocytes in the growth plate remains unexplored, and more experimental and computational studies are required to address the fluid flow boundary conditions and their influence on tissue and cell response.

The main objective of this study was to develop a poroelastic multiscale finite element model of reserve zone cells within hydrated cartilage to characterize the stress-strain environments within and around reserve zone cells caused by the movement of interstitial fluid under pressure. We believe that such a numerical approach can provide insight into the mechanotransduction events by which the

mechanical microenvironment within and around chondrocytes and stem cells regulates cell differentiation and proliferation in the reserve zone. We hypothesized that fluid flow across the cell membrane, fluid-induced shear stress at the cell surface, cell membrane strains, and cell shape changes may provide mechanotransduction signals in reserve zone chondrocytes. We hypothesized that these mechotransduction signals would be different in reserve zone cells near the subchondral bone than near the proliferative zone, and that their purported role in the process of organizing the growth plate into distinct zones of proliferation and hypertrophy during endochondral bone growth (Abad et al. 2002) would be related to these signals. To explore this we investigated the influence of loading rate and the reserve zone fluid boundary conditions on cell deformation. Such a numerical approach can enhance our understanding of the mechanical interactions between the cell and its surrounding matrix in zone of the growth plate.

5.2. Materials and Methods

5.2.1 Global macroscale model description

An idealized axisymmetric multiscale finite element model of the physis representing a 5-mm diameter cylindrical plug of bone/growth-plate-cartilage/bone was developed using Abaqus/CAE 2019 (SIMULIA, USA). The top and bottom surfaces of the model were assumed frictionless, and impermeable (Fig. 5.1). The displacements normal to bottom surface and to the axis of symmetry were blocked while, on the other hand, the lateral side parallel to the axis of symmetry was unconstrained and the pore pressure set to zero to simulate free draining from the side. The model was subjected to unconfined compression by applying a displacement to the top surface as a ramp function until it reached 0.025 mm or 5% of the overall growth plate cartilage thickness (0.5 mm) it was then held at that position until time = 1000 s, in order to simulate a stress relaxation test. The ramp loading was applied using strain rates of 0.18%/s, 5%/s, 50%/s, and 200%/s. The total reaction force at the base of the model was calculated as a function of time for comparison with experimental stress relaxation data.

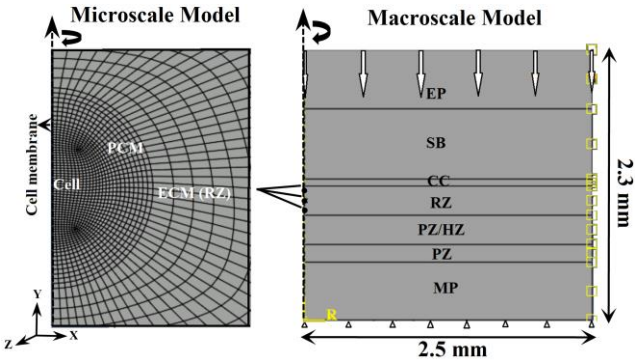

Fig.5.1. The idealized axisymmetric poroelastic model shows tissue (macroscale) and cell (microscale) levels for cells positioned at three locations within the RZ. The tissue was subjected to a displacement of 5% of the cartilage thickness parallel to the axis of axisymmetry. It is restrained at the bottom (in the y-direction) and fluid is free to drain laterally. It includes the epiphysis (EP), subchondral bone (SB), calcified cartilage (CC), growth plate cartilage (reserve zone (RZ), and proliferative/hypertrophic zone (PZ/HZ)), provisional calcification (PC), and metaphysis (MP). The microscale model consists of three chondrons embedded in the extracellular matrix (ECM). All chondrons are composed of chondrocyte cells surrounded by a thin cell membrane and enveloped by a pericellular matrix (PCM).

It was assumed that the growth plate was flat and oriented perpendicularly to the axis of symmetry of the specimen. The macroscale model included epiphyseal bone (EP), subchondral bone (SB), calcified cartilage (CC), growth plate reserve zone (RZ), growth plate proliferative/hypertrophic zone (PZ/HZ), provisional calcification (PC), and metaphyseal bone (MP). All layers were considered to be poroelastic materials with fluid phase and homogeneous solid phase. In the implementation in Abaqus it was assumed that the fluid and solid phases were incompressible. All tissues were assigned linear elastic isotropic material properties and isotropic permeability values (Tables 5. 1 & 5.2). To account for large deformation and the effect of geometrical nonlinearity NLGEOM was activated in Abaqus and finite element strains are reported as logarithmic strains. The total number of elements in the global model was 11,903. A biased mesh was used to provide a transition in mesh density and element size. Closer to the axis of symmetry, the element size was much smaller than towards the lateral side. The mean edge length

of elements in the global model was 0.48 μm. Closer to the cell region, this value decreased to about 0.2 μm.

Table 5.1. Material properties of different layers in the macroscale model.

Tissue	E (MPa)	ν	K_0 (mm^4/N.s)	e_0	M (dimensionless)	Thickness (mm)*
Subchondral bone (SB)	2000 (Moo et al. 2014)	0.2 (Moo et al. 2014)	90 (Hwang et al. 2008)	0.176 (Moo et al. 2014)	-	0.6
Calcified cartilage (CC)	300	0.2 (Fan et al. 2009)	90 (Stender et al. 2017)	1.1 (Stender et al. 2017)	-	0.06
Reserve zone (RZ)	0.98 (Gao et al. 2015)	0.125 (Sakai et al. 2015)	1.41 × 10-3 (Sergerie et al 2009)	4.25 (Sakai et al. 2015)	5.48 (Stender et al. 2017)	0.25
Proliferative/Hypertrophic zone (PZ/HZ)	0.49 (Gao et al. 2015)	0.125 (Sakai et al. 2015)	5.8×10^{-3} (Sergerie et al 2009)	3.6 (Sakai et al. 2015)	6.435** (Stender et al. 2017)	0.25
Provisional calcification (PC)	100	0.2	22.5×10^{5}***	3.5****	-	0.15
Epiphysis (EP)	1000	0.2	45.3×10^{5} (Hwang et al. 2008)	3.7 (Stender et al. 2017)	-	0.5
Metaphysis (MP)	1000	0.2	45.3×10^{5} (Hwang et al. 2008)	3.7	-	0.5

* Based on our histology of growth plate for a 480-day-old pig proximal femur (Kazemi and Williams 2020). The harvesting of tissue was exempt from IACUC review as it was obtained from euthanized animals in another University of Memphis IACUC approved study.
** This value was obtained by averaging values of the middle zone and deep zone of articular cartilage tissue.
*** This value is assumed to be half of the EP/MP permeability
**** A value close to that of the HZ.

The permeability of growth plate cartilage zones (RZ and PZ/HZ) was assumed to be strain-dependent while it was assumed to be constant within the less deformable bone and calcified cartilage regions in the model. The strain-dependent hydraulic permeability, or mobility (mm^4/N.s), was defined in terms of the void ratio and current strain by Equation 5.1 (Ficklin et al. 2009; Lai and Mow 1980), and was utilized to define the permeabilities of the RZ and PZ/HZ in the macroscale model and of the cell, cell membrane, and PCM in the microscale model.

$$k = k_0 \left[\frac{e}{e_0}\right]^2 exp\left(\frac{M}{2}\left(\left(\frac{1+e}{1+e_0}\right)^2 - 1\right)\right), \quad (1)$$

where k_0 refers to the initial hydraulic permeability at zero strain (mm^4/N.s), e_0 and e are initial and current void ratios and M is a non-dimensional constant that accounts for the additional compaction of the cartilage due to diffusive drag causing a nonuniform and nonlinear decrease of permeability with increasing strain of the tissue (Lai and Mow 1980, 1981; Ficklin et al. 2009). The initial void ratio was defined by the volume fraction of fluid divided by the volume fraction of solid at 0% strain. The current void ratio, e, can be measured from the applied strain by the relationship (Sakai et al. 2015):

$$\varepsilon = (e - e_0)/(1 + e_0) \quad (2)$$

We provided the permeability values in the Abaqus program by means of a user-defined lookup table that lists the hydraulic conductivity (mm/s) values as a function of the void ratio which were obtained by multiplying the hydraulic permeability ($mm^4/N.s$) calculated from equation 1 (Mow et al. 1980) by the specific weight of the wetting fluid (9.81×10^{-6} N/mm^3) assumed to be water at body temperature (Stender et al. 2017). All layers were assumed to be initially fully saturated with fluid. The hydraulic permeability for the marrow spaces in cancellous bone of the metaphysis and epiphysis was estimated by dividing values of bone permeability published in units of $length^2$ (Grimm and Williams 1997; Nauman et al. 1999) by the dynamic (absolute) viscosity of water.

5.2.2. Microscale submodel model description

The submodel function within Abaqus was used to transfer displacements, reaction forces, and pore pressures from the global model as boundary conditions for the microscale submodels (Fig. 1). Microscale submodels were created for three poroelastic chondrocytes surrounded by a thin cell membrane and wrapped with a narrow region of pericellular matrix (Poole et al. 1987), all embedded within the reserve zone. Cells were assumed to be perfectly bonded to the matrix. A normalized cell depth, ξ, was defined vertically from RZ-CC borders with $\xi = 0$ to the RZ-PZ/HZ border with $\xi = 1$. Cell 1 (closest to CC border) is located at $\xi = 0.08$, cell 2 (in the middle of RZ) is embedded in $\xi = 0.48$, and cell 3 (closest to PZ/HZ border) is at $\xi = 0.84$. To represent the poroelastic nature of the cartilage tissue and chondrocytes, a four-node bilinear displacement and pore pressure element (CAX4P) was used. A mesh refinement study was performed by increasing the number of elements in the cell region until the maximum principal strains and fluid velocities in the cells became independent of the mesh resolution, which occurred when the number of elements inside the cell reached 300 with edge lengths of 0.13μm or less. The material properties for the microscale model are listed in Table 5.2.

Table 5.2. Material properties used for microscale model.

Region	E (MPa)	ν	k_0 (mm^4/N.s)	e_0	M (dimensionless)*	Radius (μm)
Cell	0.002 (Gao et al. 2015)	0.04 (Alexopoulos et al. 2005)	4.2×10^{-3} (Moo et al. 2014)	4.88 (Moo et al. 2014)	5.48	5 (Kazemi and Williams 2019)
Cell membrane	4×10^{-2} (Moo et al. 2014)	0.04 (Alexopoulos et al. 2005)	3×10^{-9} (Moo et al. 2014)	3 (Moo et al. 2014)	5.48	0.1 (Moo et al. 2012)
Pericellular matrix (PCM)	0.265 (Gao et al. 2015)	0.04 (Alexopoulos et al. 2005)	4×10^{-5} (Wu and Herzog 2000)	4 (Wu and Herzog 2000)	5.48	0.5 (Kazemi and Williams 2019)

*The same value that was used for ECM (RZ) in the macroscale model (Moo et al. 2014).

To study the effect of the permeability boundary conditions at the calcified cartilage interfaces on the transient response of the cell and fluid flow across the cell membrane, a second model was developed in which the hydraulic permeability of the CC (k_0 = 90 mm^4/N.s) was replaced with very low permeability value (k_0 = 5.8× 10^{-3} mm^4/N.s) to represent a nearly impermeable interface with the reserve zone.

Cell-averaged maximum tensile principal strain, cell height, cell width strain (Kazemi and Williams 2019), and cell membrane fluid pressure were calculated for all cases. The fluid flow-induced shear stress was calculated at three locations on the cell surface (0, 90, and 180 degrees) by $\tau = \mu \, \mathrm{d}\upsilon/\mathrm{d}n$ in which μ is the dynamic fluid viscosity, defined as 10^{-3} Pa.s, and $\mathrm{d}\upsilon/\mathrm{d}n$ is the surface fluid velocity gradient perpendicular to the cell surface (Gupta et al. 2006; Lavagnino et al. 2008). All the results were extracted at 95% of the peak applied displacement (4.5% nominal strain across the growth plate cartilage) to avoid any possible numerical artifact that may result from sudden zero acceleration at the peak applied load (5% strain) in the ramp function. The data were extracted at t = 25, 0.9, 0.09 and 0.0225s for 0.18%/s, 5%/s, 50%/s and 200%/s, respectively, corresponding to the times required to reach 4.5% strain. Finite element strains are reported as logarithmic strains, while the nominal applied strains are given as engineering strains and cell deformation strains reported as % change in cell height and width compared to the unloaded circular dimensions.

5.3. Results

Depth-dependent maximum principal strains and fluid pressures in the cells are shown in bar graphs, grouped by cell location within the RZ for all the applied strain rates (Fig. 5.2 a).

5.3.1. Intracellular maximum principal strain

For the three lowest strain rates (0.18%/s, 5%/s, and 50%/s), the maximum principal strain in the cell decreased from the calcified cartilage (CC) border ($\xi = 0.08$) to the proliferative/hypertrophic (PZ/HZ) interface ($\xi = 0.84$). The highest magnitude of maximum principal strain (9%) was experienced at an applied strain rate at 5%/s by the cell nearest to the CC border, representing a 2-fold amplification of applied tissue strain. In contrast, at a loading rate of 200%/s, the maximum principal strain magnitude in the cell increased from the CC border to the PZ/HZ interface. This reversal in the pattern with cell location can be seen to already begin at a strain rate of 5% between cell locations in the middle of the reserve zone and the cell close to the proliferative zone (Fig. 5.2 a). Decreasing the permeability of the CC decreased all the strain values, but did not change the overall cellular strain pattern (Fig. 5.2 b). Restricting fluid transfer across the CC caused the maximum principal strains in the cell closest to the CC to decrease by nearly 33% and 63% at 5%/s and 50%/s respectively (Fig. 5.2 b), whereas it increased slightly (20%) for the cell near the PZ/HZ at 50%/s and 200%/s.

5.3.2. Intracellular fluid pressure

Fig. 5.2 c & d represent the fluid pressure within the cell for the conditions of a permeable and impermeable CC. Cell fluid pressures at all three locations increased with the applied strain rate. At each individual strain rate, there were no significant differences in cell fluid pressure for cells at different locations (Fig. 5.2 c). The smallest magnitude in pressure of 0.02 MPa occurred at the slowest loading rate when fluid had time to flow and the interstitial fluid pressure had dissipated. Preventing fluid exchange across the CC caused a slight increase cell fluid pressures in all locations (Fig. 5.2 d) and the highest increase happened at 5%/s (23%) and 50%/s (15%) for cell closest to CC border.

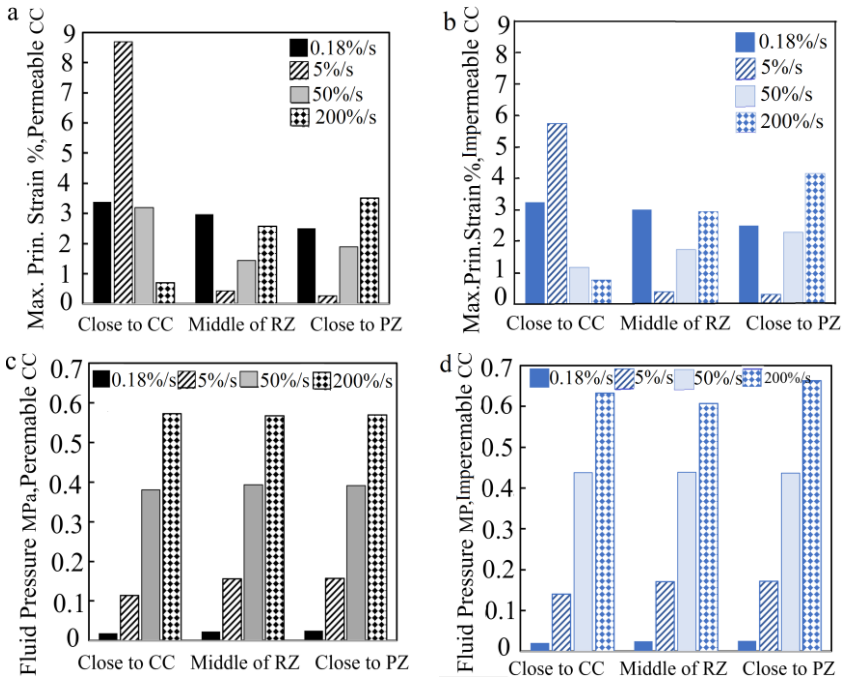

Fig. 5.2. Comparison of maximum principal strains (logarithmic strains) and fluid pressures with permeable (a&c) and impermeable calcified cartilage properties (b&d) at the 4.5% strain time point and 0.18%/s, 5%/s, 50%/s, and 200%/s strain rates for three cells embedded in the reserve zone (RZ).

5.3.3. Cell height and width strain

The magnitudes of cellular height and width strains followed a similar trend with cell location as did maximum principal strains (Fig. 5.3 a & c). The positive values of cellular width strain and negative values of height strain indicate that cells flattened under the applied compression (Fig. 5.3 a & c). The width strain values closely matched those of maximum principal strains at each equivalent cell location and strain rate, indicating that the maximum principal strains acted across the width of the cells and were highly location-dependent. Restricting fluid from crossing the CC decreased the cell height change by 27% and increased the width change by 30%, respectively, at the 5%/s strain rate for the cell nearest the CC border and caused slight increases in the cell width and height changes in the cell close to the PZ at 50%/s (21% for both height and width) and 200%/s (16% for both height and width) (Fig. 3 5.b & d).

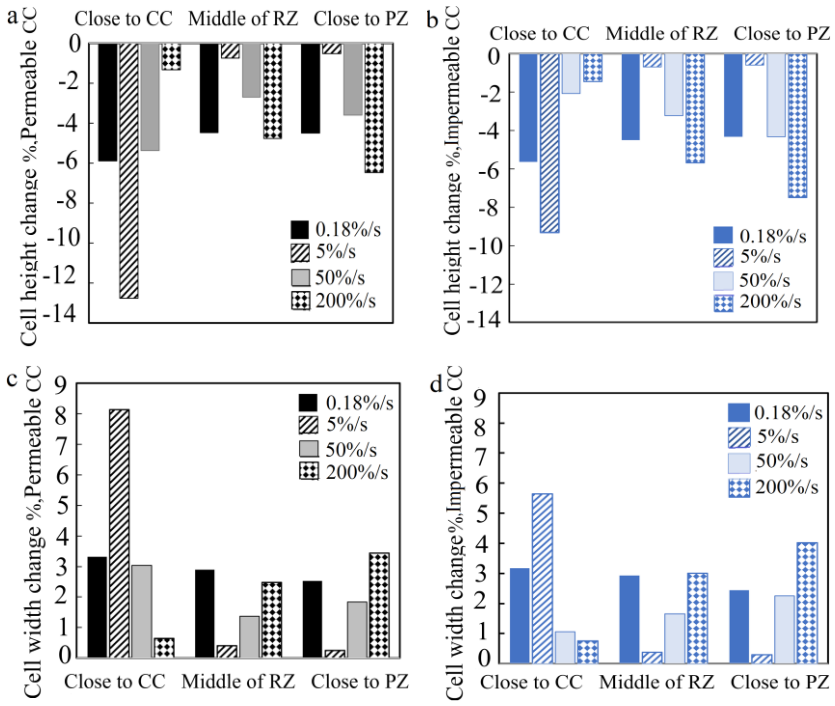

Fig.5.3. Depth-dependent cellular height- (a, b) and width- (c, d) strains with permeable (a&c) and with impermeable calcified cartilage properties (b&d) at 4.5% strain for 0.18%/s, 5%/s, 50%/s and 200%/s strain rates.

5.3.4. Fluid velocity across the cell membrane

As can be seen for the cell close to the CC the resultant fluid velocity vectors across the cell membrane are not distributed uniformly around the cell periphery (Fig. 5.4). For permeable boundary conditions at the CC/RZ interface, the maximum fluid velocity values are found at the top surface toward the subchondral bone at all applied strain rates (Fig. 5.4 a). As with cellular maximum principal strain, the maximum magnitudes of the fluid velocity occurred at 5%/s and the lowest at 200%/s. Impermeable boundary conditions at the CC/RZ interface caused the fluid velocity across the cell membrane to decrease in all cases (Fig. 5.4 b). While an impermeable CC did not affect the direction of fluid flow at the three lowest strain rates (0.18%/s, 5%/s, and 50%/s), it did cause a reversal in the direction of fluid flow across the cell membrane at the highest strain rate of 200%/s (Fig. 5.4 b -far right) such that fluid flowed into the cell over much of the top half and out of the bottom half in contrast to what happened

when the CC was permeable and the fluid mainly flowed out of the top of the cell (Fig. 5.4). Lower CC permeability also tended to change the pattern of flow direction within the cell as well (relative plots not included) as across the cell membrane for the 200%/s strain rate due to the increased resistance to flow across the CC border. For a permeable CC the peak fluid velocities across the membrane were 0.45 $x10^{-6}$, 1.63 $x10^{-6}$, 0.55 $x10^{-6}$, and 0.02 $x10^{-6}$ mm/s at the strain rates of 0.18%/s, 5%/s, 50%/s and 200%/s, respectively. For an impermeable CC the corresponding peak transmembrane fluid velocities were 0.43 $x10^{-6}$, 0.98 $x10^{-6}$, 0.16 $x10^{-6}$, and 0.006 $x10^{-6}$ mm/s.

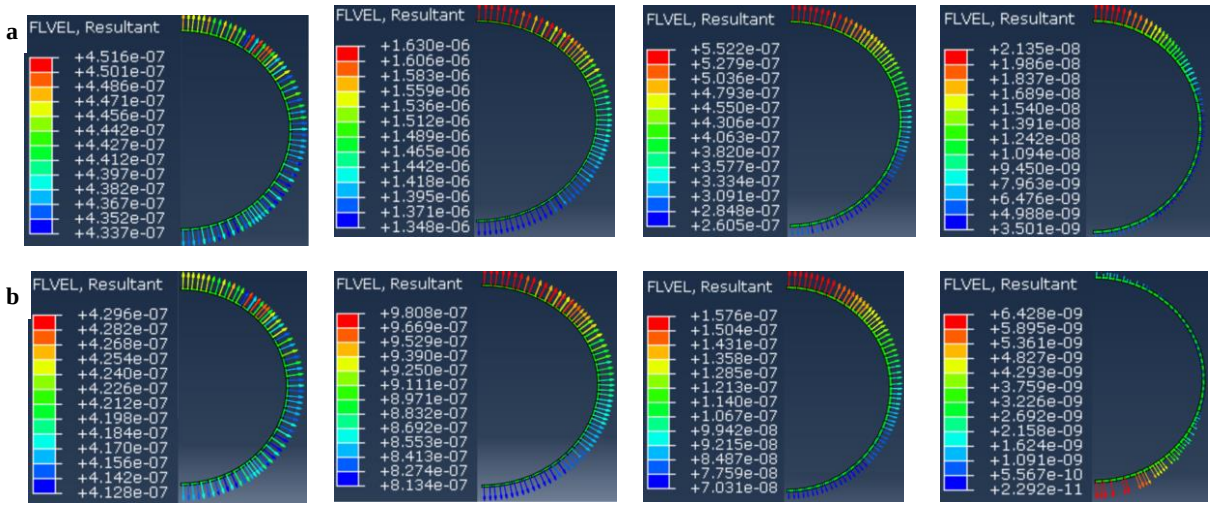

Fig. 5.4. The vector plots for fluid effective velocity (mm/s) across the cell membrane for the cell close to CC border at 4.5% applied strain, a) Permeable CC at 0.18%/s, 5%/s, 50%/s and 200%/s strain rates from left to right, respectively; and b) Impermeable CC at 0.18%/s, 5%/s, 50%/s and 200%/s strain rates from left to right, respectively.

5.3.5. Cell membrane strain

Our microscale model predicted that the maximum tensile strain in the cell membrane (logarithmic strains in the x-direction) occurred at the top and bottom of the cells, where these were acting tangentially along the membrane. For the cell located near the CC, it was generally much higher at 5%/s than at other strain rates. This strain component followed a similar trend with location to what was reported for width and height strain at all strain rates (Fig. 5.5 a). For the cell near the CC, imposing nearly impermeable conditions in the CC/RZ interface had the smallest effect at the slowest and highest

strain rates (Fig. 5.5 b). However, it caused the tangential membrane strain to decrease by about 26.5% at 5%/s and 66.5% at 50%/s for the cell closest to the impermeable CC border.

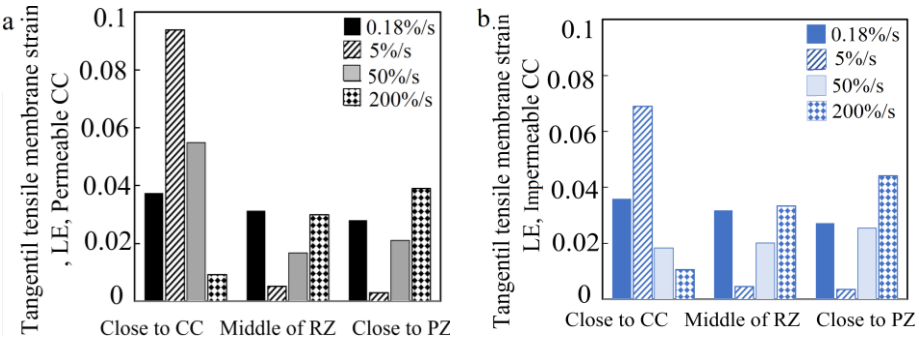

Fig. 5.5. Peak tangential tensile membrane strains for cells located at the calcified cartilage border, middle of the reserve zone, and close to proliferative/hypertrophic zone border subjected to 5% strain at four different strain rates assuming permeable (a) and impermeable (b) calcified cartilage properties.

5.3.6. Fluid flow-induced shear stress at the cell membrane surface

The magnitude of fluid flow-induced shear stress varied with position along the surface of the cell and with cell location through the RZ depth. Shear stress values are presented only for the permeable CC boundary conditions (Fig. 5.6). Strain rate had a profound effect on the localized shear stress at the cell surface with by far the greatest magnitude at 200%/s for the cell close to the CC (Fig. 5.6), where at cell equator (90-degree angle), there was a drastic 2.6 and 8 fold increase in the shear stress, compared to the shear stress values at the poles, 0 and 180 degrees, respectively (Fig. 5.6 c). At smaller rates, the north and south poles on the cell surface (0 and 180 degrees) experienced almost identical values of shear stress.

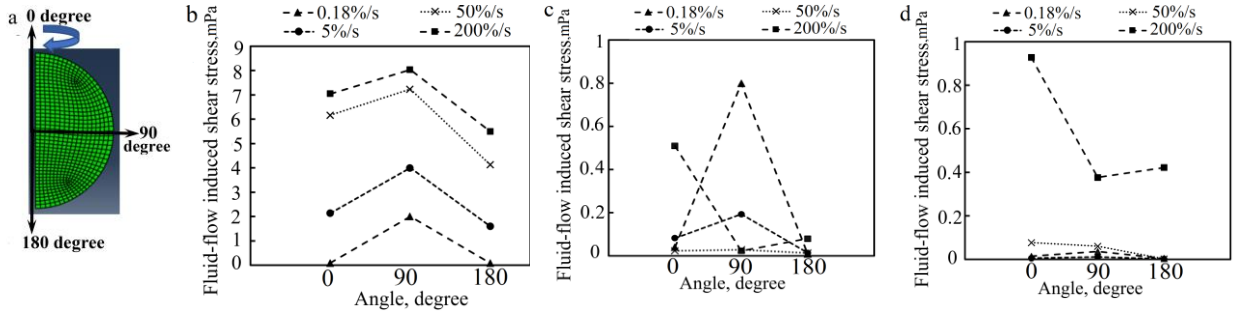

Fig. 5.6. The peak values of depth-dependent fluid flow shear stress at a) the cell surface for three angles of 0, 90, and 180 degrees, for b) the cell close to calcified cartilage border, (c) the cell in the middle of the RZ and (d) the cell close to the PZ border at 4.5% strain for four different strain rates with permeable calcified cartilage properties.

5.4. Discussion

In this study, a multiscale poroelastic model was developed to investigate the compressive behavior of the cell at various depths within the reserve zone (RZ) of the growth plate and at different strain rates using a poroelastic finite element modeling framework. The model consists of 0.5 mm layers of cancellous bone on either side of the 0.5 mm thick growth cartilage and includes the subchondral bone plate with a layer of calcified cartilage between the plate and the cartilage. Linear elastic properties were assumed for the solid structures and the permeability of growth plate cartilage was assumed to be strain-dependent while it was assumed to be constant for all the other parts of the model. Loading was applied by means of a ramp displacement function at four different strain rates until a nominal strain of 5% across the growth plate cartilage. These strain rates may be more easily interpreted in terms of the approximate time durations over which the ramp loading was applied, 25s, 0.9s, 0.09s and 0.0225s.

5.4.1. Depth-dependent pattern of cell strains and cell membrane strain

The results of the study revealed that all the cell strain magnitudes (maximum principal strain, cell width and height strains, and peak tangential membrane strains) were highly dependent on the depth of the cell within the RZ and the rate of loading. The effects of increasing loading rates on cellular strains presented a complex pattern. At the three slower rates of loading, strain measures decreased with depth for a given loading rate as the cell location within the RZ moved from the CC to the proliferative zone

(PZ). This decrease was gradual for 0.18%/s, but a drastic decrease was observed for the 5%/s rate between the cell near the CC and the cell in the middle of the RZ. At the third higher loading rate of 50%/s, all the strain measures deceased from the CC to the middle before increasing slightly near the PZ. At the fastest loading rate, a reverse pattern was observed in which all the strain measures increased steadily with cell depth within the reserve zone. This pattern may be explained by considering the internal cell pressure and the velocity of the fluid exuded from the cell.

Fluid flow has a significant influence on cell deformation. The highest cellular strain of the cell close to CC at 5%/s results from the higher fluid flow out of the cell across the cell membrane. Higher fluid flow can result from higher pore pressure within the cell than that in the matrix. A larger pore pressure implies a larger pressure gradient and consequently larger relative fluid velocities (Accadbled et al. 2008). The less permeable boundary condition at the rapid impact of 200%/s diverts most of the fluid flow around the cell resulting from the increased resistance to fluid exchange through the chondro-osseous junction.

In our study at faster strain rate, the highest tangential strain in the cell membrane occurred at the north and south poles (top and bottom), which may be the possible locations of cell damage at high strain levels and strain rates. Membrane stretch can be possible mechanism for mechanical signal transduction by activating the ion channels (Guharay and Sachs 1984; Morris and Sigurdson 1989). It has been suggested that the tangential membrane strain may have a role in chondrocyte death during compression (Moo et al. 2012). Short bouts of impulsive strain rates can lead to cell damage (Argote et al. 2019; Moo et al. 2012; Morris and Sigurdson 1989)

5.4.2. Depth-dependent intracellular fluid pressure and the influence of CC permeability

Intracellular fluid pressure was found to be relatively independent of the cell depth within the RZ and of CC permeability, increasing only slightly as the CC permeability was reduced. Cellular fluid pressures increased with increased strain rates from 0.02 MPa at 0.18%/s to about 0.58 MPa at 200%/s

representing a 30-fold increase in pressure for a 1000-fold increase in loading rate, suggesting the relative protection afforded to prevent large increases in intracellular pressure under dynamic loading conditions.

Cell fluid pressures varied with strain rates from 0.02 to 0.58 MPa for the slowest to the fastest strain rates. These values are in the range of pressure for articular cartilage (0.2-0.6 MPa) reported for simulated unconfined compression of articular cartilage plugs to 10% at 0.17%/s (Pérez and Doblaré 2006) and for chondrocytes within articular cartilage plugs under 15% imposed strains (Wu and Herzog 2000). The smallest pore pressure at the slowest strain rate is associated with the escape of fluid from the cell during the long-term compression which results in fluid pressure dissipation. Conversely, the higher fluid pressure at rapid compression relates to the fluid resistance due to the negligible fluid drainage out of the cell at a very short time (Argote et al. 2019). Similar observations were made for articular cartilage subjected to confined compression of 5% strain, in which cartilage was modeled as a hyperplastic inhomogeneous material (Moo et al. 2012). The strain rate affects the percentage of load-bearing supported by fluid and solid phases. With a higher strain rate, the contribution of fluid for load-bearing increases (Argote et al. 2019; Pérez and Doblaré 2006). At the tissue level, the fluid pressure within the cartilage is associated with the load-bearing of the joint and it can support up to 95% of the applied load while the remaining load is supported by collagen and proteoglycan of the cartilage matrix (Soltz and Ateshian 1998). This effectively increases the apparent modulus of the hydrated tissue at higher loading rates (Fig. 5.7). The total hydrostatic pressure within in the cell and the matrix is the sum of the fluid and the solid matrix pressures as accounted for the mixture theory and the volume fractions of the solid and fluid phases.

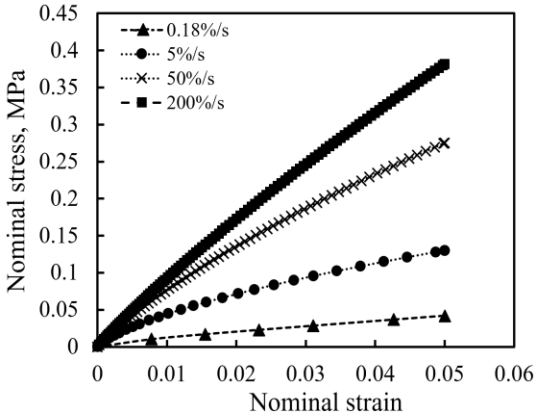

Fig. 5.7. Calculated nominal stress as a function of nominal strain during the ramp phase of loading to a 5% nominal strain.

5.4.3. Depth-dependent transmembrane fluid velocity and the influence of CC permeability

The cellular strains were affected by the boundary constraints and fluid flow across the tissue. At 0.18%/s the rate of loading the fluid had sufficient time for interstitial fluid to cross into the CC layer and to move through the extracellular matrix towards the metaphysis, and for intracellular fluid to escape across the cell membrane. Changes in CC permeability had almost no influence on the cellular strains at this slow loading rate. The slight decrease in strains with cell depth was due to the higher permeability of the PZ/HZ tissue allowing interstitial fluid to more easily flow towards the metaphyseal end. Fluid flowed out of the cell and across the cell membrane at the highest velocities for the cell closest to the CC at the 5%/s strain rate (Fig. 5.8), corresponding to when the greatest cell deformation and maximum principal strains within the cell occurred. At this strain rate, all the cell strain measures decreased through the depth of the RZ, as the velocity of the fluid extruded from the cell dropped with depth in the RZ and reached minimum values for the cell nearest the PZ. At the high nominal strain rate of 200%/s, the magnitude of the fluid velocity across the cell membrane decreased. At this loading rate, the observed pattern of cellular maximum principal strains and height and width strain increasing with depth within the RZ is similar to those obtained from a previously published single phase elastic model of in situ chondrocytes in the RZ (Kazemi and Williams 2019).

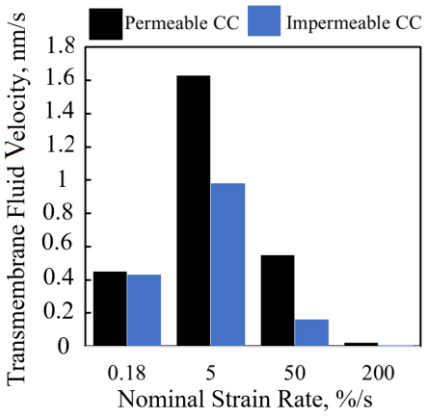

Fig. 5. 8. Peak fluid velocity across the cell membrane for the RZ cell closest to the calcified cartilage (CC).

The fluid boundary condition at the reserve zone-calcified cartilage interface has a notable effect on our results. It had the highest influence on the deformation behavior of the chondrocyte close to CC border. This means that this reserve zone cell is the most sensitive to the permeability boundary condition and that cell sensitivity decreases along the depth of RZ, farther from that border. The assumption of an impermeable CC may represent an extreme case of boundary permeability when the cartilage is close to fusing and a stiff dense subchondral bone plate has formed at the epiphyseal border. Such dense bone provides a continuous layer, acting as a barrier to fluid flow and could shut off fluid exchange (Cohen et al. 1994). The structural and mechanical properties of cartilage and its borders with the bones changes during skeletal development (Mow and Guo 2002; Wosu et al. 2012). In early stages of growth the epiphyseal border between cancellous bone and the reserve zone is open and a thin layer of bone with many perforations for blood vessels provides for a more highly permeable interface with bone marrow spaces than in the established growth plate at later stages. The compositional and structural variations influence the ability of interstitial fluid to flow through the matrix and consequent change of fluid flow pathway, which affects the permeability of cartilage chondro-osseous junctions (Berteau et al. 2016; Maroudas et al. 1968; Mow and Guo 2002). There are not enough studies on the permeability of the growth plate and chondro-osseous junctions to see how they change during skeletal development.

5.4.4. Depth-dependent pattern of flow-induces shear stress

The fluid flow around the cell and across the cell membrane generated shear stresses on the surface of the cell, which vary over the cell surface, with strain rates, and through the cartilage depth (RZ). The highest values of fluid-flow-induced shear stress occurred for the cell location closest to the CC, where it ranged from 2 mPa at 0.18%/s, increasing steadily to 8 mPa at 200%/s.

To our knowledge this is the first study to calculate interstitial fluid shear stresses around chondrocytes in growth plate cartilage. It is difficult to evaluate the stimulatory effect of these shear stresses. Interstitial fluid shear stresses through articular cartilage have been estimated from computational simulations of stress relaxation experiments to be as high as 65 mPa for 15% compression at 5%/s (Athesian et al. 2007, Mow et al. 2008). In vitro studies on the effects of convective fluid flow around cells have, with a few exceptions, mostly considered relatively large fluid-induced shear stresses, of the order of 100 mPa or more. Shear stresses of 100 mPa have been shown to stimulate spatial heterogeneity in the deposition of collagen types I and II in 250-microns scaffold-free articular cartilage constructs that were produced *de novo* by bovine articular chondrocytes; and to increase the tensile strength and moduli of the extracellular matrix (Gemmiti and Guldberg 2009). Exposure to 12 mPa 1Hz sinusoidal shear stress for 30 min/day, followed by steady flow at 0.4 mPa shear stress for the rest of the day, has been shown to stimulate aggrecan and type II collagen accumulation in 2-mm thick chondrocyte-seeded agarose hydrogels (Chen et al. 2012). Similarly, articular chondrocytes subjected to shear stresses of 0.7 to 310 mPa produced tissue with higher collagen II content than static controls (Zhong et al. 2013). Interestingly, in the same study the collagen I content of tissues formed under shear stresses between 0.7 to 4.6 mPa was the same as for static controls, but greater than controls for shear stresses above 18.9 mPa (Zhong et al. 2013). These results suggest that low levels of fluid shear stress may be beneficial for chondrocytes to maintain cartilage, but high levels may induce a fibrocartilage phenotype. Considering these in vitro studies on articular chondrocytes it seems possible that the convective fluid shear stresses around reserve zone chondrocytes calculated for 5% compression may fall in the stimulatory range for maintaining and producing cartilage tissue.

Considering only fluid shear stress values in the possibly stimulatory range of 0.4 mPa and above, it may be noted that the fluid shear stresses reached 2-8 mPa for the cell at the RZ/CC border for all loading rates; 0.5-0.8 mPa for the cell in the middle of the RZ at 0.18%/s and 200%/s, respectively; and 0.9 mPa for the cell at the RZ/PZ border only for the fastest strain rate of 200%/s. This implies a stratification in stimulatory fluid shear stresses by location within the RZ as well as loading rate. Impulsive loading rates are possibly stimulatory for cells in all locations, but much more so near the CC border. Very low strain rates may also deliver stimulatory levels of shear stress to cells at the CC border and also to those in the middle of the RZ.

The predicted shear stresses in our model fall in the range of values reported to be stimulatory for producing cartilage matrix components in vitro. This suggests that the fluid flow-induced shear stresses in our study may stimulate cells in the reserve zone and contribute to cell signal transduction at the loading rates examined in our study. Fluid shear stresses acting along the surfaces of cilia may also provide stimulatory signals to the cell. The location of maximum shear stress on the cell surface and the orientation of the cell may play a role in cell reorientation and cell alignment within the reserve zone to prepare the cells and for columnar alignment in the PZ (De Andrea et al. 2010). It has been suggested that resting chondrocytes produce a growth plate-orienting morphogen that diffuses into the proliferative zone, setting up a concentration gradient that guides the orientation of proliferative columns (Abad et al. 2002). It has also been proposed that reserve zone chondrocytes produce a morphogen that inhibits terminal differentiation of nearby proliferative zone chondrocytes (Abad et al. 2002), suggesting that the reserve zone may be partially responsible for the organization of the growth plate into distinct zones. The gradient in cellular strains and the fluid shear stresses at the cell surface predicted by our model may be the source of a mechanoregulatory component of such morphogens.

There are a number of limitations in this study. Our computational results were compared with stress relaxation data obtained from previous experiments on bone/growth plate/bone plugs in terms the time history and approximate stress magnitudes of the resulting force under prescribed displacement loading at 0.18%/s nominal strain rate (Soltz and Eng 2000), giving us confidence that the macroscale

model reproduced the overall transient response of bone/growth-plate-cartilage/bone. We did not include the complex undulations of the mammillary process of cartilage-bone interfaces in our idealized flat and level growth plate model. Such undulations and a nonlevel interface can cause a complex state of stress within the cartilage rather than pure compression and prevented a more precise quantitative comparison between the finite element model and the experimental data. The dimensions of the model in this computational study approximate those experimental samples and may represent an idealized version of the entire growth plate in a small animal. Limitations of this study include the assumption of a homogenous solid phase for cartilage structure and ignoring the collagen fiber network. The collagen network would affect the fluid flow and cell tensile strain. On the other hand, we also did not take into account the role of ions and proteoglycan fixed charge density. By assuming homogeneous isotropic properties for the PZ and HZ zone the chondron tubular structure was ignored. Perfect bonding was assumed at all interfaces when it is likely that the cell boundaries are not perfectly bonded to the pericellular matrix, but may be attached at focal points. The surface of the cell was assumed to be smooth when it is likely to have a ruffled shape. The assumption of a free boundary along one edge of the cartilage does not account for the perichondrial barrier to fluid exudation or for the possible restraining action of a thick perichondrium that exists in early growth.

5.5. Conclusions

The findings of this study are potentially important for understanding the role of the reserve zone cartilage and of the mechanical environment of reserve zone chondrocytes in the growth plate when subjected to dynamic loading conditions. The cellular strains within the reserve zone are depth-dependent and highly sensitive to the loading rate and to the permeability of the subchondral bone plate, which likely changes during development and maturation. This sensitivity to permeability decreases through reserve zone depth with distance from the epiphyseal junction. The values predicted by our model for fluid flow-induced shear stress exceed values reported to be stimulatory to cells during in vitro experiments. The gradient observed through the depth of the reserve zone in potential mechanoregulatory signals, such as cell strain, membrane strain, intracellular fluid pressure, and fluid shear stress varies with the rate of

loading. The depth-dependent patterns at very slow quasi-static loading rates and at high impact loading rates differ from those observed during intermediate loading rates. This is explained by the biphasic nature of the tissue in which the fluid component plays a more dominant role in supporting loads at higher loading rates. These strain-rate dependent gradients in the microenvironment of the cells may provide necessary signals for the hypothesized regulatory role of the reserve zone cartilage.

References

Abad V, Meyers JL, Weise M, Gafni RI, Barnes KM, Nilsson O, Baron J (2002) The role of the resting zone in growth plate chondrogenesis. Endocrinology 143(5): 1851-1857. https://doi.org/10.1210/endo.143.5.8776.

Accadbled F, Laffosse JM, Ambard D, Gomez-Brouchet A, De Gauzy JS, Swider P (2008) Influence of location, fluid flow direction, and tissue maturity on the macroscopic permeability of vertebral end plates. Spine 33(6): 612-619. https://doi.org/10.1097/BRS.0b013e318166e0d7.

Alexopoulos LG, Setton LA, Guilak F (2005) The biomechanical role of the chondrocyte pericellular matrix in articular cartilage. Acta Biomaterialia, 1(3): 317-325. https://doi.org/10.1016/j.actbio.2005.02.001.

Argote PF, Kaplan JT, Poon A, Xu X, Cai L, Emery NC, Neu CP (2019) Chondrocyte viability is lost during high-rate impact loading by transfer of amplified strain, but not stress, to pericellular and cellular regions. Osteoarthritis and Cartilage 27(12): 1822-1830. https://doi.org/10.1016/j.joca.2019.07.018

Ateshian GA, Costa KD, Hung CT (2007) A theoretical analysis of water transport through chondrocytes. Biomech Model Mechanobiol 6:91–10.

Berteau JP, Oyen M, Shefelbine SJ (2016) Permeability and shear modulus of articular cartilage in growing mice. Biomech Model Mechanobiol 15(1): 205-212. https://doi.org/10.1007/s10237-015-0671-3.

Bries AD, Weiner DS, Jacquet R, Adamczyk MJ, Morscher MA, Lowder E, Askew MJ, Steiner RP, Horne WI, Landis WJ. (2012). A study in vivo of the effects of a static compressive load on the proximal tibial physis in rabbits. J Bone Joint Surg 94(15), e111. https://doi.org/10.2106/JBJS.K.00340.

Chen T, Buckley M, Cohen I, Bonassar L, Awad HA (2012) Insights into interstitial flow, shear stress, and mass transport effects on ECM heterogeneity in bioreactor-cultivated engineered cartilage hydrogels. Biomech Model Mechanobiol 11(5): 689-702. https://doi.org/10.1007/s10237-011-0343-x.

Cohen B, Chorney GS, Phillips DP, Dick HM, Mow VC (1994) Compressive stress-relaxation behavior of bovine growth plate may be described by the nonlinear biphasic theory. J Orthop Res 12(6): 804-813. https://doi.org/10.1002/jor.1100120608.

Cancel M, Grimard G, Thuillard-Crisinel D, Moldovan F, Villemure I (2009) Effects of in vivo static compressive loading on aggrecan and type II and X collagens in the rat growth plate extracellular matrix. Bone 44(2): 306-315. https://doi.org/10.1016/j.bone.2008.09.005

Cohen B, Lai WM, Mow VC (1998) A transversely isotropic biphasic model for unconfined compression of growth plate and chondroepiphysis. ASME J Biomech Eng 120(4): 491-496. https://doi.org/10.1115/1.2798019.

Carter DR, Mikić B, Padian K (1998) Epigenetic mechanical factors in the evolution of long bone epiphyses. Zoological Journal of the Linnean Society 123(2): 163-178. https://doi.org/10.1111/j.1096-3642.1998.tb01298.x.

Carter DR, Wong M (1988) Mechanical stresses and endochondral ossification in the chondroepiphysis. J Orthop Res 6(1): 148-154. https://doi.org/10.1002/jor.1100060120.

De Andrea CE, Wiweger M, Prins F, Bovée JV, Romeo S, Hogendoorn PC (2010) Primary cilia organization reflects polarity in the growth plate and implies loss of polarity and mosaicism in osteochondroma. Laboratory Investigation 90(7): 1091-1101. https://doi.org/10.1038/labinvest.2010.81.

Eberhardt AW, Keer LM, Lewis JL, Vithoontien V (1990) An analytical model of joint contact. ASME J Biomech Eng 112(4): 407-413. https://doi.org/10.1115/1.2891204.

Fan C, Cool JC, Scherer MA, Foster BK, Shandala T, Tapp H, Xian CJ (2009). Damaging effects of chronic low-dose methotrexate usage on primary bone formation in young rats and potential protective effects of folinic acid supplementary treatment. Bone 44(1): 61-70. https://doi.org/10.1016/j.bone.2008.09.014.

Ficklin TP, Davol A, Klisch SM (2009) Simulating the growth of articular cartilage explants in a permeation bioreactor to aid in experimental protocol design. ASME J Biomech Eng , 131(4): 041008 https://doi.org/10.1115/1.3049856.

Farzaneh S, Paseta O, Gómez-Benito MJ (2015) Multi-scale finite element model of growth plate damage during the development of slipped capital femoral epiphysis. Biomech Model Mechanobiol 14(2): 371-385. https://doi.org/10.1007/s10237-014-0610-8.

Frost HM (1990) Skeletal structural adaptations to mechanical usage (SATMU): 3. The hyaline cartilage modeling problem. The Anatomical Record 226(4): 423-432. https://doi.org/10.1002/ar.1092260404.

Gao J, Roan E, Williams JL (2015) Regional variations in growth plate chondrocyte deformation as predicted by three-dimensional multi-scale simulations. PLoSONE 10(4): e0124862. https://doi.org/10.1371/journal.pone.0124862.

Gao J, Williams JL, Roan E (2014) On the state of stress in the growth plate under physiologic compressive loading. Open Journal of Biophysics 4(1):13–21. https://doi.org/10.4236/ojbiphy.2014.41003.

Gao J, Williams JL, Roan E (2017) Multiscale modeling of growth plate cartilage mechanobiology. Biomech Model Mechanobiol 16(2): 667-679. https://doi.org/10.1007/s10237-016-0844-8.

Gemmiti CV, Guldberg RE (2009) Shear stress magnitude and duration modulates matrix composition and tensile mechanical properties in engineered cartilaginous tissue. Biotechnol. Bioeng. 104(4): 809-820. https://doi.org/10.1002/bit.22440.

Guilak F, Mow VC (2000) The mechanical environment of the chondrocyte: a biphasic finite element model of cell–matrix interactions in articular cartilage. J Biomech 33(12): 1663-1673. https://doi.org/10.1016/S0021-9290(00)00105-6.

Grimm MJ, Williams JL (1997). Measurements of permeability in human calcaneal trabecular bone. J Biomech 30(7): 743-745. https://doi.org/10.1016/S0021-9290(97)00016-X.

Gupta T, Donahue TLH (2006) Role of cell location and morphology in the mechanical environment around meniscal cells. Acta Biomaterialia, *2*(5): 483-492. https://doi.org/10.1016/j.actbio.2006.05.009.

Guharay F, Sachs F (1984) Stretch-activated single ion channel currents in tissue-cultured embryonic chick skeletal muscle. The Journal of Physiology 352(1): 685-701. https://doi.org/10.1113/jphysiol.1984.sp015317

Hallett SA, Ono W, Ono N (2019) Growth plate chondrocytes: Skeletal development, growth and beyond. International Journal of Molecular Sciences 20(23): 6009. https://doi.org/10.3390/ijms20236009.

Hwang J, Bae WC, Shieu W, Lewis CW, Bugbee WD, Sah RL (2008) Increased hydraulic conductance of human articular cartilage and subchondral bone plate with progression of osteoarthritis. Arthritis &

Rheumatism: Official Journal of the American College of Rheumatology 58(12): 3831-3842. https://doi.org/10.1002/art.24069.

Kazemi M, Williams JL (2018) Elemental and histological study of the growth plate reserve zone–subchondral bone interface. Paper presented at: Orthopaedic Research Society Annual Meeting (ORS), 2018; New Orleans, LA.

Kazemi M, Williams JL (2019) Chondrocyte and pericellular matrix deformation and strain in the growth plate cartilage reserve zone under compressive loading. In: International Symposium on Computer Methods in Biomechanics and Biomedical Engineering (pp. 526-538). Springer, Cham. https://doi.org/10.1007/978-3-030-43195-2_43.

Kazemi M, Williams JL (2020) Properties of Cartilage–Subchondral Bone Junctions: A Narrative Review with Specific Focus on the Growth Plate. Cartilage https://doi.org/10.1177/1947603520924776.

Kazemi M, Williams JL (2021) On the role of the reserve zone and mechano-regulatory stimuli in the development and maturation of the growth plate: Observations and models. Mechanobiology Journal.

Komeili A, Otoo BS, Abusara Z, Sibole S, Federico S, Herzog W (2020) Chondrocyte Deformations Under Mild Dynamic Loading Conditions. Annals of Biomedical Engineering. https://doi.org/10.1007/s10439-020-02615-9.

Lavagnino M, Arnoczky SP, Kepich E, Caballero O, Haut RC (2008). A finite element model predicts the mechanotransduction response of tendon cells to cyclic tensile loading. Biomech Model Mechanobiol 7(5): 405-416. https://doi.org/10.1007/s10237-007-0104-z.

Lai WM, Mow VC (1980) Drag-induced compression of articular cartilage during a permeation experiment. Biorheology 17(1-2),:111-123. https://doi.org/10.3233/BIR-1980-171-213.

Lai WM, Mow VC, Roth V (1981) Effects of nonlinear strain-dependent permeability and rate of compression on the stress behavior of articular cartilage. ASME J Biomech Eng. 103(2): 61-66 https://doi.org/10.1115/1.3138261.

Lacroix D, Prendergast PJ, Li G, Marsh D (2002) Biomechanical model to simulate tissue differentiation and bone regeneration: application to fracture healing. Medical and Biological Engineering and Computing, 40(1): 14-21. https://doi.org/10.1007/BF02347690.

Leipzig ND, Athanasiou KA (2008) Static compression of single chondrocytes catabolically modifies single-cell gene expression. Biophysical Journal 94(6): 2412-2422. https://doi.org/10.1529/biophysj.107.114207.

Lui JC (2020) Home for a rest: stem cell niche of the postnatal growth plate. Journal of Endocrinology 246(1): R1-R11. https://doi.org/10.1530/JOE-20-0045.

Maroudas A, Bullough P, Swanson SAV, Freeman MAR (1968) The permeability of articular cartilage. The Journal of bone and joint surgery. British volume 50(1): 166-177. https://doi.org/10.1302/0301-620X.50B1.166.

Matsushita Y, Ono W, Ono . (2020) Growth plate skeletal stem cells and their transition from cartilage to bone. Bone 136: 115359. https://doi.org/10.1016/j.bone.2020.115359.

Moo EK, Han SK, Federico S, Sibole SC, Jinha A, Osman NAA, Herzog W(2014) Extracellular matrix integrity affects the mechanical behavior of in-situ chondrocytes under compre ssion. J Biomech 47(5): 1004-1013. https://doi.org/10.1016/j.jbiomech.2014.01.003.

Moo EK, Herzog W, Han SK, Osman N., Pingguan-Murphy B, Federico S (2012) Mechanical behavior of in-situ chondrocytes subjected to different loading rates: a finite element study. Biomech Model Mechanobiol 11(7): 983-993. https://doi.org/10.1007/s10237-011-0367-2.

Morris CE, Sigurdson W. (1989). Stretch-inactivated ion channels coexist with stretch-activated ion channels. Science 243(4892): 807-809. https://doi.org/10.1126/science.2536958.

Mow VC, Hou JS, Owens JM, Ratcliffe A (1990) Biphasic and quasilinear viscoelastic theories for hydrated soft tissues. In: Biomechanics of diarthrodial joints (pp. 215-260). Springer, New York, NY. https://doi.org/10.1007/978-1-4612-3448-7_8.

Mow VC, Guo XE (2002) Mechano-electrochemical properties of articular cartilage: their inhomogeneities and anisotropies. Annual Review of Biomedical Engineering 4(1): 175-209. https://doi.org/10.1146/annurev.bioeng.4.110701.120309.

Mow VC, Kuei SC, Lai WM, Armstrong CG (1980) Biphasic creep and stress relaxation of articular cartilage in compression: theory and experiments. ASME J Biomech Eng 102(1): 73-84. https://doi.org/10.1115/1.3138202.

Nauman EA, Fong KE, Keaveny TM (1999) Dependence of intertrabecular permeability on flow direction and anatomic site. Annals of Biomedical Engineering 27(4): 517-524. https://doi.org/10.1114/1.195.

Nguyen BV, Wang QG, Kuiper NJ, El Haj AJ, Thomas CR, Zhang Z (2010) Biomechanical properties of single chondrocytes and chondrons determined by micromanipulation and finite-element modelling. Journal of the Royal Society Interface *7*(53): 1723-1733. https://doi.org/10.1098/rsif.2010.0207.

Olesen SP, Claphamt D, Davies P (1988) Haemodynamic shear stress activates a K+ current in vascular endothelial cells. Nature 331(6152): 168-170.

Pauwels F (1960) Eine neue Theorie über den Einfluß mechanischer Reize auf die Differenzierung der Stützgewebe. Z Anat Entwicklung 121(6):478–515 https://doi.org/10.1007/BF00523401.

Pérez del Palomar A, Doblaré M (2006) On the numerical simulation of the mechanical behavior of articular cartilage. International Journal for Numerical Methods in Engineering 67(9): 1244-1271. https://doi.org/10.1002/nme.1638.

Poole CA, Flint MH, Beaumont BW (1987) Chondrons in cartilage: ultrastructural analysis of the pericellular microenvironment in adult human articular cartilages. J Orthop Res 5(4): 509-522. https://doi.org/10.1002/jor.1100050406.

Radhakrishnan P, Lewis NT, Mao JJ (2004) Zone-specific micromechanical properties of the extracellular matrices of growth plate cartilage. Annals of Biomedical Engineering 32(2): 284-291. https://doi.org/10.1023/B:ABME.0000012748.41851.b4.

Sakai N, Hagihara Y, Hashimoto C, Komori M, Sawae Y, Murakami T (2015) An estimation of mechanical propertes of articular cartilage for biphasic finite element analyses. Journal of Biomechanical Science and Engineering 10(4): 15-00228. https://doi.org/10.1299/jbse.15-00228.

Seeger-Nukpezah T, Golemis EA (2012) The extracellular matrix and ciliary signaling. Current Opinion in Cell Biology 24(5): 652-661. https://doi.org/10.1016/j.ceb.2012.06.002.

Sergerie K, Lacoursière MO, Lévesque M, Villemure I (2009) Mechanical properties of the porcine growth plate and its three zones from unconfined compression tests. J Biomech 42(4): 510-516. https://doi.org/10.1016/j.jbiomech.2008.11.026.

Shefelbine SJ, Carter DR (2004) Mechanobiological predictions of growth front morphology in developmental hip dysplasia. J Orthop Res 22(2): 346-352. https://doi.org/10.1016/j.orthres.2003.08.004.

Shao YY, Wang L, Welter JF, Ballock RT (2012). Primary cilia modulate Ihh signal transduction in response to hydrostatic loading of growth plate chondrocytes. Bone 50(1): 79-84. https://doi.org/10.1016/j.bone.2011.08.033.

Soltz MA, Ateshian GA (1998) Experimental verification and theoretical prediction of cartilage interstitial fluid pressurization at an impermeable contact interface in confined compression. J Biomech 31(10): 927-934. https://doi.org/10.1016/S0021-9290(98)00105-5.

Song Y, Lee D, Shin CS, Carter DR, Giori NJ (2013). Physeal cartilage exhibits rapid consolidation and recovery in intact knees that are physiologically loaded. J Biomech 46(9): 1516-1523. https://doi.org/10.1016/j.jbiomech.2013.03.026.

Stender ME, Regueiro RA, Ferguson VL (2017) A poroelastic finite element model of the bone–cartilage unit to determine the effects of changes in permeability with osteoarthritis. Computer Methods in Biomechanics and Biomedical Engineering 20(3): 319-331. https://doi.org/10.1080/10255842.2016.1233326

Sylvestre PL, Villemure I, Aubin CE (2007) Finite element modeling of the growth plate in a detailed spine model. Medical & Biological Engineering & Computing, 45(10): 977-988. https://doi.org/10.1007/s11517-007-0220-z.

Williams JL, Do PD, Eick JD, Schmidt TL (2001).Tensile properties of the physis vary with anatomic location, thickness, strain rate and age. J Orthop Res 19(6): 1043-1048. https://doi.org/10.1016/S0736-0266(01)00040-7.

Wosu R, Sergerie K, Lévesque M, Villemure I (2012) Mechanical properties of the porcine growth plate vary with developmental stage. Biomech Model Mechanobiol 11(3-4): 303-312. https://doi.org/10.1007/s10237-011-0310-6.

Wu JZ, Herzog W (2000) Finite element simulation of location-and time-dependent mechanical behavior of chondrocytes in unconfined compression tests. Annals of Biomedical Engineering 28(3): 318-330. https://doi.org/10.1114/1.271.

Wu JZ, Herzog W, Epstein M (1997) Evaluation of the finite element software ABAQUS for biomechanical modelling of biphasic tissues. J Biomech 31(2): 165-169. https://doi.org/10.1016/S0021-9290(97)00117-6.

Yellowley CE, Jacobs CR, Li Z, Zhou Z, Donahue HJ (1997) Effects of fluid flow on intracellular calcium in bovine articular chondrocytes. American Journal of Physiology-Cell Physiology 273(1): C30-C36. https://doi.org/10.1152/ajpcell.1997.273.1.C30.

Chapter 6

Summary and Conclusion

This study focused on the growth plate reserve zone-subchondral bone junction. Experimental investigations revealed evidence on how epiphyseal mamillary processes develop during the skeletal development. Computational studies investigated how reserve zone chondrocytes experience macroscopic loads applied to the tissue in terms of stress and strain and the results were explained in relation to bone growth theories.

The histological and elemental investigation of reserve zone chondro-osseous junction at three different age groups suggested that in addition to endochondral ossification at the hypertrophic end of growth plate cartilage, there is another ossification front at the reserve zone end, close to the epiphysis. The findings of this study also revealed some clusters of cells, which resemble stem cells and suggests that reserve zone chondrocytes near the epiphysis participate in a slower second endochondral ossification front that develops the subchondral bone plate and forms undulations that match those on the metaphyseal side. Computational results from elastic models indicated that the mechano-regulatory environment of cells at the chondro-epiphysis border is similar to that of hypertrophic chondrocytes, which is favorable for endochondral bone formation, and may contribute to epiphyseal mammillary process modeling or remodeling. The computational results at the microscale are consistent with mechanobiological theories for tissue level, providing evidence that such theories have relevance not only at the macroscopic tissue level, but also at the cell level.

To study the effect of the pericellular matrix (PCM) on the stress-strain distribution around reserve zone chondrocytes, a series of elastic models was developed in which the effect of fluid flow was neglected to mimic a condition when loading is applied rapidly and the interstitial fluid has insufficient time to flow through the matrix. The results found that the PCM can modulate the mechanical signals between the matrix

and cell. The PCM acts as a signal transducer by amplifying the local strains in the surrounding matrix, whilst protecting the cells by reducing intracellular pressure.

Finally, to determine the time-dependent compressive behavior of cells within hydrated soft tissues, a series of multiscale poroelastic models were developed for conditions when fluid could flow though porous matrix and induce pressure gradients in the solid phase during daily activities. The results indicate that fluid flow has a significant effect on the mechanical response of chondrocytes. These results are influenced by cell depth and applied strain rate. The results for the fastest loading rate are consistent with those found for the elastic model. Moreover, the stress-strain state around cell is sensitive to the permeability boundary conditions of the chondro-epiphyseal border, while this sensitivity decreases as the cell gets farther from that interface. Dynamic loading engenders sufficiently large fluid shear stresses around reserve zone cells that may signal reserve zone cells to orient and align in columns. Fluid shear stress can be considered as a mechanical stimulant for reserve zone chondrocyte and may act in conjunction with cilia on the cell surface to stimulate cells to respond to transient mechanical signals.

In summary, the main objectives of this study were to provide insight into mechanical origins for signal transduction at the cell level within reserve zone cartilage under conditions of dynamic compression that could explain the proposed role of the reserve zone in forming a secondary growth front at the epiphyseal border to model the epiphyseal side of the mammillary processes, and in producing morphogens that direct the alignment of the stem cell clones into proliferative columns parallel to the long axis of the bone. The information from the computational studies, along with experimental results provide new insight into the multiscale mechanics of the growth plate reserve zone, and sheds light on the possible contribution of the reserve zone to endochondral bone formation in the growth plate in terms of the cell-level mechanical environment.

Chapter 7

Recommendation for future work

In this study, the histological and elemental analysis of cells close to reserve zone-subchondral bone interface were evaluated. Moreover, the multiscale finite element methods could predict the depth-dependent stress-strain environment of reserve zone chondrocyte with and without the fluid flow effects. For continuing work, the following ideas are suggested.

In the current histology study, frozen tissues were used, which were not suitable for histochemistry studies. By using fresh samples, histochemistry techniques can be employed to provide more detail on the phenotype of cell clusters bordering on the reserve zone-subchondral bone interface.

In this study, EDX was used in the main elemental analysis of the reserve zone-subchondral bone junction and to find evidence of any chemical gradient between hard and soft tissues. However, using AFM, would also enable one to investigate any possible mechanical gradient in this junction, which would help in discovering more about the development of the epiphyseal mamillary processes and of subchondral bone formation during the final stages of growth.

In the computational study, a perfectly flat growth plate was assumed, while it has been shown that the development of mamillary processes provides undulations consisting of hills and valleys between growth plate cartilage and bone. Developing a finite element model of growth plate cartilage with such undulations to replace the current simplified idealized geometry in the macroscale model, would be desired to further explore the influence of mammillary morphology on chondrocyte stress-strain state near the epiphyseal border.

In the current poroelastic model, the solid phase was assumed to be homogenous and isotropic. However, it is well known that collagen fibers are dispersed within the matrix and provide an anisotropic, nonhomogeneous structure for cartilage. Incorporating the collagen fibers network into the computational

model of the growth plate, particularly within the reserve zone, would improve the fidelity of detecting tensile strains acting on the cells from the matrix in response to mechanical loads.

References

Brighton, C. T. (1978). Structure and function of the growth plate. Clinical Orthopaedics and Related Research, (136), 22-32.

Brighton, C. T. (1984). The growth plate. The orthopedic clinics of North America, 15(4), 571-595.

Carter, D. R., Beaupré, G. S. (2007). Skeletal function and form*:* mechanobiology of skeletal development, aging, and regeneration. Cambridge university press.

Carter, D. R., Wong, M. (1988). The role of mechanical loading histories in the development of diarthrodial joints. Journal of Orthopaedic Research, 6(6), 804-816.

Claes, L. E., Heigele, C. A. (1999). Magnitudes of local stress and strain along bony surfaces predict the course and type of fracture healing. Journal of biomechanics, 32(3), 255-266.

Frost, H. M. (1990). Skeletal structural adaptations to mechanical usage (SATMU): 2. Redefining Wolff's law: the remodeling problem. The anatomical record, 226(4), 414-422.

Frost, H. M. (1994). Wolff's Law and bone's structural adaptations to mechanical usage: an overview for clinicians. The Angle Orthodontist, 64(3), 175-188.

Frost, H. M. (1997). Defining osteopenias and osteoporoses. Bone, 20(5), 385-391.

Hueter, C. (1862). Anatomische studien an den extremitaetengelenken neugeborener und erwachsener. Archiv für pathologische Anatomie und Physiologie und für klinische Medicin, *25*(5-6), 572-599.

Newton, P. T., Li, L., Zhou, B., Schweingruber, C., Hovorakova, M., Xie, M., Suter, S. (2019). A radical switch in clonality reveals a stem cell niche in the epiphyseal growth plate. Nature, 567(7747), 234-238.

Pauwels, F. (1960). Eine neue Theorie über den Einfluß mechanischer Reize auf die Differenzierung der Stützgewebe. Zeitschrift für Anatomie und Entwicklungsgeschichte, 121(6), 478-515.

Stokes, I. A. F. (2002). Mechanical effects on skeletal growth. Journal of Musculoskeletal and Neuronal Interactions, 2(3), 277-280.

Volkmann R. (1862). Chirurgische erfahrungen uber knochenverbiegungen und knochenwachsthum. Arch f Path Anat Physiol u Klin Med. 24, 512–41.

Appendix A

1.1 EDX study of cartilage-bone interfaces

Fig. A 1 & 2 shows the map scan and line scan of the main elements within the growth plate cartilage and across its border with the epiphysis and metaphysis. Samples were collected from the proximal tibia of a yearling domestic calf of unknown sex, obtained from a slaughterhouse. The sample was prepared for SEM study as explained in Chapters 3 & 4.

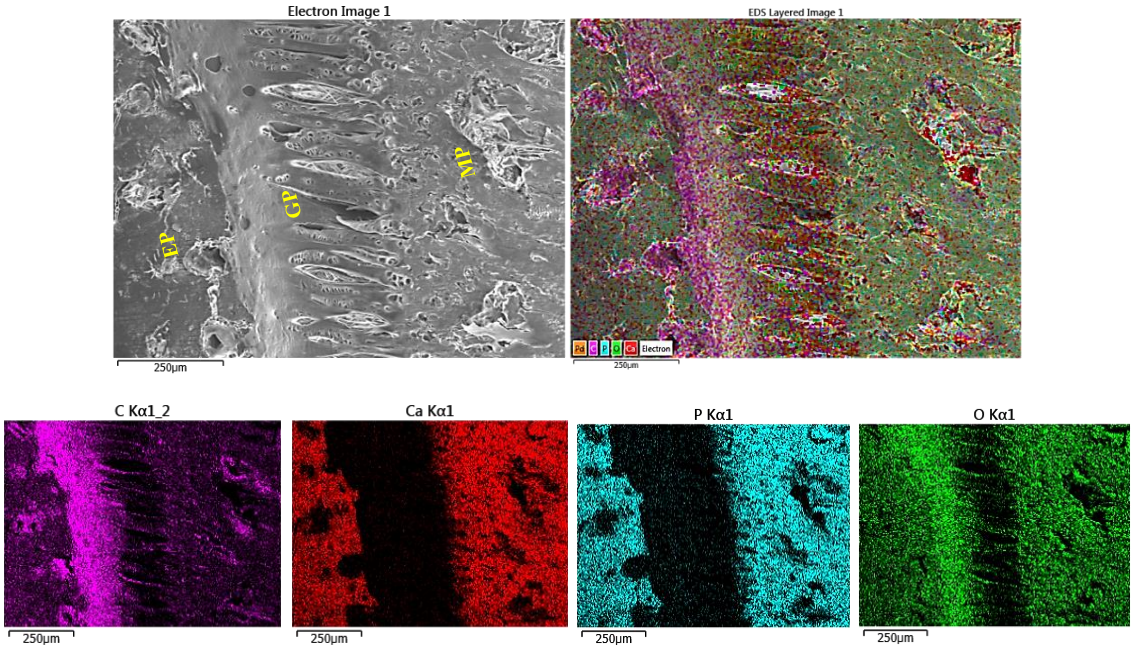

Fig. A1. The results of EDX for map scans of the main elements across the epiphysis (EP)/growth-plate Cartilage (GP)/metaphysis (MP) (12-18-month old bovine sample).

As can be seen from Fig. A1 & A2, the maximum concentrations of Ca and P are found on the bone sides, where they occur mostly in the form of hydroxyapatite, while C is found in high levels in the cartilage, where it is a major component of collagens. Fig. A2B also shows the line scan across the reserve zone chondro-osseous junction and represents the transition zone between hard tissue and soft tissue. The line profile of transition zone extended over 20-50 µm.

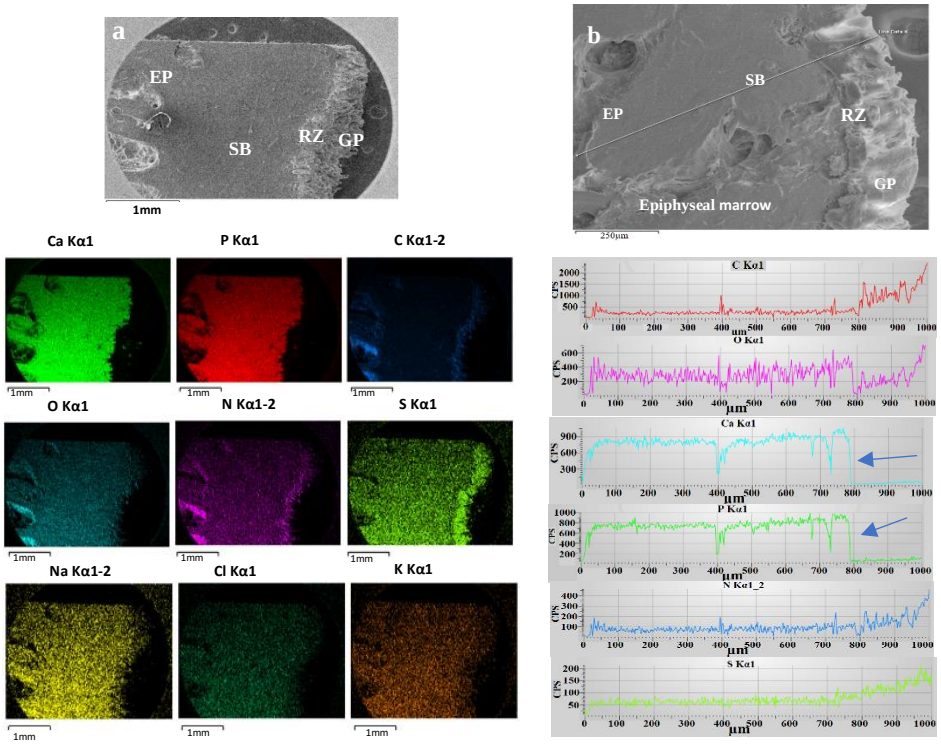

Fig. A2. The results of EDX for A) map scans and B) line scan of the main elements across the epiphyseal subchondral bone-reserve zone border (12-18-month old bovine sample), blue arrows indicate Phosphorus/Calcium gradient. RZ= reserve zone, SB=subchondral bone, GP=growth plate, EP=epiphysis. The growth plate was fractured through the proliferative zone. CPS=count per second.

1.2 Different histological stains for the cartilage-bone interface

To find out more about the collagen orientation within the reserve zone, reserve zone microstructure, and its border with the epiphysis different histological stains were tried. Using various stains provides the opportunity to find the optimum dye, which can yield more valuable information for the region of interest. Sample preparation was followed by the protocol explained for the histological study described in Chapter 3. Samples were collected from the proximal tibia of a yearling cow.

1.2.1 Picro-Sirius Red stain

Picro-Sirius Red (PSR) is a strong anionic dye, which stains collagen by reacting to its sulphonic acid groups with collagen basic groups. It increases the birefringence of collagen fibers under polarizated microscopy. PSR and a polarized light microscope is the ideal way to look at the orientation of collagen

fibers and quantify them on histological sections. Under polarized light microscopy, collagen bundles appear green, red, or yellow. The fibers will be darkest when aligned with either the polarizer or analyzer of the polarized light microscope. PSR shows collagen type I and III. Nuclei, if stained, are black but may often be grey or brown. Collagen type I is thicker and has more birefringence; therefore, it seems more reddish or yellowish in polarized images. Collagen type III is thinner and has weaker birefringence; therefore, it seems more greenish under the polarized microscope.

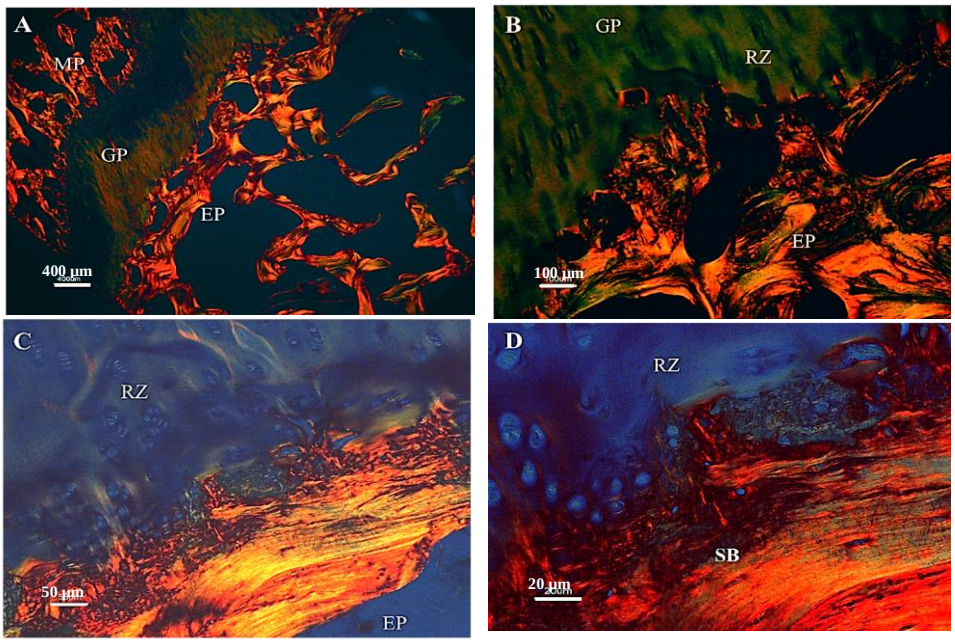

Fig. A3. Growth plate cartilage sample from a cow proximal tibia stained with Picrosirius red, A) Metaphysis (MP)/growth-plate (GP)/epiphysis (EP), B) Growth-plate (GP)/epiphysis (EP), C, D) Higher magnifications of Reserve-zone (RZ)/epiphysis (EP) border.

Collagen is not the only birefringent substance in cartilage (Fig. A3). Fibrous protein, proteoglycans, or glycosaminoglycans also have birefringent properties. To digest proteoglycans and remove them from the cartilage matrix, which results in collagen birefringent enhancement, papain was used. The time for digesting proteoglycan proteins is critical because a shorter time wouldn't be able to digest all of the proteoglycans and a longer time might remove some collagen fibers. To get the optimum time, tissue was kept in papain at four different time scales: no papain as a reference point, 15, 30, 45, and

60 minutes. Results show the continuity of collagen fibers in the interface of reserve-zone/subchondral-bone (Fig. A4).

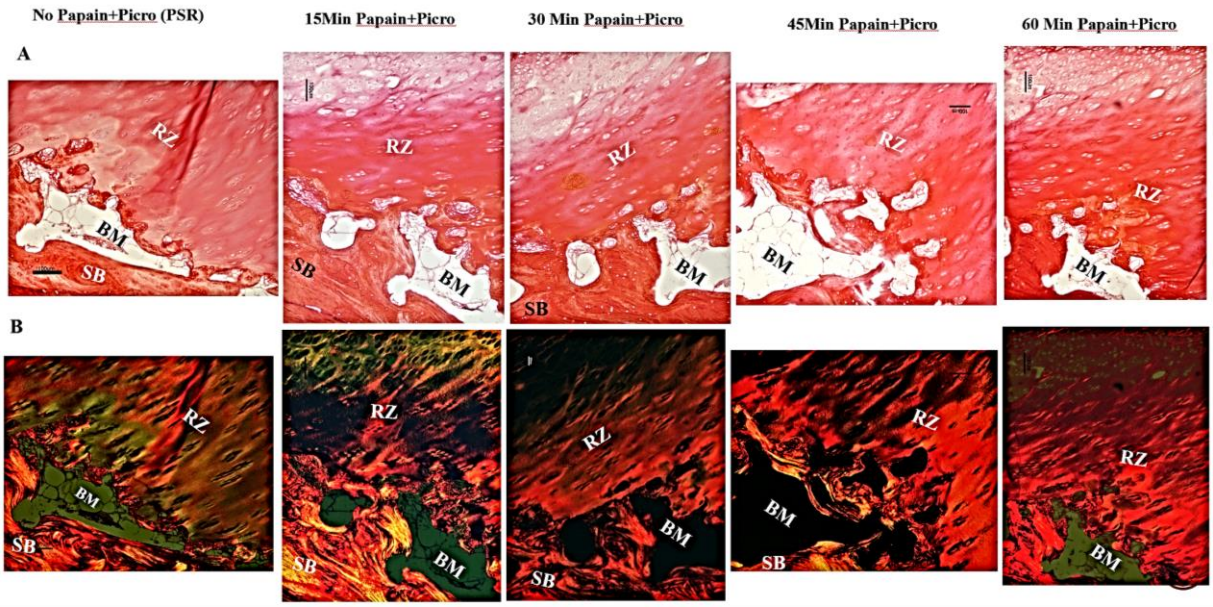

Fig. A4. Digesting proteoglycans in papain at different time scales shows the reserve-zone (RZ)/subchondral bone (SB) interface with A) light microscopy and B) polarized microscopy techniques. BM=Bone Marrow. The scale bar is 100 µm.

1.2.2 Toluidine Blue

Toluidine blue is a basic thiazine metachromatic dye with high affinity for acidic tissue components; therefore, it stains part of tissue rich in DNA and RNA. This dye contains zinc and it can show the localization of glycosaminoglycans (GAGs) in cartilage by light microscopy. It stains cartilage blue to purple (Fig. A5).

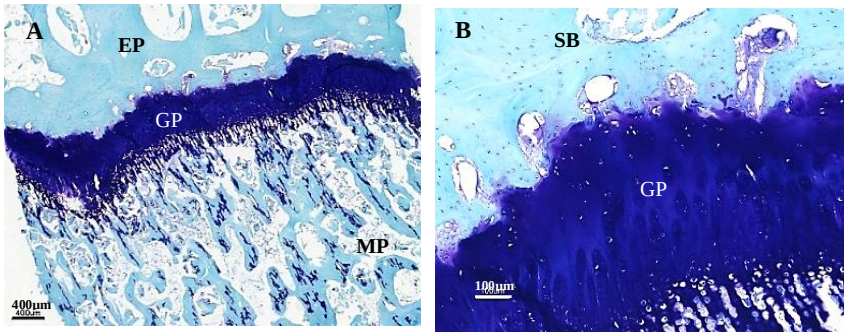

Fig. A5. Growth plate (GP) bovine sample stained with Toluidine Blue, A) Metaphysis (MP)-growth plate-epiphysis (EP), B) Higher magnification of reserve-zone/epiphyseal-subchondral bone (SB) border.

1.2.3 Alcian blue

Alcian blue stains anionic tissue components including RNA and DNA. Like Toluidine Blue, this dye stains the highly acidic proteoglycans and GAGs (Fig. A6).

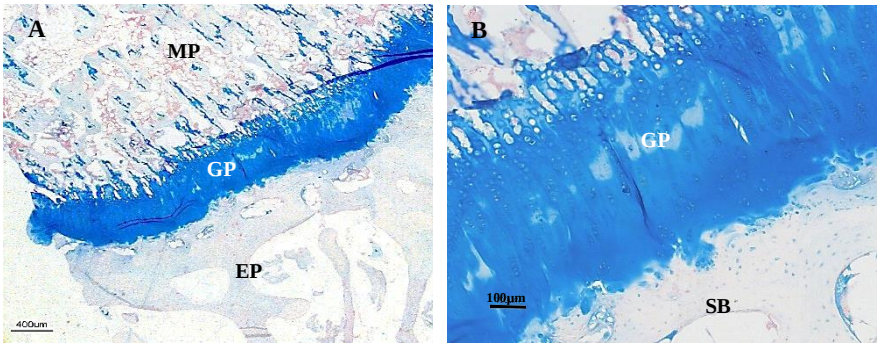

Fig. A6. Growth plate (GP) bovine sample stained with Alcian blue, A) Metaphysis (MP)/growth-plate/epiphysis (EP), B) growth plate/epiphyseal-subchondral-bone (SB) border.

1.2.4 Alizarin Red

This stain is useful for identifying bone or other high calcium structures. It is mostly for evaluating calcium deposits within the tissue. Calcium deposited sides stain orange to red (Fig. A7).

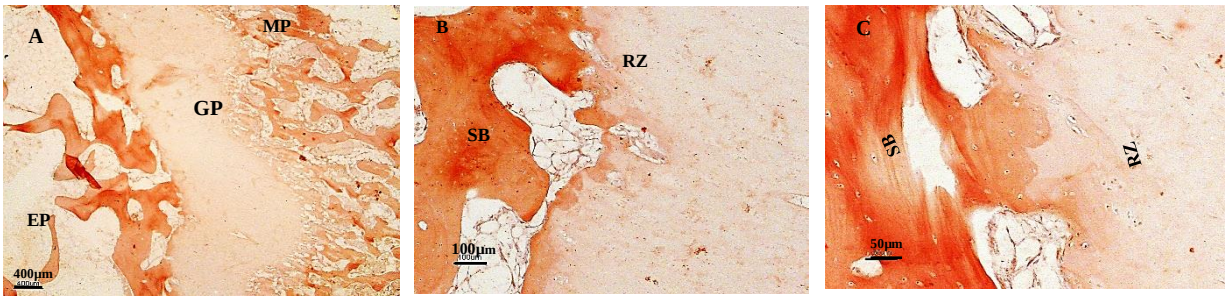

Fig. A7. Growth plate (GP) bovine sample stained with Alizarin red, A) Metaphysis (MP)/growth-plate/epiphysis (EP), B&C) Higher magnification of reserve-zone (RZ)/epiphyseal-subchondral-bone (SB) border.

1.2.5 Hematoxylin and eosin

Hemotoxin and eosin (H&E) is the most common strain used in histology studies. Hematoxylin stains cell nuclei blue, and eosin stains the extracellular matrix and cytoplasm pink. Fig. A8 &A9 show the bovine sample stained with H&E.

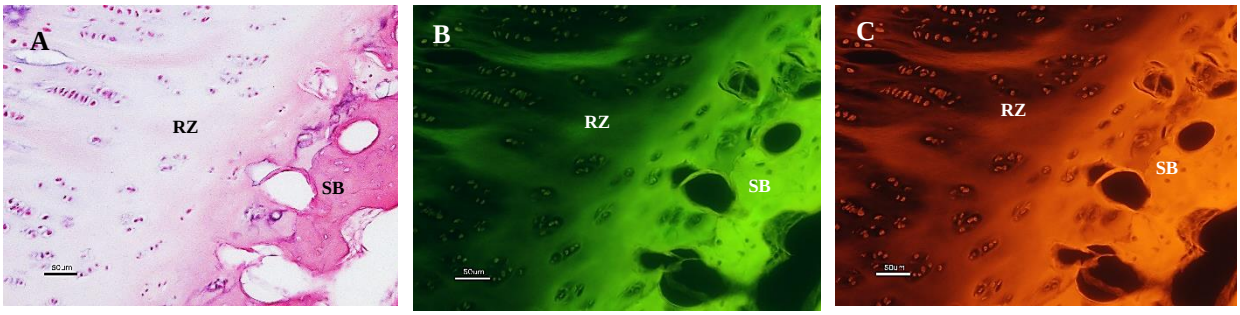

Fig. A8. Reserve-zone (RZ)/Subchondral-bone (SB) interface stained with H&E. A) light microscopy, B) Fluorescence microscopy, green channel. C) Fluorescence microscopy, red channel. Scale bar is 50μm.

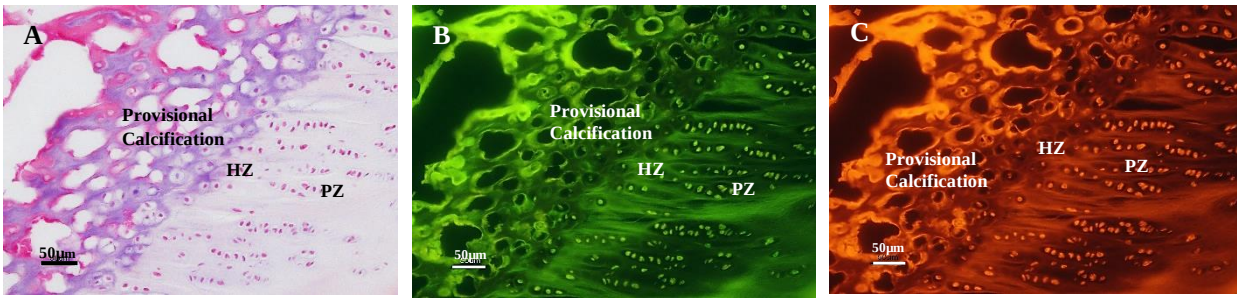

Fig. A9. Hypertrophic-zone (HZ)/metaphysis interface stained with H&E, A) light microscopy, B) Fluorescence microscopy, green channel, C) Fluorescence microscopy, red channel. PZ=Proliferative zone.

1.3 Confocal microscopy study

To measure the chondrocyte deformation as a function of the relative position within the reserve zone under physiological compression, some confocal imaging studies were carried out. Bovine samples were stained with a fluorescence probe (ActinGreen 488 ReadyProbe reagent) and a laser scanning confocal fluorescence inverted microscope (Nikon A1, Nikon Instruments, Inc. Melville, NY) was used to obtain optical serial sections (512x512 pixels) to trace labeled cells within the reserve zone and near the epiphyseal border. 3D reconstruction images of growth plate chondrocytes were created by the confocal microscope software. The results are shown in Fig. A10.

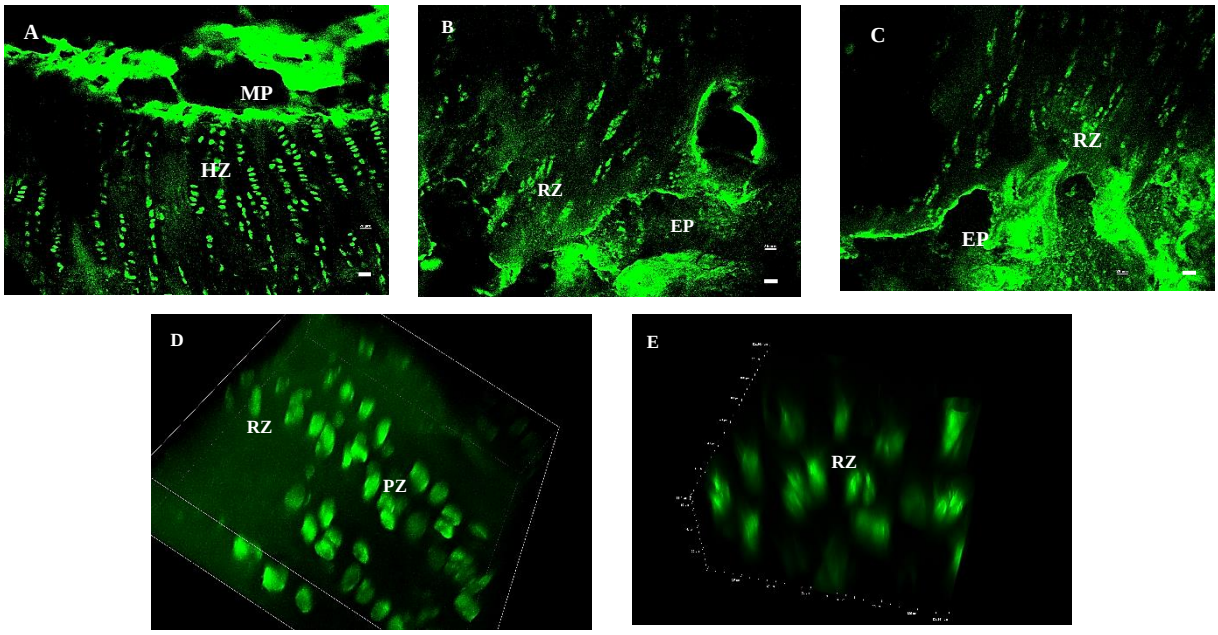

Fig. A10. Results of the confocal the microscopy study. Cells stained with ActinGreen. A) magnification of 10x from HZ-MP border, B) with a magnification of 20x from RZ-EP border, scale bar is 20µm, C) with a magnification of 20x from RZ-EP border, scale bar is 20µm, D) 3D reconstruction of cells within the bovine GP for RZ-PZ, E) 3D reconstruction of cell within the RZ of bovine GP.

2.1. Histology of a 4-month-old mouse growth plate

Distal femurs of a 4-month-old mouse were decalcified in Kristensen solution (18% Formic acid+ 3.5% Sodium formate+82% distilled water) for one week and stained with H&E. A tidemark and some clusters of large neocartilage cells can be seen between the reserve zone and subchondral bone in the 100-µm-thick growth plate cartilage (Fig A11)

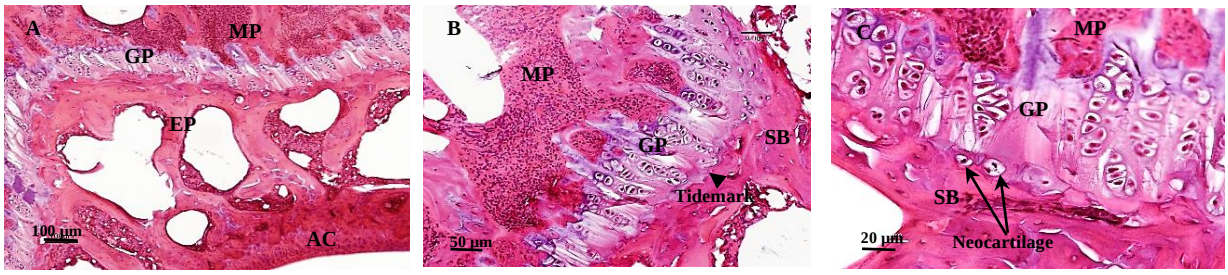

Fig. A11. Histology study of the distal femur, 116-days-old (~4-months-old), stained with H&E. AC= Articular Cartilage, GP=Growth plate, MP=Metaphysis, EP=Epiphysis, SB=Subchondral Bone.

2.2. Confocal study of a 1-month-old mouse growth plate

Images obtained through confocal microscopy (Nikon A1, Nikon Instruments, Inc. Melville, NY) serial sections (512x512 pixels) tracing fluorescently labeled (ActinGreen 488 ReadyProbe reagent) chondrocytes within the reserve zone and near the epiphyseal border (Fig. A12). Samples were cut from the distal femur of a 1-months-old mouse.

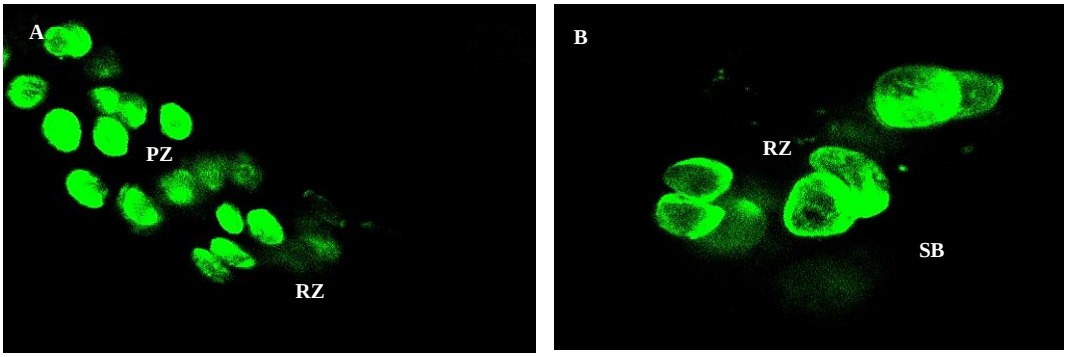

Fig. A12. Confocal microscopy of chondrocytes stained with "ActinGreen". A) proliferative chondrocytes (PZ), 20x, B) Chondrocyte within reserve zone (RZ) near subchondral bone (SB) border, 20x.

Appendix B

The following is the macro code, which was plugged into Image J to do background illumination correction for microscopic images.

For that we need to capture dark field, bright field images first as below:

I. Block the light path and capture an image, call it DarkField.

II. Open the light path, (the image is all background) and capture an image, call it BrightField

III. Capture an image from your region of interest from the specimen, call it Sample.

IV. In image J open all three images you captured, DarkField, BrightField and Sample and run the macro code below.

```
imageCalculator ("Subtract create", "BrightField.tif","DarkField.tif");
  selectWindow ("Result of BrightField.tif");
  rename ("Divisor");
 imageCalculator ("Subtract create", "Sample.tif","DarkField.tif");
  selectWindow ("Result of Smaple.tif");
  rename ("Numerator");
run ("Calculator Plus", "i1=Numerator i2=Divisor operation=[Divide: i2 = (i1/i2) x k1 + k2] k1=255 k2=0
create");
  selectWindow ("Result");
```

Appendix C

Below is the MATLAB code that was used to calculate the volume-averaged cellular hydrostatic stress and averaged cellular strain from our computational results (chapters 3 and 4).

```
%% CAX4H elements have four integration points per element. To make an average of stress/strain values
%%between 4 integration points and get one number per element, we need to run the code below, in which
%%i=number of elements for your region of interest, stress is the matrix contains all of the required
%%variables. In the stress matrix, column 3,4, 5 and 6 refers to Max. Prin strain, Max. Prin. stress, Mid.
%%Prin. stress and Min. Prin. stress respectively, which were extracted from the report file (Abaqus). This
%%code can be used for any mesh type with 4 integration points.
%%In Abaqus, the variable pressure=-hydrostatic stress, therefore, instead of calculating hydrostatic stress
%%from principal stress components, we can directly extract pressure from Abaqus.
for i=1:646                                   %% Number of elements for your region of interest (cell)
   s (i,1)=(sum (stress(4*i-3:4*i,3)))/4;     %% Average of Max. Prin. strain between four integration points
   s (i,2)=(sum (stress(4*i-3:4*i,4)))/4;     %% Average of Max. Prin. Stress between four integration points
   s (i,3)=(sum (stress(4*i-3:4*i,5)))/4;     %% Average of Mid. Prin. Stress between four integration points
   s (i,4)=(sum (stress(4*i-3:4*i,6)))/4;     %% Average of Min. Prin. Stress between four integration points
   hydro=(s(:,4)+s(:,5)+s(:,6))/3;            %% Hydrostatic stress for each element within the cell,
   AverageHydro=(sum (hydro.*v(:,2)))/(sum (v(:,2))  %%Volume averaged cellular hydrostatic stress
end
%% To calculate the volume averaged cellular hydrostatic stress: copy the elements volume (from the
%%report file of Abaqus) and paste it in MATLAB to create a matrix named v (v=[]). The AverageHydro
%% in the code above, gives you the volume averaged cellular hydrostatic stress.
%% For average cellular strain: run E=(sum(s(:,1))) and the average cellular strain=E/(number of
%%elements within your region of interest).
```

Appendix D

Fig. D1. shows the depth-dependent vector plots of maximum principal strain for three cells within the growth plate reserve zone with four growth plate cartilage thicknesses. These results are extracted from the axisymmetric elastic model subjected to 15% strain (Chapter 3). As can be seen from Fig. D1 the orientation of vector plots shows that cells are subjected to strains tending to turn and rearrange themselves under loading that might orient them for entry into the proliferative zone following division.

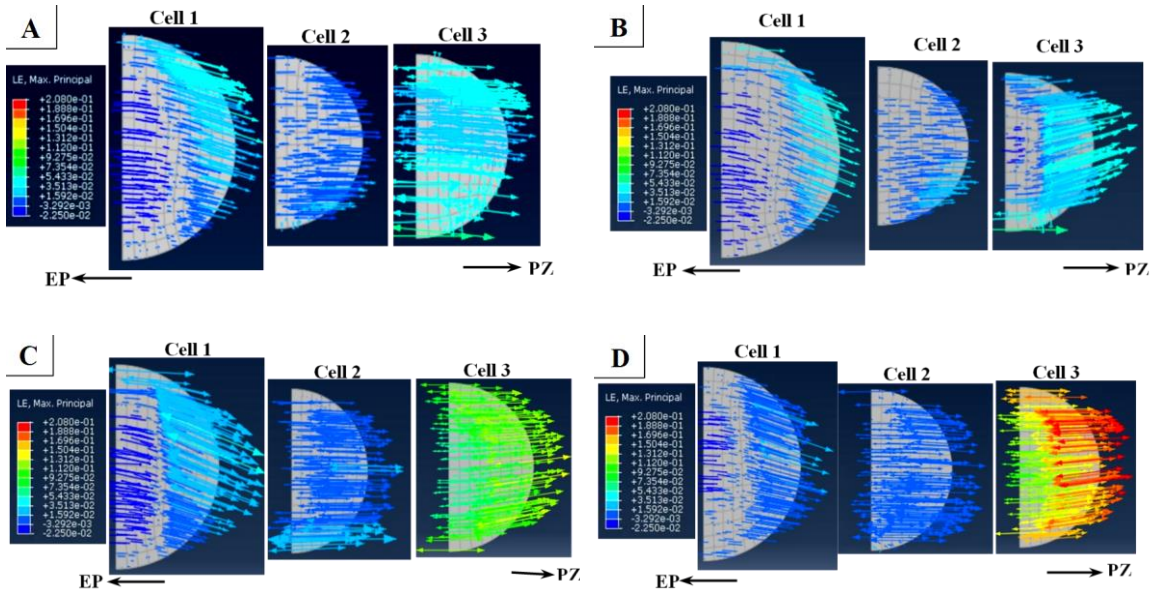

Fig. D1. Vector plots for maximum principal strain within the cell at A) 1mm thick growth plate, B) 2 mm thick growth plate, C) 4 mm thick growth plate and D) 6 mm thick growth plate. Cell 1=hypertrophic cell closest to epiphyseal border (EP), Cell 2=reserve zone cell, 20 µm away from Cell 1, representing the next closest chondrocyte to Cell 1, Cell 3= reserve zone cell closest to proliferative border (PZ).

Appendix E

From the results of the poroelastic model of growth plate cartilage, subjected to 5% strain at different strain rates of 0.18%/s, 5%.s, 50%/s and 200%/s (Chapter 5); vector plots of fluid flow across the cell membranes and within a cell close to the calcified cartilage (CC) border are shown in Figs. E1 and E2, respectively. Fig. E1 shows the results for a permeable CC, while Fig. E2 compares the results between a permeable and nearly impermeable CC. This section, also includes an input file for the poroelastic model for a cell close to the CC at the slowest strain rate.

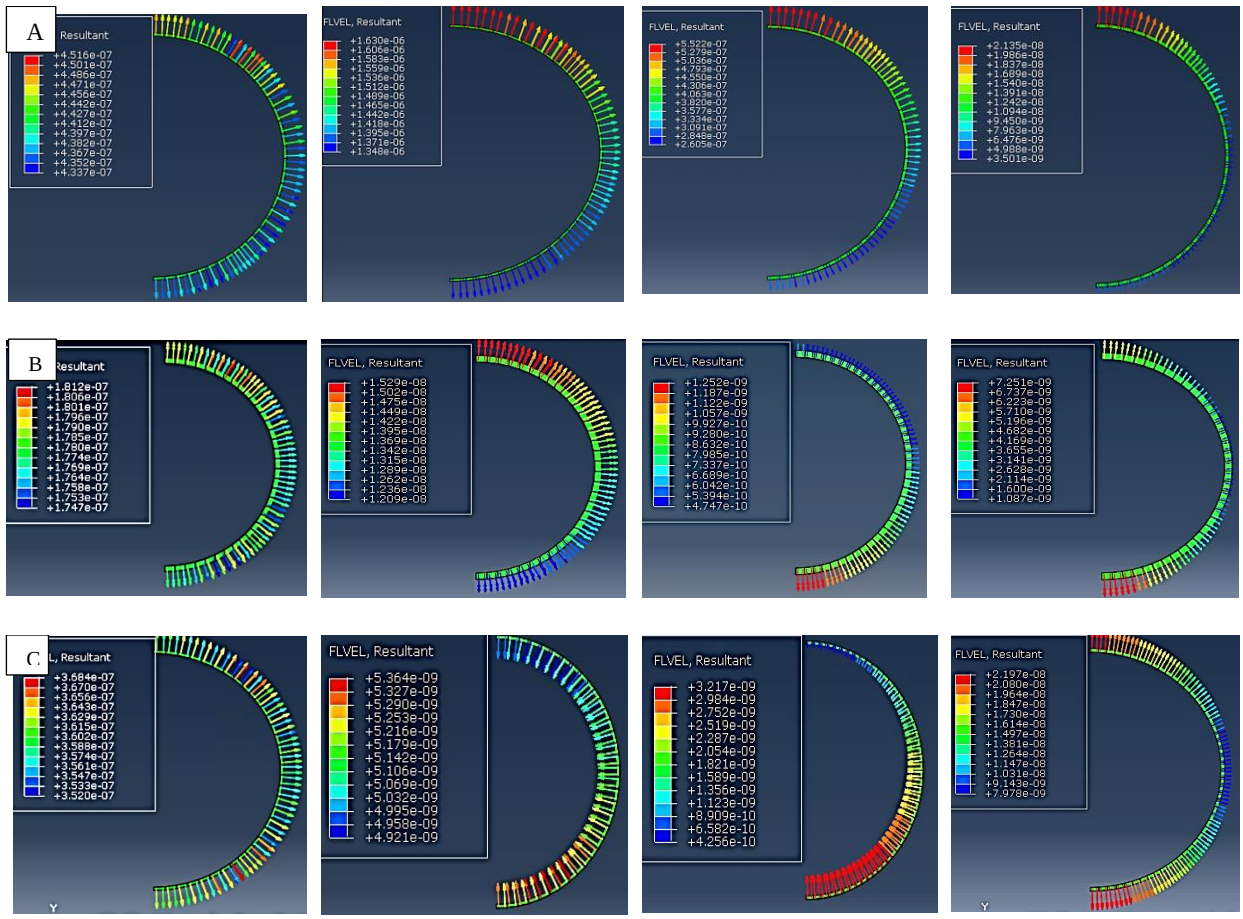

Fig. E1. Vector plots of fluid flow across the cell membrane at 4.5% strain, with a permeable calcified cartilage layer, for A) a RZ cell close to the CC, B) a cell in the middle of RZ, and C) a RZ cell close to PZ/HZ, for all three cells. Vector plots from left to right demonstrate results at strain rates of 0.18%/s, 5%/s, 50%/s, and 200%/s.

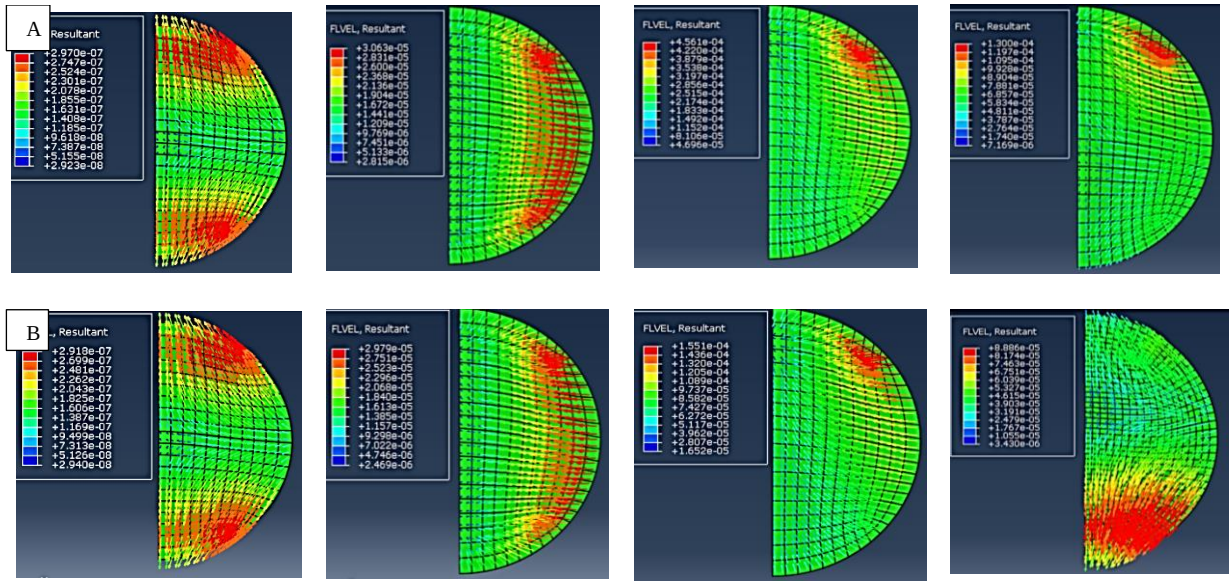

Fig E2. Vector plots of fluid flow within a cell close to the calcified cartilage (CC) with A) Permeable CC and B) Impermeable CC. From left to right, the vector plots indicate results at strain rates of 0.18%/s, 5%/s, 50%/s, and 200%/s.

The following is part of the Abaqus input file for a multiscale poroelastic model of growth plate cartilage, including one cell close to CC border. This model was subjected to 5% strain and 0.18%/s strain rate with the permeable boundary condition for the calcified cartilage (CC).

```
*Heading
** Job name: 5PercentStrain Model name: Model-1
** Generated by: Abaqus/CAE 2019
*Preprint, echo=NO, model=NO, history=NO, contact=NO
**
** PARTS
**
*Part, name=GP
*Node
** %% this model has 11863 nodes,  %%I excluded the nodes coordinate, because of space limitation%%
*Element, type=CAX4P
**%% this model has 11624 elements,  %%I excluded the nodes coordinate, because of space limitation%%
** Section: MP section
*Solid Section, elset=Set-70, material=MP,
** Section: celll
*Solid Section, elset=Set-76, material=cell,
** Section: PC section
*Solid Section, elset=Set-71, material=PC,
** Section: membrane
*Solid Section, elset=Set-77, material=membrane,
** Section: PZ/HZ section
*Solid Section, elset=Set-72, material=PZ/HZ,
** Section: PCM
*Solid Section, elset=Set-75, material=PCM,
** Section: RZ section
*Solid Section, elset=Set-74, material=RZ,
** Section: CC section
*Solid Section, elset=Set-73, material=CC,
** Section: SB
*Solid Section, elset=Set-69, material=SB,
```

```
** Section: EM section
*Solid Section, elset=Set-68, material=EP,
*End Part
**
**
** ASSEMBLY
**
*Assembly, name=Assembly
**
*Instance, name=GP-1, part=GP
*End Instance
**
*Nset, nset=Set-18, instance=GP-1
*End Assembly
**
** MATERIALS
**
*Material, name=CC
*Elastic
300., 0.2
*Permeability, specific=9.81e-06
 0.0008829, 0.5
*Material, name=EP
*Elastic
1000., 0.2
*Permeability, specific=9.81e-06
 44.4393, 2.7
*Material, name=MP
*Elastic
1000., 0.2
*Permeability, specific=9.81e-06
 44.4393, 2.7
*Material, name=PC
*Elastic
100., 0.2
*Permeability, specific=9.81e-06
 22.0725, 2.5
*Material, name=PCM
*Elastic
 0.265, 0.04
*Permeability, specific=9.81e-09
  4.6e-10,  4.1
 4.99e-10, 4.15
 5.41e-10,  4.2
 5.86e-10, 4.25
*Material, name=PZ/HZ
*Elastic
 0.49, 0.125
*Permeability, specific=9.81e-06
  6.8e-08, 3.69
 7.42e-08, 3.73
 8.15e-08, 3.78
 8.95e-08, 3.83
*Material, name=RZ
*Elastic
 0.98, 0.125
*Permeability, specific=9.81e-06
 1.61e-08, 4.35
 1.75e-08,  4.4
  1.9e-08, 4.46
 2.06e-08, 4.51
*Material, name=SB
*Elastic
2000., 0.2
*Permeability, specific=9.81e-06
 0.0008829, 0.14
*Material, name=cell
*Elastic
 0.002, 0.04
*Permeability, specific=9.81e-09
```

```
 4.81e-08, 4.99
 5.21e-08, 5.05
 5.64e-08, 5.11
 6.12e-08, 5.17
*Material, name=membrane
*Elastic
 0.04, 0.04
*Permeability, specific=9.81e-06
 3.46e-14, 3.08
 3.76e-14, 3.12
 4.08e-14, 3.16
 4.43e-14,  3.2
**
** BOUNDARY CONDITIONS
**
** Name: BC0 Type: Displacement/Rotation
*Boundary
Set-33, 2, 2
** Name: POR Type: Pore pressure
*Boundary
Set-34_PP_, 8, 8
**
** PREDEFINED FIELDS
**
** Name: CC   Type: Void ratio
*Initial Conditions, TYPE=RATIO
Set-38, 1.1
** Name: Cell   Type: Void ratio
*Initial Conditions, TYPE=RATIO
Set-44, 4.88
** Name: EP   Type: Void ratio
*Initial Conditions, TYPE=RATIO
Set-36, 3.7
** Name: MP   Type: Void ratio
*Initial Conditions, TYPE=RATIO
Set-42, 3.7
** Name: Membrane   Type: Void ratio
*Initial Conditions, TYPE=RATIO
Set-45, 3.
** Name: PC   Type: Void ratio
*Initial Conditions, TYPE=RATIO
Set-41, 3.5
** Name: PCM   Type: Void ratio
*Initial Conditions, TYPE=RATIO
Set-43, 4.
** Name: PZ   Type: Void ratio
*Initial Conditions, TYPE=RATIO
Set-40, 3.6
** Name: RZ   Type: Void ratio
*Initial Conditions, TYPE=RATIO
Set-39, 4.25
** Name: SB   Type: Void ratio
*Initial Conditions, TYPE=RATIO
Set-37, 0.176
** ----------------------------------------------------------------
**
** STEP: Load 1
**
*Step, name="Load 1", nlgeom=YES, inc=1000
5% starin load, 0.18%/s
*Soils, consolidation, end=PERIOD, utol=0.01, creep=none
1., 1., 1e-05, 1.,
**
** BOUNDARY CONDITIONS
**
** Name: Load Type: Displacement/Rotation
*Boundary
Set-35, 2, 2, -0.025
**
** CONTROLS
```

```
**
*Controls, reset
*Controls, parameters=time incrementation
, , , , , , , 15, , ,
**
** OUTPUT REQUESTS
**
*Restart, write, frequency=0
**
** FIELD OUTPUT: F-Output-1
**
*Output, field
*Node Output
CF, POR, RF, RVF, U
*Element Output, directions=YES
E, EVOL, FLVEL, LE, MVF, S, VOIDR
**
** HISTORY OUTPUT: H-Output-1
**
*Output, history, variable=PRESELECT
*End Step
** ----------------------------------------------------------------
**
** STEP: stress-relaxation 1
**
*Step, name="stress-relaxation 1", nlgeom=YES
*Soils, consolidation, end=PERIOD, utol=0.01, creep=none
1000., 1000., 0.01, 1000.,
**
** CONTROLS
**
*Controls, reset
*Controls, parameters=time incrementation
, , , , , , , 16, , ,
**
** OUTPUT REQUESTS
**
*Restart, write, frequency=0
**
** FIELD OUTPUT: F-Output-1
**
*Output, field
*Node Output
CF, POR, RF, RVF, U
*Element Output, directions=YES
E, EVOL, FLVEL, LE, MVF, S, VOIDR
**
** HISTORY OUTPUT: H-Output-1
**
*Output, history, variable=PRESELECT
*End Step
```